

Characterization of THSD7A- and PLA2R1-specific antibodies and their role in the pathogenesis of membranous nephropathy

Kumulative Dissertation zur Erlangung des Doktorgrades (Dr. rer. nat.)

an der Fakultät für Mathematik, Informatik und Naturwissenschaften

Fachbereich Biologie der Universität Hamburg

vorgelegt von Larissa Seifert (geb. 21.12.1988)

Hamburg, 2020

1. Gutachter: Priv.-Doz. Dr. Gunther Zahner

2. Gutachter: Professor Wolfgang Streit

Datum der Disputation: 26.06.2020

Prüfungskommission: Professor Wolfgang Streit
Priv.-Doz. Gunther Zahner
Professor Friedrich Koch-Nolte
Priv.-Doz. Hartwig Lüthen

Vorsitz: Priv.-Doz. Hartwig Lüthen

Table of contents

1. Introduction	2
1.1 Clinical and histological features of membranous nephropathy.....	2
1.2 Rat Animal Models of MN	4
1.3 Identification of antigens in patients with MN	5
1.4 Clinical role of autoantibody measurement	8
1.5 Structure of PLA2R1 and identification of autoantibody binding domains.....	10
1.6 Pathogenicity of autoantibodies	11
2. Materials, Methods and Results	14
3. Discussion	15
3.1 Structure of THSD7A and the role of autoantibody binding-sites in THSD7A-associated MN	15
3.2 Heterologous models of THSD7A- and PLA2R1-associated MN	22
4. Summary	30
5. Zusammenfassung	31
6. Literature	33
7. Individual contribution	39
8. Acknowledgements	40
9. Eidesstattliche Erklärung	41
10. Appendix	42

1. Introduction

1.1 Clinical and histological features of membranous nephropathy

The kidney is the most important detoxification organ of the body; it filters the blood and excretes metabolic end products and toxins into the urine. Additionally, it participates in the regulation of water and electrolyte balance, acid-base balance and blood pressure. The nephron is the structural and functional unit of the kidney consisting of the renal corpuscle connected with a renal tubule, the latter responsible for both resorption and secretion of substances. The renal corpuscle is composed of a capillary tuft called glomerulus encased by the Bowman's capsule. In healthy kidneys the glomeruli are responsible for the filtration of the primary urine. The filtration barrier of the glomerulus consists of a unique fenestrated endothelium around the glomerular capillary and a glomerular basement membrane (GBM), both negatively charged. As the third component of the barrier the glomerular epithelial cells, also called podocytes, build highly differentiated foot processes with a connecting "slit diaphragm" that localize on top of the GBM. The filtration barrier is permeable for water and smaller molecules but almost not for negatively charged and/or large molecules. Therefore, plasma proteins pass through the filter only to a very small extent. A large amount of all filtrated small molecules and water are reabsorbed during the following passage through the tubular system of the nephron, resulting in the concentrated, excreted urine.

In case of damages of the filtration barrier, high amounts of protein escape into the urine leading to a condition called proteinuria. The stage of a nephrotic syndrome has been reached if severe proteinuria is accompanied by peripheral edema, hypoalbuminemia and hyperlipidemia [1, 2]. In approximately 30% of cases, membranous nephropathy (MN) is responsible for those symptoms and thus is the most common cause of nephrotic syndrome in adult Caucasians [3]. In immunofluorescence microscopy, MN is characterized by a granular pattern of IgG together with components of the complement system along the GBM. Electron microscopy reveals subepithelial electron-dense deposits on the outer aspect of the GBM, close to the podocytes. Additionally, the podocyte foot processes are extensively effaced and the GBM is expanded. It has long been assumed that the formation of subepithelial deposits in combination with complement activation leads to the disturbance of the filtration barrier and the development of nephrotic syndrome, without notable proliferation or infiltration of inflammatory cells in the glomerulus [4, 5].

In 80% of cases MN is primary, occurring in the absence of an established cause. Nevertheless there are several conditions which are capable to induce a so called secondary MN, such as lupus erythematosus, cancer, some infections such as hepatitis B or C, or the use of certain drugs such as penicillamine or gold [6-9]. Even though the histopathological pat-

tern is very similar in these two types of MN there are some features that distinguish between them. Electron-dense deposits in primary MN are typically subepithelial and intramembranous, while mesangial deposits are uncommon [10]. In contrast, in secondary forms of MN those deposits are often located subendothelial and mesangial, suggesting a circulating immune complex [6, 11, 12]. The immune deposits in primary MN mostly contain IgG4, whereas in secondary cases IgG1, IgG2 and IgG3 are the dominant subtypes [13, 14].

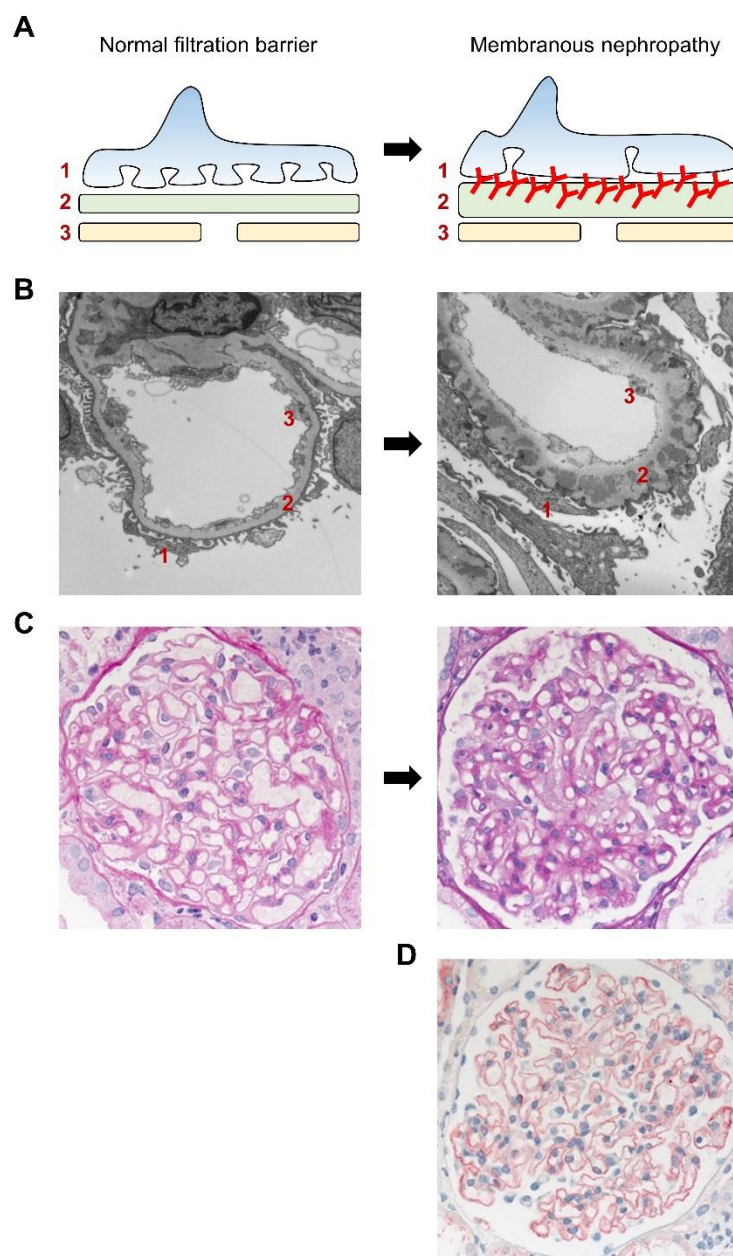


Figure 1: A schematic presentation of the filtration barrier under normal and disease conditions. 1: podocyte, 2: glomerular basement membrane, 3: endothelium B Electron microscopic image under normal and disease conditions. C PAS staining of a healthy and a damaged glomerulus. D Immunohistochemical staining for IgG in a biopsy of a patient positive for MN. All images were kindly provided by Prof. Dr. Thorsten Wiech.

The clinical outcome of MN is very diverse. While about 40% of patients accomplish spontaneous remission, another 30% end up with end stage renal disease, with a poor response to immunosuppressive treatment [15, 16]. Those patients are in need of dialysis or transplantation. Notably, even a successful transplantation is no guarantee for a favorable outcome. In approximately 40% of patients who received a kidney graft, disease will re-emerge and 45% of those patients will lose their graft due to this recurrence [17].

Because of the natural heterogeneity of this disease, it is of great importance to find predictors of the individual disease outcome. Such predictors would allow to select patients for immunosuppressive treatment who will have a benefit regarding kidney function and, conversely, to reduce adverse events from immunosuppression in individuals who will likely not benefit from such treatment. Thus, further progress in patient care depends on a deeper pathophysiological understanding of the disease processes and the identification of molecular signatures that help to predict the disease outcome.

1.2 Rat Animal Models of MN

The Heymann Nephritis (HN) in rats is the first model of experimental membranous nephropathy that was established. Two different forms were classically used to study the pathogenesis of MN, the so called active and passive HN. The active model relies on active immunization of rats with an extract of rat tubular proteins, which induces generation of autoantibodies [18]. In the passive model, heterologous antibodies from animals that were immunized with rat brush border protein extracts are transferred to rats [19, 20].

In both models, animals develop granular glomerular deposits and proteinuria. The following key characteristics of MN could be deduced from the models of active and passive Heymann nephritis:

- Binding of circulating (auto)antibodies to a resident antigen leads to *in situ* formation of subepithelial immune complexes [21, 22].
- The subepithelial localization of the detected IgG indicates that the target antigen is expressed on glomerular podocytes, which represent the outer layer of the glomerular filtration barrier [21, 22].
- Antibody binding and deposition along the glomerular filtration barrier activates the complement system, which contributes to the glomerular damage in MN [20, 23, 24].

Yet, the causal link between complement activation and disease induction is not conclusively clarified. On the one hand rats which are de-complemented with cobra venom factor

present no proteinuria in passive HN, despite the demonstrable formation of immune deposits [20]. On the other hand nephrotic syndrome is inducible in C6-deficient rats with active and passive HN [25, 26].

The relevant antigen in HN was later identified as a member of the LDL-receptor family, with a molecular weight of about 600 kDa. Due to its size this podocyte membrane protein is called Megalin (LRP2; low density lipoprotein receptor-related protein 2). Megalin is expressed on rat tubular cells and podocytes [27, 28]. In rats immunized with a small N-terminal fragment of Megalin an epitope spreading from the immunization fragment to more distal domains takes place over the time course of the experiment. This spreading is necessary for full onset of disease with remarkable proteinuria [29].

However, all these results can only be transferred to the human MN to a limited extent since human podocytes do not express Megalin. It is neither detectable in immune deposits, nor circulating antibodies are found in sera of patients with MN. Hence, Megalin is not involved in human MN.

1.3 Identification of antigens in patients with MN

The first identified human antigen in MN was the neutral endopeptidase (NEP). Antibodies against this protein cause nephrotic syndrome with possible renal failure by crossing the placenta and binding to podocytes of neonates [30]. The mothers of these children are genetically NEP deficient and were subjected to allo-immunization due to miscarriages, or during the course of the pregnancy [31, 32]. Although these cases of neonatal MN are very rare they are the first proof that a human podocyte protein can serve as an antigen targeted by circulating antibodies.

In 2009 the M-type phospholipase A2 receptor 1 (PLA2R1) was discovered as an antigen in MN. Beck *et al.* [33] tested patient sera in Western blot analyses on protein extracts of glomeruli that were isolated from healthy human kidneys. Approximately 70% of all sera tested in this study contained antibodies that bound to a 185 kDa protein. Subsequent mass spectrometry revealed that this protein was PLA2R1. Indeed all previous analyzed sera also recognized recombinant PLA2R1 in Western blot analyses. The reactivity of sera is only given under non-reducing conditions, suggesting a conformational epitope depending on disulfide bonds.

PLA2R1 is detectable in healthy human podocytes and the staining is remarkably enhanced under disease conditions. Subepithelial deposits in diseased podocytes contain PLA2R1 often co-localized with IgG4 (the dominant IgG subtype in PLA2R1-associated MN), indicating an *in situ* formation of the deposits similar to the ones in HN. Moreover, antibodies

eluted from frozen human biopsy samples detect recombinant PLA2R1 in Western blot analyses, proving that the antibodies deposited in patient glomeruli are PLA2R1-specific. PLA2R1 belongs to the mannose receptor family. All members of this family are transmembrane proteins consisting of an N-terminal cysteine rich (CysR) domain, a single fibronectin type II (FnII) domain, followed by 8 to 10 C-type lectin-like domains (CTLDs). Their cytoplasmic tail contains motifs that lead to constitutive endocytotic recycling [34, 35]. The exact function of PLA2R1 is not clear until now. However, it is known that PLA2R1 serves as a receptor for secretory PLA2 (sPLA2), which is a strong pro-inflammatory enzyme. Thereby, PLA2R1 might act in two directions, as a clearance receptor or as a positive regulator of sPLA2. This interaction can lead to different effects, for example protein kinase activation, producing lipid activators or activating DNA damage pathways [36, 37]. Furthermore PLA2R1 was proposed to alter the migratory responses to collagen type I and IV. Recombinant PLA2R1 binds to collagen I and thereby interrupts the interaction between collagen and integrin $\beta 1$ [38, 39]. Interestingly, anti-PLA2R1 autoantibodies from patients with MN interfere with the adhesion of podocytes to collagen type IV, suggesting that the disturbance of podocyte interaction with collagen type IV in the glomerular basement membrane may be involved in MN pathogenesis [40].

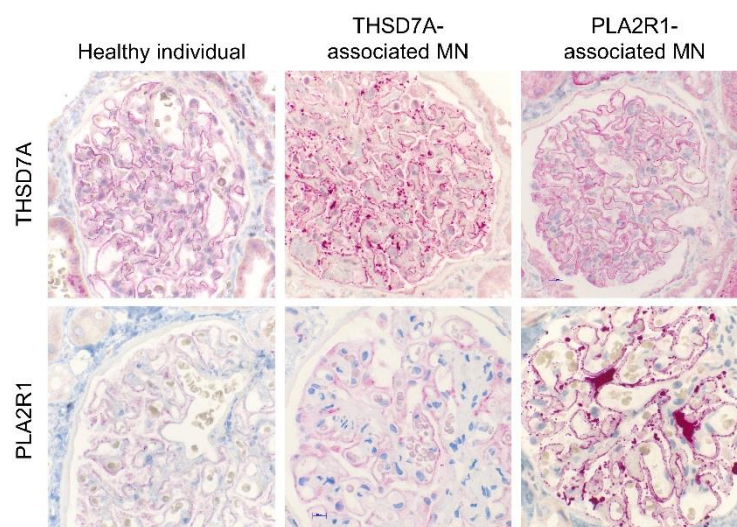


Figure 2: Immunohistochemical staining for THSD7A and PLA2R1 in renal-biopsy specimens from healthy controls and from patients with membranous nephropathy. All images were kindly provided by Prof. Dr. Thorsten Wiech.

Even though many patients with primary MN are positive for anti-PLA2R1 antibodies, the search for additional antigens went on. In 2014 thrombospondin type-1 domain containing protein 7A (THSD7A) was discovered as a further antigen in a subset of patients with primary MN. Sera from about 5% of patients contained antibodies against this protein. Comparable to PLA2R1 positive cases, the binding of antibodies is abolished under reducing

conditions in Western blot analyses and the dominant IgG subtype is IgG4 [41]. In line with the results for PLA2R1, IgG eluted from biopsies of THSD7A-positive patients detects recombinant THSD7A in Western Blot analyses. THSD7A is detectable in human podocytes with an enhanced staining under disease conditions. Worthy of note, 20% of THSD7A positive patients also presented with malignancies. THSD7A was found in their tumors, metastatic lymph nodes and also in subepithelial immune deposits, indicating a potential causal link between cancer and MN [42, 43].

THSD7A is a transmembrane glycoprotein with a large, heavily glycosylated, extracellular region, consisting of 11 thrombospondin type 1 domains (TSP-1 domains) [41]. It is prominently expressed on podocytes of humans and rodents, where it is located at the basal aspects of the foot processes [44]. During angiogenesis THSD7A mediates cell migration and tube formation in association with focal adhesion proteins in endothelial cells [45, 46]. In human cultured podocytes THSD7A expression enhances adhesion and reduces the cells' ability to migrate [47]. In summary, THSD7A likely plays a role in podocyte adhesion through the thrombospondin type 1 domains.

In very rare cases patients present with autoantibodies against both antigens THSD7A and PLA2R1. They show no different clinical features compared to single-positive patients and until now it is not known whether this double positivity is just a coincidence or caused by intermolecular spreading [48-50].

Despite the identification of THSD7A and PLA2R1, there are still cases of "double-negative" patients. Their target antigens remain elusive. In search of those antigens, new combinations of methods were implemented in experimental setups. For instance, laser microdissection and subsequent tandem mass spectrometry analysis of biopsies provided data for two new antigens, exostosin 1 and exostosin 2 (EXT1/EXT2), in immune deposits of PLA2R1-negative patients. The proteins co-localize with the granular IgG along the GBM in immunohistochemistry but no circulating antibodies against EXT1/EXT2 are detectable in sera of EXT1/EXT2 positive patients. Importantly, most patients positive for EXT1/EXT2 show clinical and biopsy features of associated autoimmune diseases. 20 out of 38 patients with EXT1/2-associated MN had co-existing systemic lupus erythematosus, indicating that EXT1/2 are markers of secondary (autoimmune) MN. However, the lack of autoantibodies challenges the concept that these are true antigens. Rather, EXT1/2 may be proteins that are upregulated by podocytes that have been injured as a consequence of another underlying glomerular disorder or circulating proteins that are trapped in the injured glomerulus [51].

In general, exostosins are endoplasmic reticulum-resident glycosyltransferases adding glycosaminoglycan to the core protein to synthesize heparin sulfate proteoglycans, an essential component of the GBM. Specifically, EXT1 and EXT2 are co-polymerases which act in the elongation of the heparin sulfate chain. EXT1 and EXT2 are expressed in podocytes and in various other mammalian tissues. The most likely explanation why both proteins are found together in all stainings is their capacity to form heterodimers with enhanced stability and activity [52-54].

The most recently identified antigen in MN is the neural epidermal growth factor-like 1 protein (NELL-1). As previously for EXT1/EXT2, also in this study microdissection, combined with tandem mass spectrometry, was used for the identification. In glomeruli dissected from PLA2R1-negative patients, the protein NELL-1 is detectable in high counts. Immunohistochemistry reveals a bright capillary wall staining for NELL-1 in co-localization with the sub-epithelial deposits. Sera of a few NELL-1 positive patients contain NELL-1 specific antibodies, dominantly of the IgG1 subtype these antibodies recognize their antigen exclusively under non-reducing conditions. None of the positive patients present features of secondary MN, such as malignancies, autoimmune disease or infections, indicating a primary type of MN [55]. NELL-1 consists of several conserved motifs including the NH₂-terminal thrombospondin1-like molecule relevant for heparin binding, a coiled coil domain, four von Willebrand-type domains, and six EGF-like repeats, which serve as protein kinase C binding domains [56, 57]. Additionally, the C-terminus mediates osteoplastic cell adhesion [58, 59]. NELL-1 is secreted mainly in tubules of the kidney. Conversely, its expression in the glomeruli is very low, suggesting that NELL-1 may be deposited in the GBM as an extracellular component [58, 60].

The studies that provide the basis for the thesis presented here focus mainly on the two most established antigens in MN, PLA2R1 and THSD7A.

1.4 Clinical role of autoantibody measurement

The discovery of PLA2R1 as a target antigen was a milestone for the understanding, diagnosis and treatment of MN. Although anti-PLA2R1 antibodies are found in some cases of secondary MN, there is no evidence for PLA2R1 positivity in other nephropathies, autoimmune diseases or in healthy individuals [61, 62]. With 100% specificity and about 78% sensitivity, these antibodies are a powerful biomarker for MN [63]. Remarkably, in some cases PLA2R1 can still be detected in deposits by immunohistochemistry in the absence of circulating antibodies. Conversely there are other patients with circulating antibodies but no

PLA2R1-deposits [64, 65]. These findings suggest a combined serological and biopsy-based approach for the diagnosis of MN is beneficial.

Because of the promising role for anti-PLA2R1 antibodies as a biomarker in PLA2R1-associated MN, an immunofluorescence assay (IF) and an enzyme-linked immunosorbent assay (ELISA) were developed to quantify circulating antibodies. In particular the ELISA can easily be used outside of expert laboratories, which paves the way for a direct application in patient diagnosis [66, 67]. The introduction of the PLA2R1 IF assay and ELISA lead to several insights into the progression of PLA2R1-associated MN. Anti-PLA2R1 antibody titers strongly correlate with disease activity. Antibody titers are high when patients present a nephrotic level of proteinuria. In contrast, during remission antibodies against PLA2R1 decline or disappear before proteinuria fully resolves. This is most likely caused by the fact that the deposit remodeling and restoration of the filtration barrier takes some time [33, 68]. Furthermore, it takes patients with high titers at the time of diagnosis substantially longer to go into remission, defined as a decrease in proteinuria to subnephrotic levels, i.e. less than 3.5 g/g albumin-to-creatinine, in comparison to patients with lower titers [69]. High anti-PLA2R1 antibody titers are associated with more rapid loss of renal function [70]. Several studies examined the course of antibody titers against PLA2R1 under immunosuppressive treatment. One possible drug for such a treatment is rituximab, a monoclonal antibody against the B cell marker CD20. By binding to CD20, rituximab is capable of depleting B cells and, as a consequence thereof, antibodies. Under treatment with rituximab the rate of remission for PLA2R1 related and unrelated cases is similar, indicating that the mere presence of anti-PLA2R1 antibodies does not predict the outcome of the patient treatment [71]. However, in patients with PLA2R1-associated MN the rate of remission is inversely correlated with antibody titer: Partial or complete depletion of antibodies against PLA2R1 precedes remission, while an increase or re-emergence of antibodies predicts a possible renal relapse [71-73].

Taken together, anti-PLA2R1 antibody levels are associated with disease activity, remission, and outcome, and measurement of anti-PLA2R1 antibodies is useful for diagnosis, individual risk assessment, and treatment monitoring in patients with MN.

For THSD7A antibody measurement in clinical practice only an IF-assay is available, but most recently an ELISA was invented and used for the analysis of patient sera [50]. Notably, it is more difficult to generate valid, statistically relevant data for THSD7A-associated MN, due to the small number of patients in this group. Nonetheless, also anti-THSD7A antibody titers strongly correlate with the level of proteinuria. Patients going into complete remission also become negative for antibodies against THSD7A. On the contrary, ongoing proteinuria correlates with persisting anti-THSD7A antibodies [43, 50]. Thus, the antibodies against

THSD7A, just as the ones against PLA2R1, are a powerful biomarker for monitoring disease activity during follow up and treatment of THSD7A-associated MN.

1.5 Structure of PLA2R1 and identification of autoantibody binding domains

PLA2R1 is a multidomain protein with 10 consecutive extracellular domains: an N-terminal cysteine rich (CysR) domain followed by a single fibronectin type II (FnII) domain and 8 C-type lectin-like domains (CTLDs) [33, 34]. Cryo-electron microscopy revealed that the domains of PLA2R1 can present at least in two different conformations.

Under acidic conditions it folds in a dense conformation, consisting of two ring-like structures. The smaller ring on top is formed by the CysR domain, the FnII domain and the first two CTLDs. The larger ring underneath contains CTLD1-6, whereas CTLD6 interacts with FnII to close the ring. Additionally there is a possible low affinity interaction between CysR and CTLD-4. On the contrary, transferring the protein to a physiological or basic environment leads to various extended conformations. It is presumed that in these extended conformations the epitopes may be more accessible for the binding of the PLA2R1-autoantibodies [74].

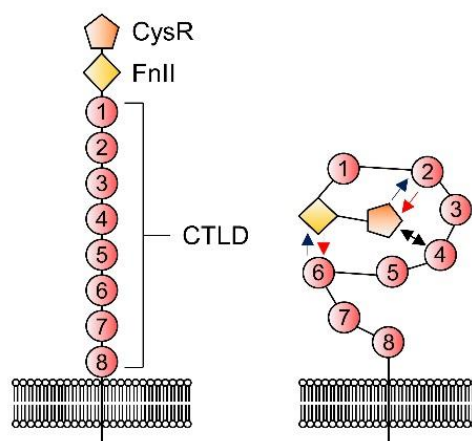


Figure 3: Schematic presentation of PLA2R with an N-terminal cysteine-rich (CysR) region, a fibronectin-like type II domain (FnII), a tandem repeat of eight C-type lectin-like domains (CTLDs), a transmembrane domain, and a short intracellular C-terminal domain. (b) A ball-and-stick model of the domains gained from cryo-electron microscopy. Blue arrow, red arrow: pH-dependent interaction, black arrow: pH-independent dynamic interactions. Model adapted from [74].

Several studies investigated the autoantibody binding sites in PLA2R1 by means of truncated versions of the protein. Kao *et al.* [75] identified a fragment consisting of CysR-FnII-CTLD1 as the epitope containing region. Later Fresquet *et al.* [76] localized one epitope to a 31 amino acid sequence within CysR. Even though this study proved that the immunodominant epitope of PLA2R1 lies within the most N-terminal region of the protein the

antibody reaction is not restricted to this area; CTLD1 and CTLD7 are also epitope containing regions [77].

In a retrospective study [77], patients whose sera only recognized CysR were younger, had lower proteinuria and exhibited a higher frequency of spontaneous remission during follow up. In contrast, those patients with recognition for all three epitope containing domains presented with a much worse disease outcome. It was suggested that this additional recognition is caused by epitope spreading from the immunodominant CysR towards the other epitope containing domains, during the time course of the disease [77]. Seitz-Polski *et al.* [78] showed that the epitope spreading associates with a decreased remission rate during follow up, independent of age, sex or baseline antibody level and strongly correlates with the anti-PLA2R1 antibody titer.

The topic of epitope spreading for PLA2R1-associated MN, has been controversially discussed over the last years. Most recently, Reinhard *et al.* [79] conducted a study in 150 consecutive patients with PLA2R1-associated MN. In line with previous studies, they found that all tested sera recognized CysR. However, all sera also recognized at least one more epitope in the more C-terminal region of the molecule, i.e. CTLD7 or a newly identified epitope in CTLD8.

Moreover, the binding of CTLD7 or 8 did not depend on the presence of antibodies against CTLD1. The authors pointed out that the detection of antibodies strongly relies on their concentration in patient serum, experimental setup and detection method chosen. 31 patients with antibodies against N- and C-terminal domains of PLA2R1 went into remission in this study, challenging the concept that a spreading of the immune response to the C-terminal region itself is a predictor of an unfavorable clinical outcome. [79]. In fact, this data indicates no relevant use of “epitope spreading” as marker for prognosis or treatment outcome in PLA2R1-associated MN. If there is an epitope spreading it must have taken place before the diagnosis of the disease. Of course, a multi-specific immune response from the beginning on is also possible.

Despite the great progress in case of PLA2R1, the questions discussed above remained widely unanswered for THSD7A. Consequently, the first part of the present work aimed at taking a closer look at the structure of THSD7A, identify the antibody binding sites and correlate the results with available clinical data of all tested patients.

1.6 Pathogenicity of autoantibodies

While the formal proof that podocyte-directed autoantibodies were causative for the development of MN was still missing, there was indirect evidence from clinical data that this is

indeed the case: (i) high autoantibody titers strongly correlate with ongoing disease activity and a poor clinical outcome [33, 68], (ii) an immunological remission (i.e. the disappearance of detectable serum autoantibodies) precedes the clinical remission and (iii) an increase of autoantibody titers frequently associates with a relapse of the disease [71-73]. Additionally, the disease can recur in the transplanted kidney, which associates with persistent or relapsing autoantibody titers [44, 66, 80].

But the question remained: Are the circulating antibodies really the pathogenic factor that drives disease in primary MN?

PLA2R1 is not expressed in rodent glomeruli, a fact that has made it difficult to finally prove this theory. However this is not the case for THSD7A. The protein is strongly expressed on rodent podocytes, offering the opportunity to perform transfer experiments with antibodies derived from patient sera [81, 82]. Indeed antibodies present in hole patient sera as well as affinity-purified THSD7A-specific human IgG (hulgG) bound to THSD7A in mouse glomeruli, resembling the histomorphological pattern of MN, and lead to the development of proteinuria. Given the purified antibodies, mice only presented with transient proteinuria and without a strong autologous phase of the disease. In contrast, mice receiving the whole serum produced large amounts of anti-hulgG antibodies at later time points of the experiment, causing a persisting proteinuria for the whole observation period of 70 days. In line with this, C3 deposits were found in mice injected with whole serum, but were absent in mice receiving purified antibodies [44]. These findings indicate that the autologous mouse antibodies bound to hulgG are necessary for a sufficient complement activation and maintenance of the disease. Yet, for the initiation of podocyte injury and proteinuria, complement activation doesn't seem to be mandatory.

THSD7A-associated MN is a rare disease, which rules out the usage of human serum for larger experimental setups. To address this issue, a heterologous model of THSD7A-associated MN was invented [83]. This model depends on heterologous antibodies, derived from rabbits immunized with human and mouse THSD7A. Transfer of purified rabbit-IgG (rbIgG) to BALB/c mice leads to pronounced granular subepithelial IgG deposits, electron-dense deposits and foot process effacement. Interestingly, proteinuria was stronger in this experiment compared with the administration of hulgG. A possible explanation could be a higher dose of antibodies and a higher polyclonality of the rabbit antibodies, effectively binding to their antigen in mice. Despite the massive proteinuria and a pronounced autologous phase, with mouse anti-rbIgG antibodies one week after starting the experiment, practically no C3 could be detected.

The lacking glomerular expression of PLA2R1 in mice necessitates the generation of a transgenic mouse line in order to enable similar proof-of-principle experiments. A previous

attempt to induce MN in mice expressing human PLA2R1 fused to a GPI anchor on their podocytes was not successful, likely due to insufficient antigen presentation or membrane incorporation of the human protein [74, 84, 85].

Thus, in the second study presented here, a new approach to establish a reliable and reproducible mouse model of PLA2R1-associated MN was pursued.

2. Materials, Methods and Results

The following two publications contain the materials and methods that were used as well as the results of the experiments performed as basis of this cumulative dissertation. The complete original publications are included into the appendix.

“The Most N-Terminal Region of THSD7A Is the Predominant Target for Autoimmunity in THSD7A-Associated Membranous Nephropathy.”

Seifert L, Hoxha E, Eichhoff AM, Zahner G, Dehde S, Reinhard L, Koch-Nolte F, Stahl RAK, Tomas NM

J Am Soc Nephrol. 2018 May. 29(5)

“A novel mouse model of phospholipase A2 receptor 1-associated membranous nephropathy mimics podocyte injury in patients.”

Meyer-Schwesinger C, Tomas NM, Dehde S, Seifert L, Hermans-Borgmeyer I, Wiech T, Koch-Nolte F, Huber TB, Zahner G

Kidney Int. 2019 Nov.

3. Discussion

3.1 Structure of THSD7A and the role of autoantibody binding-sites in THSD7A-associated MN

In the first study presented in this thesis (The most N-terminal region of THSD7A is the predominant target for autoimmunity in THSD7A-associated membranous nephropathy), a deeper look at the predicted structure of THSD7A was taken and epitope containing domains were identified. Structure based alignments of THSD7A with data of TSP-1 domains from the protein data bank (pdb) revealed that 21 TSP-1 (d1_d21) domains are part of the THSD7A structure. These domains show a high homology either to the TSP-1 domains of thrombospondin 1 (THBS1, pdb code 3r6b) or complement component 6 (C6, pdb code 3t5o, containing two TSP-1 domains) and F-spondin (pdb 1szl, containing one TSP-1 domain) [86-88]. Both types of TSP-1 domains form three antiparallel peptide strands, their structure only differs in the position of their third disulfide bridge. While it connects the second and the third strand in THBS1 (C3-C4), it is located between C4 on the second and C0 on the first strand in C6/F-spondin.

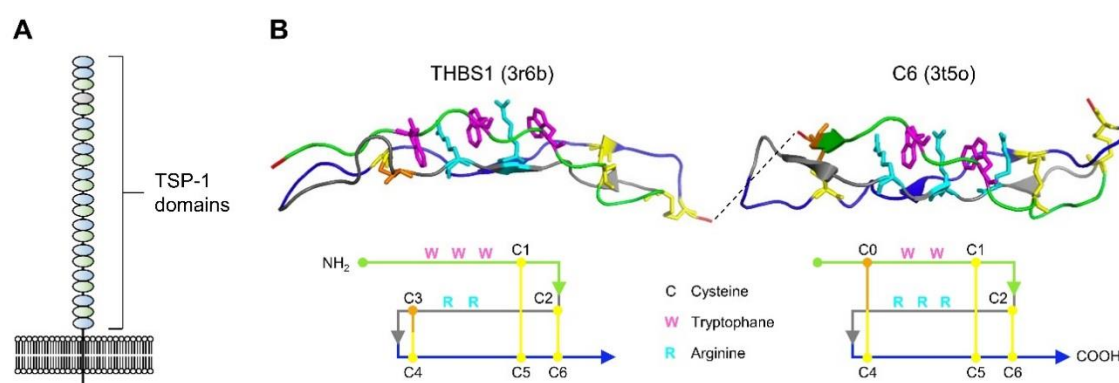


Figure 4: **A** Schematic presentation of THSD7A. The extracellular part consists of 21 thrombospondin type 1 (TSP-1) domains and one coiled coil domain. **B** Predicted three-dimensional structure and schematic view of THBS1- and complement component 6 (C6)-like domains with three strand-connecting disulfide bonds each (yellow/orange).

Interestingly, the first two N-terminal domains of THSD7A are both THBS1 like domains, followed by two C6-like domains separated by a highly basic coiled coil domain. The domains d5 to d21 then show an alternating pattern of THBS1- and C6-like domains. THBS1 is a multi-domain matrix glycoprotein that is involved in cellular responses to growth factors, cytokines and injury. It regulates cell proliferation, migration and apoptosis in a variety of physiological and pathological settings [89]. In particular, the TSP-1 domains of thrombospondin 1 interact in a complex network with proteins of the extracellular matrix [90], cell receptors [91-93] and proteases [94] resulting in activation of downstream signaling path-

ways, alterations of protein localization and protein internalization [95]. The strong homology between the TSP-1 domains of THSD7A and those of THBS1 may give a hint for different biological functions of THSD7A that are unknown until now.

We used this newly gained knowledge of the THSD7A structure to produce fragments of THSD7A recombinantly in HEK cells for autoantibody testing. When this project was started, studies on PLA2R1-associated MN already revealed that only 3 parts of the protein contain epitopes for autoantibodies, CysR and CTLD1 in the most N-terminal region as well as CTLD7, located closer to the C-terminus of the protein [77]. Hence, we went for an unbiased approach and expressed 3 parts of THSD7A for our screening of patient sera, comprising the whole extracellular region of the protein (d1_d4, d5_d10, d11_d21). Surprisingly, many patient sera recognized all three parts of THSD7A. To resolve their recognition sites in more detail, smaller fragments of THSD7A were produced, consisting of two or three consecutive domains (d1_d2, d2_d3, d3_d4, d5_d6, d7_d8, d9_d10, d11_d12, d13_d14, d15_d16, d17_d18, d19_d21). These fragments were used for all further screenings of patient sera in Western Blot and Dot Blot analysis under non-reducing conditions. This mapping, indeed, revealed an antibody binding distributed over the whole length of the extracellular region of THSD7A, with epitope profiles that largely vary between different patients. Antibodies that were purified using the recombinant recognition domain failed to bind any other domain in THSD7A. Thus any relevant cross-reactivity of the autoantibodies with different, highly homologous TSP-1 domains of THSD7A was excluded, emphasizing the true polyclonal nature of autoantibodies in THSD7A-associated MN.

The most N-terminal part d1_d2 was recognized by 87% of all tested patient sera. Even though the N-terminal antigen region was not recognized by all tested patient sera, it is strong evidence that the N-terminus is the predominant target in THSD7A-associated MN. The function of the N-terminus as the major target for antibodies was further supported by experimental data generated from THSD7A-immunized rabbits and mice. Both species develop a dominant antibody response against the N-terminal domains d1_d2, when immunized with human and mouse THSD7A cDNA. The resemblance of the situation in the patient cohort was completed by additional recognition of several other domains within THSD7A. The d1_d2 regions in rabbit, mouse and human THSD7A are highly homologous; therefore a lack of homology in this region could not be the reason for a preferred antibody generation against this part of THSD7A. Probably, other features of the N-terminal region, such as epitope accessibility, are responsible for the predominant antibody response. Worthy of note, the antibodies derived from rabbits were very potent in inducing experimental MN in mice [83].

In 2019 Stoddard *et al.* [96] presented an in silico 3-D structure of THSD7A. In line with our results, they defined the extracellular domains of the protein as a mixture of THBS1-like and C6/F-spondin like domains. While they also ended up with 21 domains, the numbering shifted. In contrast to our work, they labelled the coiled coil domain as an additional THBS1-like domain with a polybasic region, resulting in the alternating pattern of THBS1- and C6-like domains, already from domain 2 on. They assumed that the polybasic region mentioned above serves as a glycosaminoglycan binding site for heparan sulfate or similar proteoglycans. Heparan sulfate is a component of the glomerular basement membrane. THSD7A may serve as an adhesion protein, anchoring the basal aspects of podocyte foot processes to the GBM. Disruption of this anchor by autoantibodies binding in the C-terminal region of the antigen represents a potential mechanism of glomerular injury in MN. Whereas we identified a THBS1-like domain at the C-terminal end of the extracellular region of THSD7A, the study points out that this domain most probably does not fold into a proper structure, due to a low number of residues in the sequence corresponding to the C-strand of the predicted domain. As a consequence, they defined the extracellular region of THSD7A as the part from domain 1 to domain 21, the latter being the equivalent to domain 20 in our terminology. Strikingly, the predicted favorable epitopes in the extracellular region of THSD7A investigated by Stoddard *et al.* correspond very well with our experimental data. In their analysis, 18 domains of THSD7A are predicted to contain epitopes and 3 domains are not. Compared with our results, this holds true for all fragments we tested except for one. None of the patient sera that we tested recognized the fragment d3-cc-d4, corresponding to domains 3, 4 and 5 in their study. Additionally, Stoddard *et al.* suggest that hydrophobic and polar uncharged residues are most likely to be involved in epitope sites. In their study this was the case for all predicted epitope containing domains, with eleven having mostly hydrophobic residues, five consisting of mostly polar uncharged residues and two with a mixture of both kinds of residues. Taken together our data and the study by Stoddard *et al.* strongly support and strengthen each other.

Next, epitope recognition patterns were correlated with anti-THSD7A antibody levels and clinical characteristics of the investigated patient cohort. Patients whose sera recognized more than two fragments of THSD7A had higher antibody titer measured in IF than patients with recognition of only one or two fragments. Furthermore, they presented with higher proteinuria (not reaching statistical significance) and tended to go into remission less often during follow-up. After analyzing the sera of 31 untreated patients diagnosed with THSD7A-associated MN, experiments with follow-up sera from 16 of them were performed and results were correlated with available clinical data. During follow-up, the epitope profile re-

remained unchanged in five patients. They had stable anti-THSD7A titers and suffered nephrotic-range proteinuria during the whole time of observation. Seven patients lost recognition of one or more constructs, which was accompanied by a decrease of antibody level and remission of proteinuria. Taken together, several conclusions can be drawn from our data. First, the vast majority of patient sera contain antibodies against the most N-terminal region of the antigen. This strongly suggests that this area is of enhanced immunogenicity. One could speculate that the disease starts with a break of tolerance in this region. Second, most patients recognize multiple additional domains along the antigen. This demonstrates that THSD7A-associated MN is a polyclonal disease with poly-reactive autoantibodies. Third, a high overall anti-THSD7A antibody titer correlates with the number of recognized domains and a decrease in the overall titer is associated with a reduction in the number of recognized domains. This situation strongly suggests that the epitope recognition profiles depend on the anti-THSD7A antibody titer. However, from these clinical data alone it is not possible to deduce whether the epitope profile or the number of recognized epitopes have a direct impact on disease severity. It is possible that the more epitopes are bound the stronger are the immunological effector mechanisms, such as complement activation, that take place at the podocyte foot processes. Further experimental studies are warranted to dissect the pathogenic role of the targeted domains in THSD7A-associated MN.

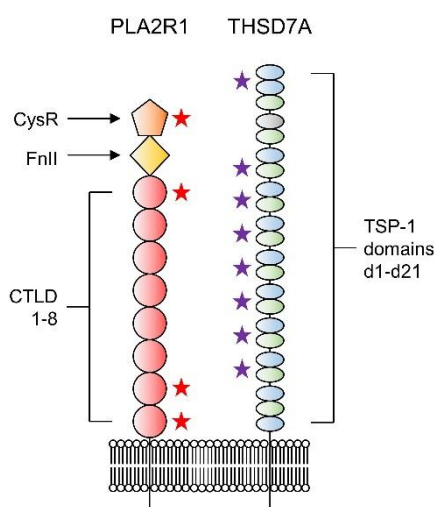


Figure 5: Asterisks mark domains of PLA2R1 and THSD7A that are detectable with patient autoantibodies.

These data are largely in line with the published data for PLA2R1-associated MN, where patient autoantibodies also show a strong predominance for the most N-terminal region of the antigen. In fact, all investigated patients recognize the most N-terminal CysR domain [76, 77]. Moreover, the majority of patients additionally recognize epitopes in the more C-terminal area, i.e. in CTLD7 and CTLD8 [77, 79]. Nevertheless, the immune response in THSD7A-associated MN seems to be more widespread as in PLA2R1-associated MN as more different domains are recognized.

Similar to our data also in PLA2R1-associated MN the total antibody level against PLA2R1 correlates with the number of recognized domains and a lower total PLA2R1 antibody level usually leads to a higher remission rate and a better outcome of the disease [69].

Although four patients had a change in their epitope recognition pattern during follow up, we could not find clear evidence for any epitope spreading over time.

Inter-and intra-molecular epitope spreading was observed in several antibody-mediated autoimmune diseases, such as bullous pemphigoid, multiple sclerosis and encephalomyelitis [97-100]. The phenomenon is defined by an expansion of epitope specificity from an initial immune response against a dominant epitope within a self or foreign protein, towards sub-dominant and/or cryptic epitopes on that protein (intramolecular spreading) or other proteins (intermolecular spreading). Because MN is considered to be a very slowly developing disease and patients are usually not under clinical observation at the origin of disease, it is very difficult to verify epitope spreading in human disease. To address this problem specific animal models that mimic the human disease are very useful [101].

Indeed, for the experimental MN model of Heymann Nephritis an epitope spreading from the immunization construct, a small N-terminal fragment of Megalin, to more distal domains could be shown [29].

Epitope spreading was reported in 2014 for PLA2R1-associated MN, and it was suggested to be useful for prediction of disease development regarding spontaneous remission and/or response to treatment [77]. Besides Western Blot analyses, an ELISA with PLA2R1 fragments was used to investigate domain specific antibody titers. Two groups were defined in these studies, (i) patients whose sera only recognize the CysR domain and (ii) patients in whom the recognition had spread towards CTLD1 and CTLD7. Members of the second group were older, showed active disease and a poor renal prognosis. During follow up, antibodies against CTLD1 and CTLD7 disappeared with disease remission and reappeared with disease relapse [77, 78]. Additionally, a reversal of epitope spreading could be induced by treatment with rituximab.

The role of epitope spreading in PLA2R1-associated MN was severely weakened by the most recent study of Reinhard *et al.* [79] which not only identified a new recognition site of antibodies in CTDL8, but could not find any evidence for epitope spreading in their cohort during the whole time course of observation. All tested patients recognized more than one fragment of PLA2R1 at baseline. Some patients achieved spontaneous remission, regardless of existing antibodies against N-and C-terminal domains in their sera. They [79] also mentioned that the method applied, the dilution of sera, the composition of sera and the accuracy in performance are besides further aspects of great importance for the detection of epitope specific antibodies in PLA2R1-associated MN. For example, if they used higher

dilutions of sera, recognition of domains in the C-terminal area disappeared, while new recognitions appeared if lower dilutions were used. Taken together this refutes the occurrence of an epitope spreading during the time of follow up. It is more likely that the antibody repertoire already exists from the beginning of the disease. Consequently, only the autoantibody titer decides whether recognition is seen at the domain level or not.

In fact, we could not rule out either that epitope profiles would have changed if we had applied additional methods, like an ELISA, or changed the serum dilutions. A dilution of 1:100 was used for all experiments, raising the possibility that antibody concentration against specific fragments of THSD7A were below the detection limit for some patient sera. Therefore it has to be carefully considered whether profiles of recognized protein fragments are a valid tool to predict disease outcome at the moment.

Nonetheless, if larger cohorts of patients with THSD7A-associated MN are available in the future it would be a good approach to establish a similar ELISA as in PLA2R1-associated MN because the identification of the precise epitopes in THSD7A-associated MN is still of high interest for several reasons. Some domains of THSD7A may interact with other molecules, so that antibody binding to these domains specifically interferes with the natural function of the protein, leading to a structural and functional alteration of slit diaphragm permeability. It is already known, that anti-THSD7A antibodies induce cytoskeletal rearrangements in primary cultured murine glomerular epithelial cells [44].

Furthermore, the autoimmunity in THSD7A-associated MN is possibly caused by a molecular mimicry between microbial antigens and host proteins [102, 103]. Knowing the precise epitopes would allow deeper analyses to address this theory. The term molecular mimicry describes the pathogenic consequence of cross-reactivity between common B or T cell reactive epitopes of microorganisms or environmental agents and the host. It can occur in several different forms including complete identity at the protein level, homology at the protein level, structural similarity and similarity at the level of amino acid sequences [104]. For instance, PLA2R1 and THSD7A share a signature motif in their N-terminal domains, which is suggested to be an epitope involved in the initial B cell triggering event in MN. Parts of this motif are also present in sequences of proteins from *Clostridium*, *Saccharomyces cerevisiae* and *Pseudomonas HrcC Type*, raising the opportunity that exposure to microbes may play a role in the development of MN [105].

Importantly, the precise epitopes could serve as a basis for innovative and individualized treatments, specific for THSD7A-associated MN (see below). To design and apply those future therapies properly and expediently, the remaining question should be answered: is it an individual epitope profile, the number of recognized epitopes, the antibody titer alone or a combination of these factors that drives disease?

One way to answer this question is to generate multiple domain-specific antibodies and investigate the conditions that are required for disease development in mice. For this purpose we already started to generate monoclonal antibodies using THSD7A-knockout mice (*Thsd7a*^{-/-} mice). The mice are immunized with the mouse orthologues of the TSP-1 domains that were most frequently recognized by patient autoantibodies, afterwards spleens and lymph nodes are taken and fused with a multiple myeloma cell line. Cell clones that produce THSD7A-specific antibodies are then selected for further cell culture and production of larger amounts of antibodies. IgG subtypes can be determined and antibodies can even be sequenced and potentially be modified to different IgG subtypes. Once a proper antibody library is generated, antibodies will be transferred to mice. Thereby, modification of the variables „antibody amount“ (i.e. a certain anti-THSD7A titer), „epitope profile“ (i.e. a certain domain recognition profile) and „antibody polyreactivity“ (i.e. targeting different numbers of domains) can be freely modified in order to further comprehend what drives disease on a molecular level. One example would be the transfer of antibodies against two domains versus transfer of antibodies against four or five domains, while the injected amount is adapted to identical antibody titers circulating in the serum of mice. This experimental setup will allow to understand whether antibodies targeting multiple domains along the antigen induce more severe disease (e.g. via more efficient complement activation) in comparison to a more restricted antibody distribution. Preliminary experiments have already shown that polyclonal IgG against THSD7A derived from *Thsd7a*^{-/-} mice has indeed the capacity to induce experimental MN in wild type BALB/c mice.

However, such monoclonal antibodies have a variety of potential applications regarding the investigation of disease pathogenesis. (1) Our collaboration partner has established a podocyte cell line that stably expresses THSD7A. These antibodies can now be applied on this podocyte cell line and transcriptomic and proteomic analyses over time may reveal different signaling programs, depending on which or how many epitopes are targeted. (2) In preliminary studies, we have identified the *in vitro* THSD7A interactome, i.e. the direct or indirect binding partners of THSD7A. The monoclonal antibodies can be used to analyze whether such protein-protein interactions are disrupted due to binding of certain domains by IgG. Those interactions may be an integral part of the yet unknown function of THSD7A for the podocyte. (3) The precise structure of the THSD7A antigen has not been defined yet by experimental methods such as cryo-electron microscopy or x-ray crystallography. It is unclear how the antigen structure is involved in THSD7A function under physiological conditions or whether an alteration in antigen structure plays a role in MN pathogenesis. To this end, the monoclonal antibodies can be co-crystallized with the antigen in direct comparison to the crystal structure of the unbound antigen.

It is essential to emphasize that this approach is based on an immunological reaction in mice, resulting in antibodies against mouse THSD7A. Even though mouse and human THSD7A share over 90% of amino acid sequence homology, the application of such innovative therapeutic approaches in patients with MN will rely on further characterization of the antigen/antibody interaction in human disease.

In summary, in the first study presented in this thesis, the structure of THSD7A was analyzed for the first time using *in silico* structure-based alignments of THSD7A with TSP-1 domains. Additionally, the epitope-containing domains were identified that are involved in the pathogenesis of MN, and patient recognition patterns were correlated with clinical data. *In vivo* immunization experiments revealed that the most N-terminal part of the antigen contains particular immunogenicity, as an antibody response against this region was not only found in patient sera but also in sera of mice and rabbits after immunization with THSD7A. The presented data build the basis for a variety of studies that will shed further light on the role of the targeted epitopes in this antibody-mediated autoimmune disease and, not last, may help to develop specific, pathogenesis-based treatments in the near future.

3.2 Heterologous models of THSD7A- and PLA2R1-associated MN

In the second study presented in this thesis, the direct pathogenicity of anti-PLA2R1 antibodies was demonstrated for the first time and a reproducible animal model of PLA2R1-associated MN was established by means of transgenic overexpression of the PLA2R1 antigen in podocytes of BALB/c mice. It is known for some time that autoantibodies against THSD7A are the pathogenic factor in THSD7A-associated MN. Purified antibodies, derived from sera of patients with THSD7A-associated MN, are capable of inducing proteinuria and the typical histopathological features of MN in wild type BALB/c mice [44]. In order to transfer this insight into a reproducible and valid experimental model of MN, a heterologous approach, using rabbit antibodies against THSD7A was pursued [83].

These experiments were feasible because THSD7A is expressed on mouse podocytes with over 90% homology with the human protein.

The situation is more complicated for PLA2R1-associated MN as the protein is not expressed on mouse podocytes. To enable experiments in mice, a transgenic approach had to be applied. The first attempts, to express the human PLA2R1 on mouse podocytes were not successful. Most probably due to the complex structure of PLA2R1 with high internal flexibility of the human PLA2R1 ectodomains [74], resulting in insufficient antigen expression or possible membrane incorporation of the human protein in mice.

Therefore we decided to design a mouse line that expresses mouse PLA2R1 (mPLA2R1-positive mice) on its podocytes, comparable to the natural expression of THSD7A on podocytes of wild type BALB/c mice.

First the expression pattern and the possible consequences of the transgenic protein expression were examined. Under basal conditions the mice express the transgenic mPLA2R1 protein strongly in their cytoplasm and cell membrane. In the podocyte membrane, mPLA2R1 is specifically localized to podocyte foot processes, since PLA2R1 staining partially merged with the slit diaphragm protein nephrin. The number of podocytes identified was not changed in mPLA2R1 expressing mice in comparison to non-PLA2R1 expressing littermates. Furthermore, in light microscopy and electron microscopy, no alteration in the glomerular morphology, especially for the GBM, the podocyte foot processes or the glomerular endothelium could be detected. We also looked for signs of ER-stress and a possible overload of cellular degradation/repair systems, caused by the transgenic expression of the large, strongly glycosylated protein in podocytes. All performed experiments demonstrated podocyte tolerance towards transgenic mPLA2R1 expression with normal expression of all investigated stress markers in both mPLA2R1-negative and -positive mice. Importantly, the albumin/creatinine ratio in PLA2R1-positive mice showed no anomalies when compared to PLA2R1-negative mice, leading to the conclusion that a transgenic mouse line that is suitable for further applications was successfully generated.

In an attempt to reproduce the proof of principle experiment that was already successful for THSD7A, human antibodies against PLA2R1, derived from patients with PLA2R1-associated MN, were transferred to the transgenic mice. While the application of the antibody led to a slightly positive staining of hulgG in the glomerulus, no proteinuria or additional features of MN could be observed. Most probably the homology of 72% between human and mouse PLA2R1 is not enough for a sufficient binding of patient antibodies to the mouse orthologue in the transgenic mice. This assumption was also supported by the finding that the detection of mPLA2R1 by human autoantibodies was very weak in Western blot analyses.

Further approaches for a successful expression of the human protein in mice are in progress to finally prove the pathogenicity of human anti-PLA2R1 antibodies in PLA2R1-associated MN.

In order to investigate whether anti-PLA2R1 antibodies in general are capable of inducing proteinuria and the classical histopathology of MN, antibodies against mPLA2R1 were produced in rabbits immunized with mPLA2R1 cDNA, similar to the approach that was undertaken for the heterologous model of THSD7A-associated MN [83]. In accordance with patient sera from PLA2R1-associated MN, the rabbit antibodies strongly recognized the N-

terminal region of mouse PLA2R1 (CysR-CTLD1). While the antibody binding was also detectable in fragments comprising CTLD2-6 and CTLD2-8, in contrast to patient data, no recognition was found for the CTLD7-8 region. This strengthens the hypothesis that, like it the case for THSD7A, also the N-terminal region of PLA2R1 is of particularly enhanced immunogenicity.

In line with the characteristics of patient anti-PLA2R1 antibodies, the rabbit antibodies showed no binding under reducing conditions in Western Blot analyses, indicating binding to conformation dependent epitopes.

The purified total rabbit antibodies were injected into PLA2R1-positive and -negative mice and the animals were observed for seven days. PLA2R1-positive mice developed severe proteinuria persisting over the whole time course of the experiment, while PLA2R1-negative mice or those who received control rblgG (i.e. rblgG without recognition of mPLA2R1) remained unaffected. Additionally, the mice presented the typical histomorphological signs of human MN. Granular and subepithelial deposition of rblgG, as well as an enhanced membrane staining for mPLA2R1 could be detected. Electron microscopy revealed electron-dense deposits in a strictly subepithelial location within the GBM and areas of foot process broadening in mPLA2R1-positive mice. The slit diaphragm is an early target of antibody immune complex formation in experimental THSD7A-associated MN [47]. This might be also the case for the mPLA2R1-anti-mPLA2R1 complex formation in our experiment, suggested by electron-dense deposits in close proximity to the podocyte slit diaphragms and a co-localization of mPLA2R1 and the deposited rblgG with the slit-diaphragm protein nephrin found in high-resolution confocal imaging.

For the first time we demonstrate that anti-PLA2R1 antibodies directly cause MN in animals. Moreover, we generated the first animal model of PLA2R1-associated MN which is reliable and reproducible at the same time. The proof for the pathogenicity of anti-PLA2R1 antibodies is of particular importance as it builds a pathomechanistic rationale for future therapies aiming for the elimination of the pathogenic factor (i.e. the antibodies) or of the source of the pathogenic factor (i.e. the antibody-producing cells).

The experimental model is highly comparable with the one of THSD7A-associated MN, with one major difference. While glomerular deposition of C3 was barely detectable in the model of THSD7A-associated MN, here C3 was found in partial co-localization with the bound rblgG at day seven, suggesting complement activation in the area of immune complex deposition. However, whether the absence of C3 in the model of THSD7A-associated MN holds true, is currently under investigation using highly sensitive methods.

Until today it remains a major question how antibodies lead to the glomerular damage in MN, in particular the foot process effacement of podocytes and the consecutive loss of

plasma proteins into the urine. Several injury pathways are conceivable and have been discussed extensively in the field of MN. With both PLA2R1- and THSD7A-related models now successfully running; we have the opportunity to systematically investigate different postulated mechanisms:

(1) Antibodies bind to the target antigen, leading to the activation of the complement cascade which ends with the formation of the final product C5b9, also known as the membrane attack complex. C5B9 gets inserted into the podocyte membranes, resulting in a "sublytic"-damage of the cells. The knowledge about this role of the complement system for the development of glomerular damage in MN has been derived from several investigations in the Heymann nephritis model [20, 23, 24]. However, other studies have strongly challenged this pathophysiological concept [25, 26]. It has to be considered that the classic protocols for both active and passive HN involve antibodies against a multitude of tubular and glomerular proteins. In active HN these antibodies develop in rats due to direct immunization with a cocktail of rat tubular proteins. In passive HN the antibodies were derived from immunization of sheep with the identical protein cocktail and subsequently transferred to rats. This stands in strong contrast to the pathophysiology of MN, where the immune system predominantly targets one membrane-expressed podocyte antigen (i.e. PLA2R1 or THSD7A).

The heterologous mouse models of PLA2R1- and THSD7A-associated MN now allow investigating the role of the complement system in a more specific way. To this regard, a mouse line genetically lacking C3 was generated. C3 is the center complement component without it all activation pathways of the complement system stop at the level of C3 cleavage, preventing the membrane attack complex to be formed. We already crossed the mouse line to a BALB/c background and currently crossing it with the PLA2R1-positive mice to set up proof of principle experiments involving anti-THSD7A and anti-PLA2R1 antibodies. In addition, we have established the use of small interfering RNA (siRNA) depleting specific complement components, to answer the question whether a complement-targeted therapy is promising in MN. siRNAs are small RNA molecules that are 20 to 25 base pairs in length. They are important for the regulation of gene expression and can temporarily switch off certain genes, in our case genes for the expression of complement components [106]. We will inject this siRNA before the induction or during the course of the experimental MN models. Thus, we can examine whether the complement factors are sufficiently suppressed in mice, and whether the outcome of the disease is ameliorated in the models.

(2) Important structural functions of the antigen are disrupted due to the binding of the autoantibodies. Such a mechanism has already been demonstrated for the antibody-mediated autoimmune skin disease pemphigus vulgaris. This disease is characterized by separation of skin layers and consequently blistering of the skin caused by antibodies against

desmoglein-3, a protein of the cadherin family that is a component of the skin desmosome [107]. Both PLA2R1 and THSD7A are large multidomain membrane proteins expressed on podocyte foot processes, likely interacting with other surrounding molecules. For example, PLA2R1 was shown to interact with collagen type IV (the collagen subtype that is the main constituent of the GBM) [38, 39], and the TSP-1 domains of THSD7A may interact with heparan sulfate (an essential component of the GBM) [96]. Thus, it is possible that PLA2R1 and THSD7A contribute to the integrity of the glomerular filtration barrier by anchoring podocyte foot processes to the outer aspect of the GBM. Anti-PLA2R1 [40] and anti-THSD7A antibodies might directly interfere with this structural function. In the heterologous mouse models of PLA2R1 and THSD7A-associated MN, it will be possible to investigate this hypothesis directly, e.g. by structural and ultrastructural spacial resolution of the glomerular filtration barrier in high-resolution immunofluorescence imaging and ultrastructural electron microscopy analyses.

(3) If autoantibodies bind to the target antigen, intracellular signaling is altered. This is the case, for example, in Grave's disease, a disorder of the thyroid gland which is characterized by clinically relevant hyperthyroidism. The Autoantibodies target the thyrotropin receptor (or TSH receptor) activate it and induce a G-protein signal cascade with intracellular formation of cAMP. This leads to activation of all functional aspects of the thyroid cells, including thyroid hormone release [108]. Until today the physiological functions of PLA2R1 and THSD7A are largely unknown and it is unclear whether PLA2R1 and THSD7A serve as receptors for specific ligands and transmit signals from the outside to the inside of cells, e.g. podocytes. PLA2R1 may be a regulator of inflammation by binding sPLA2s [36, 37], even though the *in vivo* relevance of this mechanism is not well understood.

With regard to THSD7A it was recently shown that the expression of the protein is accentuated at filopodia on podocytes. THSD7A overexpression in cell culture podocytes is associated with increased cell size and cell adhesion (e.g. to collagen IV) and a decreased cell migratory potential [47]. This suggests that THSD7A may be involved in outside-in signaling. Thus, it is possible that anti-PLA2R1 and anti-THSD7A antibodies interfere with (to date largely unknown) signaling pathways and that this process contributes to the cellular damage in MN. The heterologous models of PLA2R1- and THSD7A-associated MN can be applied to elucidate such potential pathomechanisms. After the disease is induced by transfer of rblgG, whole glomeruli or even podocytes, endothelial cells and mesangial cells can be isolated using FACS-sorting [109]. The isolated samples can be investigated for alterations in signaling pathways, e.g. by performing transcriptomic and proteomic analyses. This may reveal PLA2R1- and THSD7A-dependent signaling pathways that are activated by the respective antibodies. The identified pathways then can be validated in patients with MN

(e.g. by immunostaining for the identified targets) and further investigated regarding their involvement in MN pathogenesis, e.g. by generating mice that are genetically deficient for the identified target. Finally, such pathways may serve as druggable targets, which can be evaluated in the models of PLA2R1- and THSD7A-associated MN.

Besides investigations regarding PLA2R1- and THSD7A-related pathomechanisms in MN, the models can be applied to evaluate innovative, antigen-specific treatments *in vivo*:

(1) Epitope blocking therapy using non-pathogenic antibodies/nanobodies. For such an approach, it would be feasible to use specifically engineered antagonists to block several epitopes, for example nanobodies. The nanobodies would bind to the antigen and thereby prevent the binding of the pathogenic antibody. Nanobodies are small, recombinantly produced antigen binding VHH fragments, derived from cameloid heavy chain IgG antibodies [110]. It has already been shown that nanobodies are capable of blocking epitopes on molecules and interrupt the biological function of the targeted protein [111, 112]. For such a blocking strategy, the already generated monoclonal antibodies (see 3.1) could be applied in case that they share recognition of identical (or at least overlapping) epitopes with the patient autoantibodies. The antigen recognition site of the monoclonal antibodies can be analyzed by antibody sequencing and then be fused to an immunologically inactive IgG or a nanobody VHH backbone. Such blocking antibodies could be applied in the models of PLA2R1- and THSD7A-associated MN, e.g. initially as a pretreatment strategy to evaluate whether the disease will be attenuated as a consequence of epitope blocking.

(2) Antibody extraction using epitope-specific immunoabsorption. This method has been proven to be a possible tool in the treatment of pemphigus vulgaris (see above). When patient sera were adsorbed on sepharose, loaded with the parts of desmoglein-3 that bind the patient autoantibodies, all pathogenically active antibodies were eliminated [113]. In a neonatal mouse model of pemphigus vulgaris such depleted sera failed to induce the disease at all, giving a strong hint for the usefulness of this strategy as future therapy [114]. In the heterologous models of PLA2R1- and THSD7A-associated MN comparable proof-of-concept studies could be performed.

(3) Antibody extraction using endogenous degradation systems. For this approach, fragments of THSD7A and PLA2R1, containing the epitopes of pathogenic antibodies, are fused to the constant region of the mouse IgG heavy chain (Fc-region) and produced recombinantly. Genetic modifications in the Fc region (the region of the antibody that binds to Fc receptors) can enhance binding to the FcγIIb receptor. This receptor is highly expressed on liver sinusoidal epithelial cells, which play an important role in clearance of blood components as a part of the reticuloendothelial system. Binding of immune complexes via the Fc

part of the involved antibody leads to rapid internalization and degradation of the immune complex [115, 116]. Thus, such re-engineered heavy chain antibodies, also called sweeping antibodies, can be applied to scavenge pathogenic antibodies from a living organism. This mechanism can be evaluated in the models of PLA2R1- and THSD7A-associated MN by generating sweeping antibodies involving the antigen domains that are recognized by the pathogenic rIlgG.

Despite the broad applicability of these passive transfer models, there are certain limitations. First, the course of the model is acute, with high levels of proteinuria developing within days after transfer of anti-PLA2R1 or anti-THSD7A antibodies. This stands in contrast to the development of MN in patients, where the disease is usually clinically invisible for a certain time with slowly developing proteinuria. Interestingly, a recent study analyzing longitudinal serum samples found presence of anti-PLA2R1 antibodies months to years before a definite diagnosis of MN was made [117]. Second, the heterologous rIlgG serves as a foreign antigen itself and induces an immune response leading to the formation of mouse anti-rIlgG and consecutively binding of these antibodies to the deposited rIlgG in glomeruli. This creates large immune complexes consisting of PLA2R1–rabbit anti-PLA2R1–mouse anti-rIlgG (or THSD7A–rabbit anti-THSD7A–mouse anti-rIlgG) at the filtration barrier, where the mouse anti-rIlgG is a confounder that does not have a correlate in patients with MN. Third, the models do not contain true autoimmunity, which means that there is no autoimmune response against the antigen itself, i.e. no antigen presentation by antigen presenting cells, neither T cell activation nor B cell activation with subsequent differentiation of the B cell clones producing the pathogenic antibodies. Consequently, therapeutic strategies targeting the antibody-producing cells cannot be tested in the passive models of PLA2R1- and THSD7A-associated MN.

Thus, the establishment of a true autoimmune model is imperative for an even better modeling of the MN pathophysiology and for the development of highly innovative therapies targeting the pathogenic B cell clones. In preliminary experiments we could already show that mice, immunized with mouse THSD7A or fragments of the protein develop detectable antibody titers. Indeed, these antibodies bind to THSD7A in the glomerulus of the mice, causing proteinuria and the typical histopathological features of THSD7A-associated MN. A similar approach is envisaged for the PLA2R1-positive transgenic mice.

One promising therapeutic strategy to eliminate pathogenic B cell clones is the generation of chimeric autoantibody receptor (CAAR) T cells, a modification of the oncotherapeutic strategy of chimeric antigen receptor (CAR) T cells. This strategy involves the isolation of peripheral blood mononuclear cells (PBMCs) from the patient's blood using leukapheresis.

Stimulation of specific B cells using interleukin-2 and anti-CD3 antibodies lead to their proliferation. Afterwards the T cells are transduced with a construct encoding for the CAR of interest, e.g. the antigen-binding domain of an anti-CD19 antibody fused to intracellular signaling domains [118]. The resulting CAR T cells are transfused back to the patient, serving as a “living drug” to eliminate all cells expressing, in this case, CD19, a marker of B cells. This therapeutic strategy has recently been used with remarkable success, for example in refractory or relapsed B cell lymphoma [119-121]. For the treatment of antibody-mediated autoimmune diseases, this approach can be modified by expressing a CAAR on T cells. This CAAR does not recognize a certain antigen, but rather contains domains of an antigen itself, enabling binding to a B cell receptor of interest. The B cell receptor is a membrane bound immunoglobulin, corresponding to the antibody that is produced by this particular B cell. Thus, the engineered CAAR T cell will bind to the B cell of interest and eliminate it. In an animal model of pemphigus vulgaris, CAAR T cells specifically and efficiently eliminated anti-desmoglein 3-specific autoreactive B cells even in the presence of circulating autoantibodies, and without relevant off-target toxicity [122]. A huge advantage of this approach is the potential for the generation of long-term memory CAAR T cells, which offer the opportunity for constant elimination of newly emerging autoreactive B cells without the need for repetitively application of the treatment.

Once the mice models with active B cells are available such a CAAR T cell strategy could be applied, to investigate whether the elimination of specific B cell will ameliorate the disease. Perhaps, those studies can be combined with insights gained from the passive transfer of specific monoclonal antibodies (see 3.1). If the severity of disease depends on the binding of autoantibodies to a specific region of THSD7A, it might be sufficient to eliminate only B cell clones which produce antibodies targeting this part of the protein.

Taken together the heterologous animal models of THSD7A and PLA2R1-associated MN already represent powerful tools to investigate disease mechanisms and new therapeutic strategies. In future these opportunities will be expanded by the development of models that will involve autoantibody producing B cells, resulting in true autoimmunity.

4. Summary

Primary membranous nephropathy (MN) is an autoimmune disease and a major cause of nephrotic syndrome in adult patients. The disease is caused by the formation of immune deposits on the outer aspect of the glomerular basement membrane, which contain podocyte antigens and circulating antibodies specific for these antigens, resulting in severe damage of the filtration barrier. Two podocyte expressed proteins have been identified as antigens in MN so far, phospholipase A2 receptor 1 (PLA2R1) and thrombospondin type 1 domain containing protein 7A (THSD7A). Most of the patients develop antibodies against PLA2R1 (70-80% of MN cases), while cases with anti-THSD7A antibodies are less frequent (3-5% of MN cases). The outcome of the disease varies, with about 30% of patients experiencing spontaneous remission, whereas another 20-30% develop end stage renal disease within 10 years. Because of this heterogeneity it is inevitable to find the individual predictors of disease outcome. In order to do this and to test newly generated therapeutic strategies, valid animal models have to be established.

In our first study, presented here, we in *silico* analyzed the structure of THSD7A, and identified the autoantibody binding sites within the protein. We found out that the extracellular region of THSD7A is composed of a tandem string of 21 thrombospondin type one domains showing structural homology either to the TSP-1 domains of thrombospondin 1 (THBS1) or complement component 6 (C6). The 31 serum samples tested for the study revealed a polyreactive immune response against the whole extracellular region of THSD7A with a predominance for the most N-terminal part of the protein, the latter was also confirmed by animal models of active immunization with THSD7A.

In our second study, we generated a transgenic mouse line expressing the murine full-length PLA2R1 in podocytes (mPLA2R1-positive mice). The transfer of rabbit anti-THSD7A antibodies to these mice caused nephrotic range proteinuria, hypercholesterolemia, and the histomorphological signs of MN. We established the first animal model for PLA2R1 associated MN that can be used to gain deeper insights in disease development and investigate future therapeutic strategies.

In summary, the two studies presented in this thesis close a gap in the field of MN research. The domains that were targeted by antibodies in PLA2R1-associated MN were already defined, while a sufficient animal model for the disease was still missing. Vice versa, a model for THSD7A-associated MN existed, but the binding sites of patient antibodies were unknown. This work thus synchronizes research on these two antigens. Furthermore, the work presented in this thesis builds the base for a variety of potential future projects that will help to deepen the knowledge about the pathophysiology of the disease. For example, the role of the targeted epitopes can be investigated using domain-specific monoclonal antibodies

and the PLA2R1- and THSD7A-specific mouse models can be used to uncover the unknown signaling pathways that lead to glomerular damage in MN. Not last, innovative therapeutic strategies targeting antigen-specific disease mechanisms, such as extraction of pathogenic antibodies or elimination of autoantibody-producing B cells, can be investigated based on the work presented herein.

5. Zusammenfassung

Die primäre membranöse Glomerulonephritis (MN) ist eine Autoimmunerkrankung und eine der Hauptursachen für das nephrotische Syndrom bei erwachsenen Patienten. Verursacht wird sie durch die Bildung von Immunablagerungen auf der Außenseite der glomerulären Basalmembran, die zu einer schweren Schädigung der Filtrationsbarriere führen. Diese Ablagerungen enthalten Podozytenantigene und an sie gebundene Antikörper. Bisher wurden zwei Antigene identifiziert: Phospholipase A2 receptor 1 (PLA2R1) und Thrombospondin type 1 domain containing protein 7A (THSD7A). Die meisten Patienten entwickeln Antikörper gegen PLA2R1 (70-80% der MN-Fälle), während Anti-THSD7A-Antikörpern weniger häufig sind (3-5% der MN-Fälle). Der Ausgang der Krankheit ist unterschiedlich: Etwa 30% der Patienten erreichen eine spontane Remission, während weitere 20 bis 30% innerhalb von 10 Jahren eine Nierenerkrankung im Endstadium entwickeln. Aufgrund dieser Diversität ist es wichtig Indikatoren zu identifizieren, die es einem erlauben den Verlauf der Erkrankung zu prognostizieren, um passende Therapien anwenden zu können. Sowohl für die Analyse solcher Erkrankungsmarker als auch für die Testung neuer und innovativer Therapiemöglichkeiten, sind Tiermodelle unabdingbar, die die Erkrankungssituation möglichst genau reproduzieren.

In der ersten, hier vorgestellten, Studie wurde die Struktur von THSD7A *in silico* analysiert und die Autoantikörper-Bindungsstellen innerhalb des Proteins identifiziert. Wir konnten zeigen, dass die extrazelluläre Region von THSD7A aus einer Tandemkette von 21 Thrombospondin-Typ-1-Domänen besteht, die entweder eine strukturelle Homologie zu den TSP-1 Domänen von Thrombospondin 1 (THBS1) oder zu denen der Komplement Komponente 6 (C6) aufweisen. Die 31 für die Studie getesteten Serumproben zeigten eine polyreaktive Immunantwort gegen die gesamte extrazelluläre Region von THSD7A mit einer Dominanz für den Teil des Proteins der am äußersten N-terminus des Proteins liegt. Letzteres wurde auch durch aktiven Immunisierungen mit THSD7A in mehreren Tiermodellen bestätigt.

In der zweiten Studie wurde eine transgene Mauslinie erzeugt, die das murine PLA2R1 auf Podozyten (mPLA2R1-positive Mäuse) exprimiert. Der Transfer von Kaninchen-Anti-

THSD7A Antikörpern in diese Mäuse verursachte eine Proteinurie im nephrotischen Bereich, Hypercholesterinämie und alle histomorphologischen Anzeichen der MN. Es wurde somit das erste Tiermodell für die PLA2R1-assoziierte MN etabliert, mit dem tiefere Einblicke in die Krankheitsentwicklung gewonnen und therapeutische Strategien untersucht werden können.

Die beiden, in dieser Arbeit vorgestellten Studien, schließen jeweils eine Lücke auf dem Gebiet der MN bezogenen Forschung. Im Bereich der PLA2R1 assoziierten MN fehlte bis dato ein Tiermodell, während die Domänen des Proteins, welche von Autoantikörpern gebunden werden, bereits bekannt waren. Umgekehrt existierte bereits ein Modell für THSD7A-assoziiertes MN, aber die Bindungsstellen der Patientenantikörper waren unbekannt. Schlussendlich synchronisiert diese Arbeit somit die Forschung an diesen beiden Antigenen. Darüber hinaus bildet sie die Grundlage für eine Vielzahl potenzieller zukünftiger Projekte, die dazu beitragen werden, das Wissen um die Pathophysiologie dieser Krankheit zu vertiefen. Beispielsweise kann die Rolle der Zielepitope untersucht werden, indem man domänenspezifische monoklonale Antikörper verwendet. Außerdem bieten die PLA2R1- und THSD7A-spezifischen Mausmodelle eine Möglichkeit bisher unbekannte Signalwege zu identifizieren, die zu glomerulären Schäden führen. Nicht zuletzt liefert die hier vorgestellte Arbeit die notwendige Grundlage um innovative Therapiestrategien, wie die Extraktion pathogener Antikörper oder die Eliminierung von Autoantikörper-produzierenden B Zellen, zu entwickeln und zu testen.

6. Literature

1. Menon, M.C., P.Y. Chuang, and C.J. He, *The glomerular filtration barrier: components and crosstalk*. Int J Nephrol, 2012. **2012**: p. 749010.
2. Kodner, C., *Diagnosis and Management of Nephrotic Syndrome in Adults*. Am Fam Physician, 2016. **93**(6): p. 479-85.
3. Maisonneuve, P., et al., *Distribution of primary renal diseases leading to end-stage renal failure in the United States, Europe, and Australia/New Zealand: results from an international comparative study*. Am J Kidney Dis, 2000. **35**(1): p. 157-65.
4. Fogo, A.B., et al., *AJKD Atlas of Renal Pathology: Membranous Nephropathy*. Am J Kidney Dis, 2015. **66**(3): p. e15-7.
5. Segawa, Y., et al., *IgG subclasses and complement pathway in segmental and global membranous nephropathy*. Pediatr Nephrol, 2010. **25**(6): p. 1091-9.
6. Jennette, J.C., S.S. Iskandar, and F.G. Dalldorf, *Pathologic differentiation between lupus and nonlupus membranous glomerulopathy*. Kidney Int, 1983. **24**(3): p. 377-85.
7. Johnson, R.J. and W.G. Couser, *Hepatitis B infection and renal disease: clinical, immunopathogenetic and therapeutic considerations*. Kidney Int, 1990. **37**(2): p. 663-76.
8. Radford, M.G., Jr., et al., *Reversible membranous nephropathy associated with the use of nonsteroidal anti-inflammatory drugs*. JAMA, 1996. **276**(6): p. 466-9.
9. Bjorneklett, R., et al., *Long-term risk of cancer in membranous nephropathy patients*. Am J Kidney Dis, 2007. **50**(3): p. 396-403.
10. Larsen, C.P., et al., *Determination of primary versus secondary membranous glomerulopathy utilizing phospholipase A2 receptor staining in renal biopsies*. Mod Pathol, 2013. **26**(5): p. 709-15.
11. Takekoshi, Y., et al., *Immunopathogenetic mechanisms of hepatitis B virus-related glomerulopathy*. Kidney Int Suppl, 1991. **35**: p. S34-9.
12. Davenport, A., et al., *Do mesangial immune complex deposits affect the renal prognosis in membranous glomerulonephritis?* Clin Nephrol, 1994. **41**(5): p. 271-6.
13. Imai, H., et al., *IgG subclasses in patients with membranoproliferative glomerulonephritis, membranous nephropathy, and lupus nephritis*. Kidney Int, 1997. **51**(1): p. 270-6.
14. Kuroki, A., et al., *Glomerular and serum IgG subclasses in diffuse proliferative lupus nephritis, membranous lupus nephritis, and idiopathic membranous nephropathy*. Intern Med, 2002. **41**(11): p. 936-42.
15. Polanco, N., et al., *Spontaneous remission of nephrotic syndrome in membranous nephropathy with chronic renal impairment*. Nephrol Dial Transplant, 2012. **27**(1): p. 231-4.
16. Glasscock, R.J., *Diagnosis and natural course of membranous nephropathy*. Semin Nephrol, 2003. **23**(4): p. 324-32.
17. Grupper, A., et al., *Recurrent Membranous Nephropathy After Kidney Transplantation: Treatment and Long-Term Implications*. Transplantation, 2016. **100**(12): p. 2710-2716.
18. Heymann, W., et al., *Production of nephrotic syndrome in rats by Freund's adjuvants and rat kidney suspensions*. Proc Soc Exp Biol Med, 1959. **100**(4): p. 660-4.
19. Barabas, A.Z. and R. Lannigan, *Induction of an autologous immune-complex glomerulonephritis in the rat by intravenous injection of heterologous anti-rat kidney tubular antibody. I. Production of chronic progressive immune-complex glomerulonephritis*. Br J Exp Pathol, 1974. **55**(1): p. 47-55.
20. Salant, D.J., et al., *A new role for complement in experimental membranous nephropathy in rats*. J Clin Invest, 1980. **66**(6): p. 1339-50.

21. Van Damme, B.J., et al., *Experimental glomerulonephritis in the rat induced by antibodies directed against tubular antigens. V. Fixed glomerular antigens in the pathogenesis of heterologous immune complex glomerulonephritis*. Lab Invest, 1978. **38**(4): p. 502-10.
22. Couser, W.G., et al., *Experimental glomerulonephritis in the isolated perfused rat kidney*. J Clin Invest, 1978. **62**(6): p. 1275-87.
23. Cybulsky, A.V., et al., *Complement-induced glomerular epithelial cell injury. Role of the membrane attack complex in rat membranous nephropathy*. J Clin Invest, 1986. **77**(4): p. 1096-107.
24. Kerjaschki, D., et al., *Transcellular transport and membrane insertion of the C5b-9 membrane attack complex of complement by glomerular epithelial cells in experimental membranous nephropathy*. J Immunol, 1989. **143**(2): p. 546-52.
25. Leenaerts, P.L., et al., *Active Heymann nephritis in complement component C6 deficient rats*. Kidney Int, 1995. **47**(6): p. 1604-14.
26. Spicer, S.T., et al., *Induction of passive Heymann nephritis in complement component 6-deficient PVG rats*. J Immunol, 2007. **179**(1): p. 172-8.
27. Kerjaschki, D. and M.G. Farquhar, *The pathogenic antigen of Heymann nephritis is a membrane glycoprotein of the renal proximal tubule brush border*. Proc Natl Acad Sci U S A, 1982. **79**(18): p. 5557-61.
28. Kerjaschki, D. and M.G. Farquhar, *Immunocytochemical localization of the Heymann nephritis antigen (GP330) in glomerular epithelial cells of normal Lewis rats*. J Exp Med, 1983. **157**(2): p. 667-86.
29. Shah, P., A. Tramontano, and S.P. Makker, *Intramolecular epitope spreading in Heymann nephritis*. J Am Soc Nephrol, 2007. **18**(12): p. 3060-6.
30. Debiec, H., et al., *Antenatal membranous glomerulonephritis due to anti-neutral endopeptidase antibodies*. N Engl J Med, 2002. **346**(26): p. 2053-60.
31. Debiec, H., et al., *Role of truncating mutations in MME gene in fetomaternal alloimmunisation and antenatal glomerulopathies*. Lancet, 2004. **364**(9441): p. 1252-9.
32. Ronco, P., H. Debiec, and V. Guignonis, *Mechanisms of disease: Alloimmunization in renal diseases*. Nat Clin Pract Nephrol, 2006. **2**(7): p. 388-97.
33. Beck, L.H., Jr., et al., *M-type phospholipase A2 receptor as target antigen in idiopathic membranous nephropathy*. N Engl J Med, 2009. **361**(1): p. 11-21.
34. East, L. and C.M. Isacke, *The mannose receptor family*. Biochim Biophys Acta, 2002. **1572**(2-3): p. 364-86.
35. Zvaritch, E., G. Lambeau, and M. Lazdunski, *Endocytic properties of the M-type 180-kDa receptor for secretory phospholipases A2*. J Biol Chem, 1996. **271**(1): p. 250-7.
36. Lambeau, G. and M.H. Gelb, *Biochemistry and physiology of mammalian secreted phospholipases A2*. Annu Rev Biochem, 2008. **77**: p. 495-520.
37. Augert, A., et al., *The M-type receptor PLA2R regulates senescence through the p53 pathway*. EMBO Rep, 2009. **10**(3): p. 271-7.
38. Takahashi, S., et al., *C-type lectin-like domain and fibronectin-like type II domain of phospholipase A(2) receptor 1 modulate binding and migratory responses to collagen*. FEBS Lett, 2015. **589**(7): p. 829-35.
39. Watanabe, K., et al., *Human soluble phospholipase A2 receptor is an inhibitor of the integrin-mediated cell migratory response to collagen-I*. Am J Physiol Cell Physiol, 2018. **315**(3): p. C398-C408.
40. Skoberne, A., et al., *Serum with phospholipase A2 receptor autoantibodies interferes with podocyte adhesion to collagen*. Eur J Clin Invest, 2014. **44**(8): p. 753-65.
41. Tomas, N.M., et al., *Thrombospondin type-1 domain-containing 7A in idiopathic membranous nephropathy*. N Engl J Med, 2014. **371**(24): p. 2277-2287.

42. Hoxha, E., et al., *A Mechanism for Cancer-Associated Membranous Nephropathy*. N Engl J Med, 2016. **374**(20): p. 1995-6.
43. Hoxha, E., et al., *An Indirect Immunofluorescence Method Facilitates Detection of Thrombospondin Type 1 Domain-Containing 7A-Specific Antibodies in Membranous Nephropathy*. J Am Soc Nephrol, 2017. **28**(2): p. 520-531.
44. Tomas, N.M., et al., *Autoantibodies against thrombospondin type 1 domain-containing 7A induce membranous nephropathy*. J Clin Invest, 2016. **126**(7): p. 2519-32.
45. Wang, C.H., et al., *Thrombospondin type I domain containing 7A (THSD7A) mediates endothelial cell migration and tube formation*. J Cell Physiol, 2010. **222**(3): p. 685-94.
46. Kuo, M.W., et al., *Soluble THSD7A is an N-glycoprotein that promotes endothelial cell migration and tube formation in angiogenesis*. PLoS One, 2011. **6**(12): p. e29000.
47. Herwig, J., et al., *Thrombospondin Type 1 Domain-Containing 7A Localizes to the Slit Diaphragm and Stabilizes Membrane Dynamics of Fully Differentiated Podocytes*. J Am Soc Nephrol, 2019. **30**(5): p. 824-839.
48. Larsen, C.P., L.N. Cossey, and L.H. Beck, *THSD7A staining of membranous glomerulopathy in clinical practice reveals cases with dual autoantibody positivity*. Mod Pathol, 2016. **29**(4): p. 421-6.
49. Wang, J., et al., *Circulating Antibodies against Thrombospondin Type-I Domain-Containing 7A in Chinese Patients with Idiopathic Membranous Nephropathy*. Clin J Am Soc Nephrol, 2017. **12**(10): p. 1642-1651.
50. Zaghrini, C., et al., *Novel ELISA for thrombospondin type 1 domain-containing 7A autoantibodies in membranous nephropathy*. Kidney Int, 2019. **95**(3): p. 666-679.
51. Sethi, S., et al., *Exostosin 1/Exostosin 2-Associated Membranous Nephropathy*. J Am Soc Nephrol, 2019. **30**(6): p. 1123-1136.
52. Busse, M. and M. Kusche-Gullberg, *In vitro polymerization of heparan sulfate backbone by the EXT proteins*. J Biol Chem, 2003. **278**(42): p. 41333-7.
53. Busse, M., et al., *Contribution of EXT1, EXT2, and EXTL3 to heparan sulfate chain elongation*. J Biol Chem, 2007. **282**(45): p. 32802-10.
54. Busse-Wicher, M., K.B. Wicher, and M. Kusche-Gullberg, *The exostosin family: proteins with many functions*. Matrix Biol, 2014. **35**: p. 25-33.
55. Sethi, S.e.a., *Neural epidermal growth factor-like 1protein (NELL-1) associated membranous nephropathy*. Kidney International, 2019.
56. Zhang, X., et al., *The role of NELL-1, a growth factor associated with craniosynostosis, in promoting bone regeneration*. J Dent Res, 2010. **89**(9): p. 865-78.
57. Kuroda, S., et al., *Biochemical characterization and expression analysis of neural thrombospondin-1-like proteins NELL1 and NELL2*. Biochem Biophys Res Commun, 1999. **265**(1): p. 79-86.
58. Hasebe, A., et al., *Efficient production and characterization of recombinant human NELL1 protein in human embryonic kidney 293-F cells*. Mol Biotechnol, 2012. **51**(1): p. 58-66.
59. Hasebe, A., et al., *The C-terminal region of NELL1 mediates osteoblastic cell adhesion through integrin alpha3beta1*. FEBS Lett, 2012. **586**(16): p. 2500-6.
60. Watanabe, T.K., et al., *Cloning and characterization of two novel human cDNAs (NELL1 and NELL2) encoding proteins with six EGF-like repeats*. Genomics, 1996. **38**(3): p. 273-6.
61. Hoxha, E., et al., *An immunofluorescence test for phospholipase-A(2)-receptor antibodies and its clinical usefulness in patients with membranous glomerulonephritis*. Nephrol Dial Transplant, 2011. **26**(8): p. 2526-32.
62. Qin, W., et al., *Anti-phospholipase A2 receptor antibody in membranous nephropathy*. J Am Soc Nephrol, 2011. **22**(6): p. 1137-43.

63. Du, Y., et al., *The diagnosis accuracy of PLA2R-AB in the diagnosis of idiopathic membranous nephropathy: a meta-analysis*. PLoS One, 2014. **9**(8): p. e104936.
64. Pourcine, F., et al., *Prognostic value of PLA2R autoimmunity detected by measurement of anti-PLA2R antibodies combined with detection of PLA2R antigen in membranous nephropathy: A single-centre study over 14 years*. PLoS One, 2017. **12**(3): p. e0173201.
65. Debiec, H. and P. Ronco, *PLA2R autoantibodies and PLA2R glomerular deposits in membranous nephropathy*. N Engl J Med, 2011. **364**(7): p. 689-90.
66. Stahl, R., E. Hoxha, and K. Fechner, *PLA2R autoantibodies and recurrent membranous nephropathy after transplantation*. N Engl J Med, 2010. **363**(5): p. 496-8.
67. Dahnrich, C., et al., *Development of a standardized ELISA for the determination of autoantibodies against human M-type phospholipase A2 receptor in primary membranous nephropathy*. Clin Chim Acta, 2013. **421**: p. 213-8.
68. Hofstra, J.M., et al., *Anti-phospholipase A(2) receptor antibodies correlate with clinical status in idiopathic membranous nephropathy*. Clin J Am Soc Nephrol, 2011. **6**(6): p. 1286-91.
69. Hoxha, E., et al., *Phospholipase A2 receptor autoantibodies and clinical outcome in patients with primary membranous nephropathy*. J Am Soc Nephrol, 2014. **25**(6): p. 1357-66.
70. Hoxha, E., et al., *M-type phospholipase A2 receptor autoantibodies and renal function in patients with primary membranous nephropathy*. Clin J Am Soc Nephrol, 2014. **9**(11): p. 1883-90.
71. Ruggenenti, P., et al., *Anti-Phospholipase A2 Receptor Antibody Titer Predicts Post-Rituximab Outcome of Membranous Nephropathy*. J Am Soc Nephrol, 2015. **26**(10): p. 2545-58.
72. Beck, L.H., Jr., et al., *Rituximab-induced depletion of anti-PLA2R autoantibodies predicts response in membranous nephropathy*. J Am Soc Nephrol, 2011. **22**(8): p. 1543-50.
73. Bech, A.P., et al., *Association of anti-PLA(2)R antibodies with outcomes after immunosuppressive therapy in idiopathic membranous nephropathy*. Clin J Am Soc Nephrol, 2014. **9**(8): p. 1386-92.
74. Dong, Y., et al., *Structure of Human M-type Phospholipase A2 Receptor Revealed by Cryo-Electron Microscopy*. J Mol Biol, 2017. **429**(24): p. 3825-3835.
75. Kao, L., et al., *Identification of the immunodominant epitope region in phospholipase A2 receptor-mediating autoantibody binding in idiopathic membranous nephropathy*. J Am Soc Nephrol, 2015. **26**(2): p. 291-301.
76. Fresquet, M., et al., *Identification of a major epitope recognized by PLA2R autoantibodies in primary membranous nephropathy*. J Am Soc Nephrol, 2015. **26**(2): p. 302-13.
77. Seitz-Polski, B., et al., *Epitope Spreading of Autoantibody Response to PLA2R Associates with Poor Prognosis in Membranous Nephropathy*. J Am Soc Nephrol, 2016. **27**(5): p. 1517-33.
78. Seitz-Polski, B., et al., *Phospholipase A2 Receptor 1 Epitope Spreading at Baseline Predicts Reduced Likelihood of Remission of Membranous Nephropathy*. J Am Soc Nephrol, 2018. **29**(2): p. 401-408.
79. Reinhard, L.e.a., *Clinical Relevance of Domain-Specific Phospholipase A2 Receptor 1 Antibody Levels in Patients with Membranous Nephropathy*. J Am Soc Nephrol, 2019.
80. Seitz-Polski, B., et al., *Prediction of membranous nephropathy recurrence after transplantation by monitoring of anti-PLA2R1 (M-type phospholipase A2 receptor) autoantibodies: a case series of 15 patients*. Nephrol Dial Transplant, 2014. **29**(12): p. 2334-42.

81. Meyer-Schwesinger, C., G. Lambeau, and R.A. Stahl, *Thrombospondin type-1 domain-containing 7A in idiopathic membranous nephropathy*. N Engl J Med, 2015. **372**(11): p. 1074-5.
82. Godel, M., F. Grahammer, and T.B. Huber, *Thrombospondin type-1 domain-containing 7A in idiopathic membranous nephropathy*. N Engl J Med, 2015. **372**(11): p. 1073.
83. Tomas, N.M., et al., *A Heterologous Model of Thrombospondin Type 1 Domain-Containing 7A-Associated Membranous Nephropathy*. J Am Soc Nephrol, 2017. **28**(11): p. 3262-3277.
84. Zahner G, M.-S., Tomas N, Hoxha E, Wiech T, Stahl RA, *Development and morphologic characterization of a mouse model of membranous nephropathy involving the human phospholipase A2 receptor*. J Am Soc Nephrol, 2014.
85. Zahner G, H., Helmchen U, Stahl RA, *The generation of inducible specific human phospholipase A2 receptor transgenic mice*. J Am Soc Nephrol 2012.
86. Klenotic, P.A., et al., *Expression, purification and structural characterization of functionally replete thrombospondin-1 type 1 repeats in a bacterial expression system*. Protein Expr Purif, 2011. **80**(2): p. 253-9.
87. Aleshin, A.E., et al., *Structure of complement C6 suggests a mechanism for initiation and unidirectional, sequential assembly of membrane attack complex (MAC)*. J Biol Chem, 2012. **287**(13): p. 10210-22.
88. Paakkonen, K., et al., *Solution structures of the first and fourth TSR domains of F-spondin*. Proteins, 2006. **64**(3): p. 665-72.
89. Chen, H., M.E. Herndon, and J. Lawler, *The cell biology of thrombospondin-1*. Matrix Biol, 2000. **19**(7): p. 597-614.
90. Galvin, N.J., et al., *Interaction of human thrombospondin with types I-V collagen: direct binding and electron microscopy*. J Cell Biol, 1987. **104**(5): p. 1413-22.
91. Asch, A.S., et al., *Thrombospondin sequence motif (CSVTCG) is responsible for CD36 binding*. Biochem Biophys Res Commun, 1992. **182**(3): p. 1208-17.
92. Calzada, M.J., et al., *Identification of novel beta1 integrin binding sites in the type 1 and type 2 repeats of thrombospondin-1*. J Biol Chem, 2004. **279**(40): p. 41734-43.
93. Calzada, M.J., et al., *Recognition of the N-terminal modules of thrombospondin-1 and thrombospondin-2 by alpha6beta1 integrin*. J Biol Chem, 2003. **278**(42): p. 40679-87.
94. Bein, K. and M. Simons, *Thrombospondin type 1 repeats interact with matrix metalloproteinase 2. Regulation of metalloproteinase activity*. J Biol Chem, 2000. **275**(41): p. 32167-73.
95. Resovi, A., et al., *Current understanding of the thrombospondin-1 interactome*. Matrix Biol, 2014. **37**: p. 83-91.
96. Stoddard, S.V., et al., *Structure and function insights garnered from in silico modeling of the thrombospondin type-1 domain-containing 7A antigen*. Proteins, 2019. **87**(2): p. 136-145.
97. Hashimoto, T., et al., *Demonstration of epitope spreading in bullous pemphigoid: results of a prospective multicenter study*. J Invest Dermatol, 2011. **131**(11): p. 2175-7.
98. Di Zenzo, G., et al., *Demonstration of epitope-spreading phenomena in bullous pemphigoid: results of a prospective multicenter study*. J Invest Dermatol, 2011. **131**(11): p. 2271-80.
99. McRae, B.L., et al., *Functional evidence for epitope spreading in the relapsing pathology of experimental autoimmune encephalomyelitis*. J Exp Med, 1995. **182**(1): p. 75-85.
100. Goebels, N., et al., *Repertoire dynamics of autoreactive T cells in multiple sclerosis patients and healthy subjects: epitope spreading versus clonal persistence*. Brain, 2000. **123 Pt 3**: p. 508-18.

101. Vanderlugt, C.L. and S.D. Miller, *Epitope spreading in immune-mediated diseases: implications for immunotherapy*. Nat Rev Immunol, 2002. **2**(2): p. 85-95.
102. Wucherpfennig, K.W., *Mechanisms for the induction of autoimmunity by infectious agents*. J Clin Invest, 2001. **108**(8): p. 1097-104.
103. Kain, R., et al., *Molecular mimicry in pauci-immune focal necrotizing glomerulonephritis*. Nat Med, 2008. **14**(10): p. 1088-96.
104. Oldstone, M.B., *Molecular mimicry: its evolution from concept to mechanism as a cause of autoimmune diseases*. Monoclon Antib Immunodiagn Immunother, 2014. **33**(3): p. 158-65.
105. Fresquet, M., et al., *Autoantigens PLA2R and THSD7A in membranous nephropathy share a common epitope motif in the N-terminal domain*. J Autoimmun, 2019: p. 102308.
106. Dana, H., et al., *Molecular Mechanisms and Biological Functions of siRNA*. Int J Biomed Sci, 2017. **13**(2): p. 48-57.
107. Porro, A.M., et al., *Pemphigus vulgaris*. An Bras Dermatol, 2019. **94**(3): p. 264-278.
108. Menconi, F., C. Marocci, and M. Marino, *Diagnosis and classification of Graves' disease*. Autoimmun Rev, 2014. **13**(4-5): p. 398-402.
109. Boerries, M., et al., *Molecular fingerprinting of the podocyte reveals novel gene and protein regulatory networks*. Kidney Int, 2013. **83**(6): p. 1052-64.
110. Wesolowski, J., et al., *Single domain antibodies: promising experimental and therapeutic tools in infection and immunity*. Med Microbiol Immunol, 2009. **198**(3): p. 157-74.
111. Farajpour, Z., et al., *A nanobody directed to a functional epitope on VEGF, as a novel strategy for cancer treatment*. Biochem Biophys Res Commun, 2014. **446**(1): p. 132-6.
112. Danquah, W., et al., *Nanobodies that block gating of the P2X7 ion channel ameliorate inflammation*. Sci Transl Med, 2016. **8**(366): p. 366ra162.
113. Langenhan, J., et al., *Specific immunoadsorption of pathogenic autoantibodies in pemphigus requires the entire ectodomains of desmogleins*. Exp Dermatol, 2014. **23**(4): p. 253-9.
114. Hofrichter, M., et al., *Immunoadsorption of Desmoglein-3-Specific IgG Abolishes the Blister-Inducing Capacity of Pemphigus Vulgaris IgG in Neonatal Mice*. Front Immunol, 2018. **9**: p. 1935.
115. Chu, S.Y., et al., *Reduction of total IgE by targeted coengagement of IgE B-cell receptor and FcγRIIb with Fc-engineered antibody*. J Allergy Clin Immunol, 2012. **129**(4): p. 1102-15.
116. Ganesan, L.P., et al., *FcγRIIb on liver sinusoidal endothelium clears small immune complexes*. J Immunol, 2012. **189**(10): p. 4981-8.
117. Burbelo, P.D., et al., *Detection of PLA2R Autoantibodies before the Diagnosis of Membranous Nephropathy*. J Am Soc Nephrol, 2020. **31**(1): p. 208-217.
118. June, C.H. and M. Sadelain, *Chimeric Antigen Receptor Therapy*. N Engl J Med, 2018. **379**(1): p. 64-73.
119. Park, J.H., et al., *Long-Term Follow-up of CD19 CAR Therapy in Acute Lymphoblastic Leukemia*. N Engl J Med, 2018. **378**(5): p. 449-459.
120. Maude, S.L., et al., *Tisagenlecleucel in Children and Young Adults with B-Cell Lymphoblastic Leukemia*. N Engl J Med, 2018. **378**(5): p. 439-448.
121. Schuster, S.J., et al., *Tisagenlecleucel in Adult Relapsed or Refractory Diffuse Large B-Cell Lymphoma*. N Engl J Med, 2019. **380**(1): p. 45-56.
122. Ellebrecht, C.T., et al., *Reengineering chimeric antigen receptor T cells for targeted therapy of autoimmune disease*. Science, 2016. **353**(6295): p. 179-84.

7. Individual contribution

All publications described in this thesis are the result of collaborations with other scientists whose names are listed in the respective author list. The weighting of individual contributions was agreed with all respective co-authors with mutual agreement. I contributed a significant part of the presented publications, which I would like to describe briefly below.

The Most N-Terminal Region of THSD7A Is the Predominant Target for Autoimmunity in THSD7A-Associated Membranous Nephropathy.

This study was conceptualized by Dr. Nicola Tomas, Prof. Friedrich Koch-Nolte and me. I designed the experimental setups with regular consultation of my supervisor during the time course of the project. All experimental work contained in this study (design, expression and purification of antigen domain constructs as well as characterization of epitope domains targeted by human and animal antibodies using different methodology such as Western and native blotting) was independently carried out by me. All clinical data were analyzed by Elion Hoxha. All obtained data was interpreted together with Dr. Nicola Tomas. The manuscript was written by me together with Dr. Nicola Tomas.

A novel mouse model of phospholipase A2 receptor 1-associated membranous nephropathy mimics podocyte injury in patients.

This study was designed by Priv.-Doz. Dr. Gunther Zahner. The major experimental work was carried out by Priv.-Doz. Gunther Zahner and Prof. Dr. Catherine Meyer-Schwesinger. I significantly contributed to the study by performing the following experiments: purification of antibodies, regular monitoring of mice and obtaining of urine, measurement of urinary albumin excretion, animal sacrifice, and preparation of renal tissue and serum samples. Additionally, I was significantly involved in writing of the manuscript and the final proofreading of the publication.



Dr. Nicola Tomas



Priv.-Doz. Dr. Gunther Zahner

8. Acknowledgements

I want to express a special thanks to my supervisor Dr. Nicola Tomas. He not only give me the opportunity to perform all my experiments in his working group but also helped me a lot with his intensive support, his scientific instinct and good ideas. Without this support and personal commitment, my work would not have been possible.

Furthermore, I want to thank the supervisor of my dissertation Priv.-Doz. Gunther Zahner. Who was immediately willing to examine my dissertation and always stood by my side to help me during the whole time course of the project. Thank you for a lot of fruitful discussions.

I also want to thank our collaboration partner Prof. Friedrich Koch-Nolte and his whole team. Their work, ideas and support are an important cornerstone of this doctoral thesis.

Thanks to all my colleagues in the AG Tomas/Zahner who worked with me over the time. Especially to Silke Dehde, who was my “partner in crime” for everything, experiment related or not.

I want to thank Prof. Dr. med. Ulf Panzer, Prof. Dr. med. Tobias B. Huber and Prof. Dr. Rolf A.K. Stahl for the opportunity to carry out my work within the Sonderforschungsbereich 1192.

I wish to thank all my friends, especially my boyfriend, who encouraged me to start over new with this project and who irrefragably presumed that it will be successful in the end.

Last but not least, I want to thank my mother for her loving and unconditional support, I wouldn't have gotten this far without her.

9. Eidesstattliche Erklärung

Hiermit erkläre ich an Eides statt, dass ich die vorliegende Dissertationsschrift selbstständig und ohne fremde Hilfe verfasst und keine anderen als die angegebenen Quellen und Hilfsmittel verwendet habe.

Hamburg, April 2020

Larissa Seifert

10. Appendix

The Most N-Terminal Region of THSD7A Is the Predominant Target for Autoimmunity in THSD7A-Associated Membranous Nephropathy

Larissa Seifert,¹ Elion Hoxha,¹ Anna M. Eichhoff,² Gunther Zahner,¹ Silke Dehde,¹ Linda Reinhard,¹ Friedrich Koch-Nolte,² Rolf A.K. Stahl,¹ and Nicola M. Tomas¹

¹III. Medizinische Klinik and ²Institute of Immunology, University Medical Center Hamburg-Eppendorf, Hamburg, Germany

ABSTRACT

Background Thrombospondin type 1 domain-containing 7A (THSD7A) has been identified as a pathogenic autoantigen in membranous nephropathy (MN). However, the THSD7A epitopes targeted by patient autoantibodies are unknown.

Methods We performed an *in silico* analysis of the THSD7A multidomain structure, expressed the folded domains in HEK293 cells, and tested for domain reactivity with 31 serum samples from patients with THSD7A-associated MN using Western and native blotting. Immunogenicity of the antigen domains was further investigated by cDNA immunization of rabbits and mice.

Results We characterized the extracellular topology of THSD7A as a tandem string of 21 thrombospondin type 1 domains. Overall, 28 serum samples (90%) recognized multiple epitope domains along the molecule. Detailed epitope mapping revealed that the complex consisting of the first and second N-terminal domains (amino acids 48–192) was recognized by 27 of 31 patient serum samples (87%). Serum recognizing one or two epitope domains showed lower anti-THSD7A antibody levels than serum recognizing three or more epitope domains. During follow-up, a loss of epitope recognition was observed in seven of 16 patients, and it was accompanied by decreasing antibody levels and remission of proteinuria. In four of 16 patients, epitope recognition patterns changed during follow-up. Notably, immunization experiments in rabbits and mice revealed that induced antibodies, like patient autoantibodies, preferentially bound to the most N-terminal domains of THSD7A.

Conclusions Our data show that the immune response in THSD7A-associated MN is polyreactive and that autoantibodies predominantly target the most N-terminal part of THSD7A.

J Am Soc Nephrol 29: 1536–1548, 2018. doi: <https://doi.org/10.1681/ASN.2017070805>

Primary membranous nephropathy (MN) is an autoimmune disease and a major cause of nephrotic syndrome in adult patients. The clinical outcome

Received July 27, 2017. Accepted February 9, 2018.

L.S. and E.H. contributed equally to this work.

Published online ahead of print. Publication date available at www.jasn.org.

Correspondence: Dr. Nicola M. Tomas, III. Medizinische Klinik, Universitätsklinikum Hamburg-Eppendorf, Martinistrasse 52, D-20246 Hamburg, Germany. Email: n.tomas@uke.de

Copyright © 2018 by the American Society of Nephrology

Significance Statement

Membranous nephropathy (MN) is an autoimmune disease in which autoantibodies against the podocyte surface proteins THSD7A or PLA2R1 are found. The autoantibody binding domains of THSD7A are unknown. This paper identifies autoantibodies against multiple epitopes in patients with THSD7A-associated MN and characterizes the most N-terminal part of THSD7A as an immunologic hotspot region. The preferential antibody generation against this region could be reproduced in immunization experiments in mice and rabbits. This study presents novel data regarding the pathogenesis of MN and may pave the way for innovative epitope-specific therapeutic approaches.

varies, with about 30% of patients experiencing spontaneous remission, whereas another 20%–30% develop ESRD within 10 years.¹ Two podocyte-expressed autoantigens have been identified in primary MN so far: phospholipase A2 receptor 1 (PLA2R1) and thrombospondin type 1 domain-containing 7A (THSD7A).^{2,3} Anti-PLA2R1 antibody levels associate with clinical outcome of affected patients.^{4–6} Therefore, measurement of anti-PLA2R1 antibodies is useful for diagnosis, individual risk assessment, and monitoring of treatment in patients with MN, including the time after transplantation.^{7–10} The prevalence of THSD7A-associated MN is significantly lower compared with that of PLA2R1-associated MN, and the clinical usefulness of anti-THSD7A autoantibody measurement is currently under investigation.¹¹ Noteworthy, 20% of white patients with THSD7A-associated MN have concurrent malignancies, suggesting that intensive screening for malignancies is advised in these patients.^{12,13}

The identification of antigen epitopes in renal autoimmune diseases, such as anti-glomerular basement membrane disease and ANCA vasculitis, has contributed to the understanding of the disease mechanisms in these entities.^{14,15} Recently, the most N-terminal part of PLA2R1 was identified as the immunodominant epitope region in patients with PLA2R1-associated MN.^{16,17} PLA2R1 contains at least two more epitope regions involved in autoimmune processes in MN, and epitope spreading from the N-terminus toward the C-terminus might associate with a poor clinical outcome and a reduced response to immunosuppressive therapy.^{18,19}

In this study, we identified the autoantibody binding sites in THSD7A. Furthermore, we characterized the association of individual epitope profiles and changes of epitope recognition patterns over time with the clinical presentation. Additionally, we experimentally investigated the immune response against THSD7A using animal models of active immunization.

METHODS

Design and Generation of THSD7A Fragments

THSD7A was split into three parts: d1_d4 (Ala-48 to Ala-423), d5_d10 (Thr-424 to Gln-831), and d11_d21 (Ser-832 to His-1535). To define more precise epitope regions, we designed fragments of THSD7A containing three or two domains each: d1_d2 (Ala-48 to Gln-192), d2_d3 (Trp-117 to Cys-246), d3_d4 (Gln-193 to Ala-423), d5_d6 (Thr-424 to Tyr-574), d7_d8 (Asp-575 to Thr-695), d9_d10 (Val-696 to Gln-831), d11_d12 (Ser-832 to Asp-959), d13_d14 (Lys-960 to Asn-1095), d15_d16 (Gln-1096 to Tyr-1220), d17_d18 (His-1221 to Tyr-1341), and d19_d21 (Arg-1342 to His-1535). An additional d1_d3 (Ala-48 to Cys-246) construct was designed for purification of domain-specific antibodies. All variants were generated by PCR and cloned into the eukaryotic expression vector pCSE2.5 (provided by Thomas Schirrmann, Braunschweig, Germany). This vector has been optimized for secretory protein production in suspension cultures of HEK293–6E

cells.²⁰ The cDNA of a full-length, flag-tagged THSD7A variant served as the PCR template (Origene). All constructs were designed to be secreted to the cell culture medium. All constructs contained a C-terminal 6× his tag. Full sequencing validated the accuracy of all constructs.

Cell Culture, Cell Transfection, and Recombinant Protein Expression

HEK293 cells were kept in culture and transfected with the generated constructs. Cells were harvested and lysed in 50 mM Tris (pH 7.4), 1 mM EDTA, 150 mM NaCl, and 1% Triton. All expressions were validated by Western blot and immunologic detection using an anti-his antibody (1:1000; Thermo Scientific, Cramlington, United Kingdom). Details on these procedures are presented in Supplemental Material.

Western Blot and Immunologic Detection

If reducing conditions were desired, samples were heated in 20% β -mercaptoethanol. Proteins were separated by electrophoresis and subsequently transferred to methanol-soaked polyvinylidene difluoride membranes. Membranes were then blocked for 2 hours at room temperature followed by incubation with the primary antibody. Sera (human, mouse, and rabbit) were diluted 1:100. All sera were tested using horseradish peroxidase-conjugated anti-human IgG4 and anti-total human IgG, and protein bands were visualized using a chemiluminescence substrate. Details on these procedures and the used materials are presented in Supplemental Material.

Native Blotting (Dot Blot Analyses) and Immunologic Detection

His-tagged thrombospondin type 1 (TSP-1) domain constructs (d1_d2 to d19_d21) were purified under native conditions using an Ni-NTA resin (His-Pur, 88221; Thermo Scientific) and applying the batch method according to the manufacturer's instructions. Purified proteins were then dotted on nitrocellulose membranes and allowed to dry for 10 minutes at room temperature. Membranes were then blocked in 4% dry milk in PBS plus Tween 0.08% (PBS-T) for 3 hours followed by incubation with human serum (1:100) or anti-his antibody (1:1000) in PBS-T with 0.5% dry milk. Horseradish peroxidase-conjugated secondary anti-human or anti-mouse IgG was used as the secondary antibody. Details of these procedures and the used material are presented in Supplemental Material.

Purification of Domain-Specific Antibodies from Patient Sera

The shortest protein fragment containing the epitope of interest was transferred to a polyvinylidene difluoride membrane in the highest possible quantity. The protein-containing part of the membrane was cut out and incubated in patient serum (1:100) in 0.5% skim milk in PBS-T overnight at 4°C with agitation. After washing the membrane three times with

PBS-T, the bound antibodies were eluted from the membrane by three subsequent incubations with 200 μ l IgG elution buffer for 5 minutes (Thermo Scientific) at room temperature. The eluted solution was immediately neutralized with 1 M Tris-HCl (pH 9). Before use as the primary antibody for immunologic detection, 0.5% skim milk in PBS-T was added.

Statistical Analyses

Remission of proteinuria was defined as proteinuria of <3.5 g/24 h and at least 50% reduction from the time of inclusion. Data are given as median and interquartile range (IQR). A Mann–Whitney *U* test was performed to assess for statistical significance. For analyses of categorical data, a Fisher exact test was performed. Statistical significance was defined as $P < 0.05$.

Animal Care

Wild-type male BALB/c mice (8–12 weeks old) were bred in the animal facility of the University Medical Center Hamburg-Eppendorf. Animals had free access to water and standard animal chow.

Immunization of Rabbits and Mice with THSD7A cDNA

A mixture of expression constructs encoding full-length mouse and human THSD7A was conjugated to 1- μ m gold particles (Bio-Rad Laboratories, Munich, Germany). These were ballistically injected into rabbits and mice at the antibody core unit of the University Medical Center Hamburg-Eppendorf. The rabbits received four immunizations in 3- to 6-week intervals, each with 12 shots of plasmid-conjugated gold particles (1 μ g DNA per 1 mg gold per shot). The mice received four immunizations in 3- to 6-week intervals, each with four shots of plasmid-conjugated gold particles (1 μ g DNA per 1 mg gold per shot). Serum was obtained 3 weeks after the last immunization. The specificity of the antiserum for native mouse and human THSD7A was verified using immunofluorescence staining of transfected Chinese hamster ovary cells as described previously.²¹ All animal experiments were performed according to national and institutional animal care and ethical guidelines, and they were approved by the veterinarian agency of Hamburg and the local animal care committee.

Epitope Domains in Mouse THSD7A

Eleven mouse TSP-1 fragments corresponding to the previously designed human TSP-1 constructs were designed: d1_d2 (Ala-37 to Gln-181), d2_d3 (Trp-106 to Glu-236), d3_d4 (Lys-182 to Ala-412), d5_d6 (Thr-413 to Tyr-563), d7_d8 (Asp-564 to Thr-684), d9_d10 (Val-685 to His-820), d11_d12 (Ser-821 to Asp-888), d13_d14 (Lys-889 to Asn-1084), d15_d16 (Gln-1085 to Tyr-1208), d17_d18 (His-1209 to Tyr-1329), and d19_d21 (Arg-1330 to Arg1523). All variants were generated by PCR, cloned into the eukaryotic expression vector pCSE2.5, and expressed in HEK293 cells as described above for human TSP-1 domains.

Immunohistochemical Analyses

Immunohistochemical analyses were performed essentially as described previously.²¹ Details are presented in Supplemental Material.

RESULTS

Domain Analyses of THSD7A

THSD7A is a glycosylated 250-kD type 1 transmembrane protein composed of a large extracellular N-terminal region, a single-pass transmembrane domain, and a short intracellular C-terminal tail.³ On the basis of automated basic local alignment search tool analyses, THSD7A was previously reported to contain 11 TSP-1 (Pfam domain PF00090) repeats.³ We now took into consideration the relative position of conserved cysteine, tryptophan, and arginine residues and performed position-sensitive iterative basic local alignment search tool searches and structure-based alignments of THSD7A with TSP-1 domains from the Protein Data Bank (pdb). This re-evaluation of the THSD7A architecture revealed a tandem string of 21 TSP-1 domains (d1–d21) (Figure 1A, Supplemental Figure 1), most of which are separated by short linkers of one to nine amino acid residues. These TSP-1 domains show high structural homology either to the TSP-1 domains of thrombospondin 1 (THBS1; pdb code 3r6b) or complement component 6 (C6; pdb code 3t5o; containing two TSP-1 domains) and F-spondin (pdb 1szl; containing one TSP-1 domain).^{22–24} THBS1 and C6 domains both consist of three antiparallel peptide strands (Figure 1B). The first strand contains two or three tryptophan residues that interlace with two or three arginine residues from the second strand. The three peptide strands are tightly connected by three disulfide bridges between cysteine residues. The first disulfide bridge connects the first strand and the third strand (C1–C5), and the second disulfide bridge connects the second strand and the third strand (C2–C6). However, THBS1 and C6 domains differ in the position of the third disulfide bridge. In THBS1, it connects the second and third strands (C3–C4), whereas in C6, it connects C4 to C0, a cysteine near the N-terminus of the first strand (Figure 1B).

The first two (N-terminal) TSP-1 domains of THSD7A are tandem THBS1-like domains, and the third and fourth TSP-1 domains are C6-like domains separated by a unique and highly basic coiled coil domain (Figure 1A). Domains d5–d21 are arranged in an alternating fashion of THBS1-like and C6-like domains. Six linker regions contain a proline residue, which is often found in linker regions of TSP-1 domains in the pdb and likely stabilizes the angle between the adjacent THBS1- and C6-like domains due to limited flexibility. The overall domain architecture of THSD7A is highly conserved in vertebrate evolution. It is found in all extant teleost and cartilaginous fish, including the elephant shark (*Callorhynchus milii*), the slowest evolving of all known vertebrates.²⁵

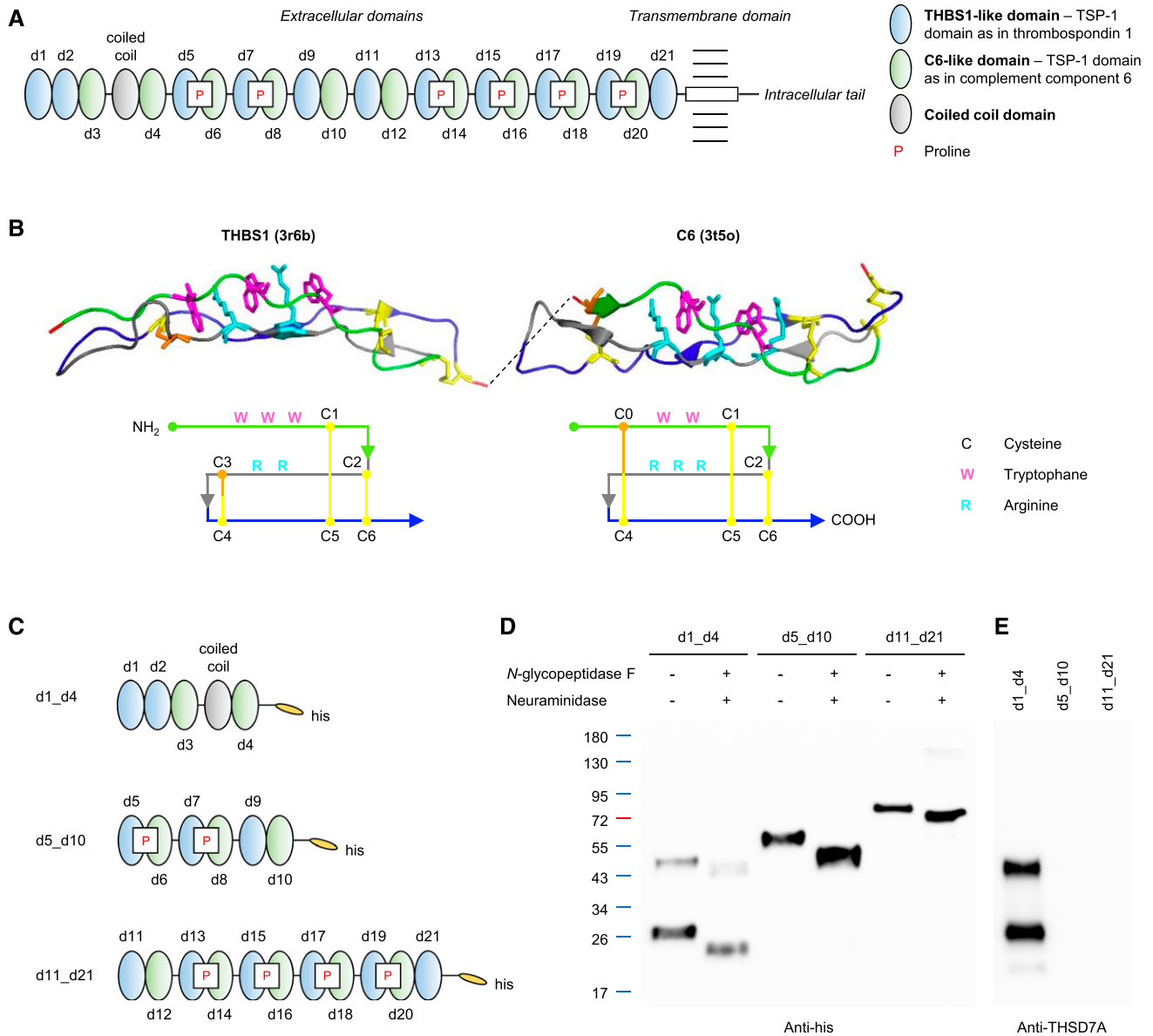


Figure 1. Structural analysis of thrombospondin type 1 domain-containing 7A (THSD7A) reveals 21 consecutive thrombospondin type 1 (TSP-1) domains. (A) Schematic view of the THSD7A structure. The extracellular part consists of 21 thrombospondin type 1 (TSP-1) domains (referred to as d1–d21) and one coiled coil domain. P, proline. (B) Predicted three-dimensional structure and schematic view of THBS1- and complement component 6 (C6)-like domains with three strand-connecting disulfide bonds each (yellow/orange). (C) Schematic view of the three his-tagged THSD7A fragments. (D) Western blot of the three THSD7A fragments before and after deglycosylation with *N*-glycopeptidase F and neuraminidase with an anti-his antibody under reducing conditions. (E) Western blot of THSD7A fragments with a coiled coil domain-directed commercial antibody.

Expression of Three THSD7A Fragments

To define epitope regions targeted by anti-THSD7A autoantibodies, we designed three fragments of the antigen. The first fragment contained the first four TSP-1 domains, including the coiled coil domain interposed between the two C6-like domains (d1_d4) (Figure 1C). The middle fragment contained the three subsequent THBS1–C6 pairs (d5_d10), and the third fragment ranged from the 11th to the last TSP-1 domain shortly before the transmembrane region (d11_d21). Transfection of HEK293 cells with subsequent Western blotting under reducing

and nonreducing conditions revealed efficient expression of all constructs (Figure 1D, Supplemental Figure 2). The fragments d5_d10 and d11_d21 showed single bands at 60 and 90 kD, respectively, whereas detection of d1_d4 revealed two distinct bands, the predicted band at 50 kD and an additional band at 30 kD, suggesting post-translational proteolytic cleavage.²⁶ All three fragments were found to be glycosylated and showed a shift in size after enzymatic deglycosylation with *N*-glycopeptidase F and neuraminidase (Figure 1D). Immunologic detection with a commercially available anti-THSD7A

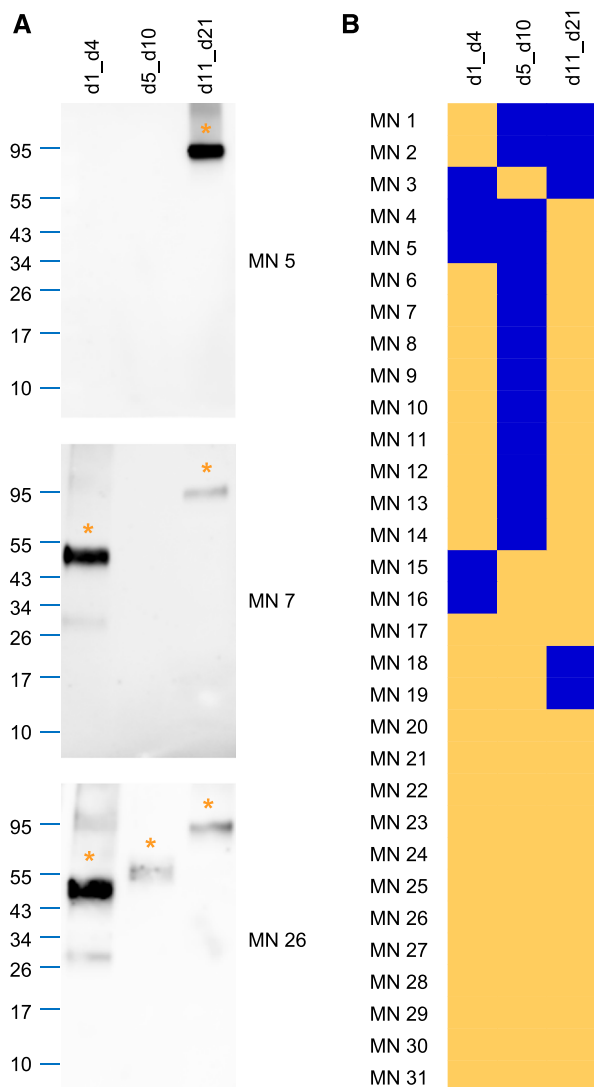


Figure 2. Patient autoantibodies recognize thrombospondin type 1 (TSP-1) domains along the whole extracellular part of thrombospondin type 1 domain-containing 7A (THSD7A). (A) Representative Western blots of the d1_d4, d5_d10, and d11_d21 fragments with three different sera under nonreducing conditions (serum dilution 1:100, anti-IgG4 as secondary antibody). Asterisks mark the recognized THSD7A fragments. (B) Heat map depicting the reactivity profiles of sera from 31 patients with THSD7A-associated membranous nephropathy (MN) with the three THSD7A fragments. Yellow indicates serum recognition of the construct, whereas blue indicates no reactivity. Patients were clustered according to their epitope recognition profiles.

antibody raised against the coiled coil domain exclusively recognized the d1_d4 construct (Figure 1E).

Clinical Characteristics and Serum Recognition of the Three THSD7A Fragments in the Study Cohort

We tested the reactivity of sera from 31 patients with biopsy-proven MN with the three THSD7A fragments by Western

blotting under nonreducing conditions. Before study inclusion, all patients tested positive for anti-THSD7A antibodies in the serum by a recently developed indirect immunofluorescence test.¹¹ Nineteen (61%) patients were men, and the median age was 67 years old (IQR, 53.5–74.5 years old). The median time between renal biopsy and first serum collection was 1 month (IQR, 0.0–1.0 months), median proteinuria at the time of first serum collection was 7.1 g/d (IQR, 4.8–9.9 g/d), and median serum creatinine was 1.3 mg/dl (IQR, 0.8–1.6 mg/dl). Nine of the patients were diagnosed with a malignant tumor before diagnosis of MN or during follow-up (median time, 3 months; IQR, 1–6 months).

All sera reacted with at least one of the expressed constructs (Figure 2, Supplemental Figure 3). The d1_d4 and the d11_d21 constructs were each recognized by 84% of patient sera, whereas the d5_d10 construct was recognized by 58% of patient sera. More than one fragment was recognized by 84%, and all three fragments were recognized by 42% of the sera. Sera from healthy control individuals that were analyzed under identical conditions failed to react with any of the THSD7A fragments (Supplemental Figure 4A). Taken together, these results suggest the presence of multiple autoantibody binding sites in THSD7A, with most reactivity in the more N-terminal and the more C-terminal extracellular parts of the antigen.

Identification of Epitope Regions in THSD7A

To more deeply map the epitopes for anti-THSD7A autoantibodies, we designed smaller fragments of the THSD7A antigen. These fragments contained two to three adjacent TSP-1 domains (d1_d2, d2_d3, d3_d4, d5_d6, d7_d8, d9_d10, d11_d12, d13_d14, d15_d16, d17_d18, and d19_d21). Transfection of HEK293 cells with subsequent Western blotting revealed efficient expression of all constructs (Figure 3A, Supplemental Figure 5). All constructs were found to be glycosylated, except d1_d2 and d11_d12 (Supplemental Figure 6).

We next tested the reactivity of the 31 sera with the TSP-1 domain constructs using Western blotting under nonreducing conditions. All but the d3_d4 and the d19_d21 constructs were each recognized by at least three of the sera (Figure 3B, Supplemental Figure 7). Sera that reacted with d1_d4 in the first screening round also reacted with d1_d2 in the second screening round, whereas only nine (35%) of these sera additionally recognized d2_d3. Serum reactivity was independent of the glycosylation status of the protein (Supplemental Figure 8). The recognition of the TSP-1 domain constructs corresponded to the previously described recognition of the larger THSD7A fragments in all but one serum (MN 17). The one mismatched serum was positive for all three larger THSD7A fragments but failed to react with one of the smaller TSP-1 domain constructs in the d11_d21 area (Supplemental Figures 3 and 7). This suggests that this particular epitope was not covered with the chosen antigen fragmentation or that the sensitivity of detection was too low to show autoantibody binding in this case. Sera from healthy control individuals

failed to react with any of the TSP-1 domain constructs (Supplemental Figure 4B).

To investigate the presence of epitopes that are sensitive to denaturation by SDS, we applied native blotting (dot blot analysis). All constructs were well recognized by an anti-his antibody under native conditions (Figure 3C). Subsequently, we tested 30 of the previously tested 31 patients with available serum. Twenty-one sera (70%) showed identical epitope profiles in native and Western blotting. However, three sera did not recognize a TSP-1 domain construct that was previously recognized using Western blotting (Supplemental Figure 9A), and two sera did not show any reactivity in native blotting (data not shown). Interestingly, four sera recognized additional TSP-1 domain constructs in native blotting, showing the presence of denaturation-sensitive epitopes in these patients (Figure 3C, Supplemental Figure 9B). Epitope recognition profiles as deduced from Western blotting and native blotting are shown in Figure 3D. Altogether, 28 of 31 (90%) serum samples recognized multiple domains, and d1_d2 (amino acids 48–192) was most frequently recognized (27 of 31 patients; 87%) followed by d15_d16, d9_d10, and d13_d14, which were recognized by 61%, 52%, and 45% of the sera, respectively (Figure 3E).

All Western blot experiments were performed using anti-human IgG4 and anti-total human IgG as secondary antibodies. Two sera recognized additional TSP-1 domain constructs when tested with anti-total IgG compared with anti-IgG4, showing the presence of domain-specific autoantibodies different from IgG4 in these patients (Figure 4, A and B). Both patients did not have an associated malignant disease. Taken together, these data show that autoantibodies from patients with THSD7A-associated MN preferentially bind to the most N-terminal region of THSD7A (amino acids 48–192) and that most sera recognize multiple epitope domains present in THSD7A.

Domain and Conformation Specificity of Identified Autoantibodies

We next investigated whether the identified autoantibodies were indeed distinct domain-specific antibodies or whether one clone of antibodies recognized several epitopes along the antigen due to sequence homology between the TSP-1 domains (Supplemental Figure 1A). We purified domain-specific IgG using recombinant d1_d3 and d9_d10 from a patient serum that recognized d1_d2, d7_d8, and d9_d10 (Figure 4C). The d1_d3-purified antibodies exclusively recognized d1_d2, whereas the d9_d10-purified antibodies showed exclusive reactivity with d9_d10 in Western blot analysis (Figure 4, D and E). The experiment was repeated with three more patient sera with consistent results (not shown). These results indicate that the variety of domain recognition in our patients is due to distinct autoantibodies against several epitopes present in THSD7A.

Autoantibodies from patients with THSD7A-associated MN have been reported to recognize THSD7A exclusively

under nonreducing conditions in Western blot analysis, suggesting autoantibody binding to a conformation-dependent epitope within the antigen.³ We tested nine of the previously analyzed sera under both reducing and nonreducing conditions in a standardized side by side Western blot experiment. Sera were probed on full-length THSD7A; the d1_d4, d5_d10, and d11_d21 fragments; and the small TSP-1 domain constructs. Under reducing conditions, all investigated sera completely lost reactivity with full-length THSD7A; partially or completely lost reactivity with d1_d4, d5_d10, and d11_d21; and completely retained reactivity with the small TSP-1 domain constructs (Figure 5) (not shown). Sera from healthy control individuals failed to react with the TSP-1 domain constructs under reducing conditions (Supplemental Figure 4). These experiments suggest that the small TSP-1 fragments are capable of refolding after loss of the reducing agent during protein transfer.

Association of Epitope Recognition Profiles with Clinical Characteristics and Epitope Recognition during Follow-Up

We next analyzed the association of the THSD7A epitope profiles (Figure 3D) with clinical characteristics of the study cohort (Table 1). Patients whose sera recognized only one or two TSP-1 domain constructs had significantly lower anti-THSD7A antibody levels and statistically nonsignificant lower proteinuria compared with patients whose sera recognized at least three TSP-1 domain constructs ($P=0.02$ and $P=0.07$, respectively). Remission of proteinuria was achieved by 86% of patients whose sera recognized one or two TSP-1 domain constructs, but it was only achieved by 50% of patients whose sera recognized three or more TSP-1 domains ($P=0.18$) (Table 1).

Follow-up sera were available from 16 of 31 patients in the study, and they were examined for changes in epitope recognition over time. In five patients, epitope profiles did not change during follow-up (Supplemental Figure 10). All of these patients had stable anti-THSD7A antibody levels as measured by immunofluorescence test and nephrotic-range proteinuria throughout the follow-up time. Sera from seven patients lost reactivity with one or more constructs (Supplemental Figure 11). The anti-THSD7A antibody levels decreased in six of these patients, and five patients had a remission of proteinuria. The remaining four patients had a change in their epitope profile during follow-up (Supplemental Figure 12). We found no specific patterns for the loss or gain of epitope recognition (*i.e.*, preferential loss or gain of reactivity with one specific TSP-1 domain construct compared with another) (Supplemental Table 1).

Immune Response against THSD7A after Active Immunization

We next evaluated the epitope regions in human and mouse THSD7A that are targeted by antibodies raised against THSD7A in three rabbits by coimmunization with human

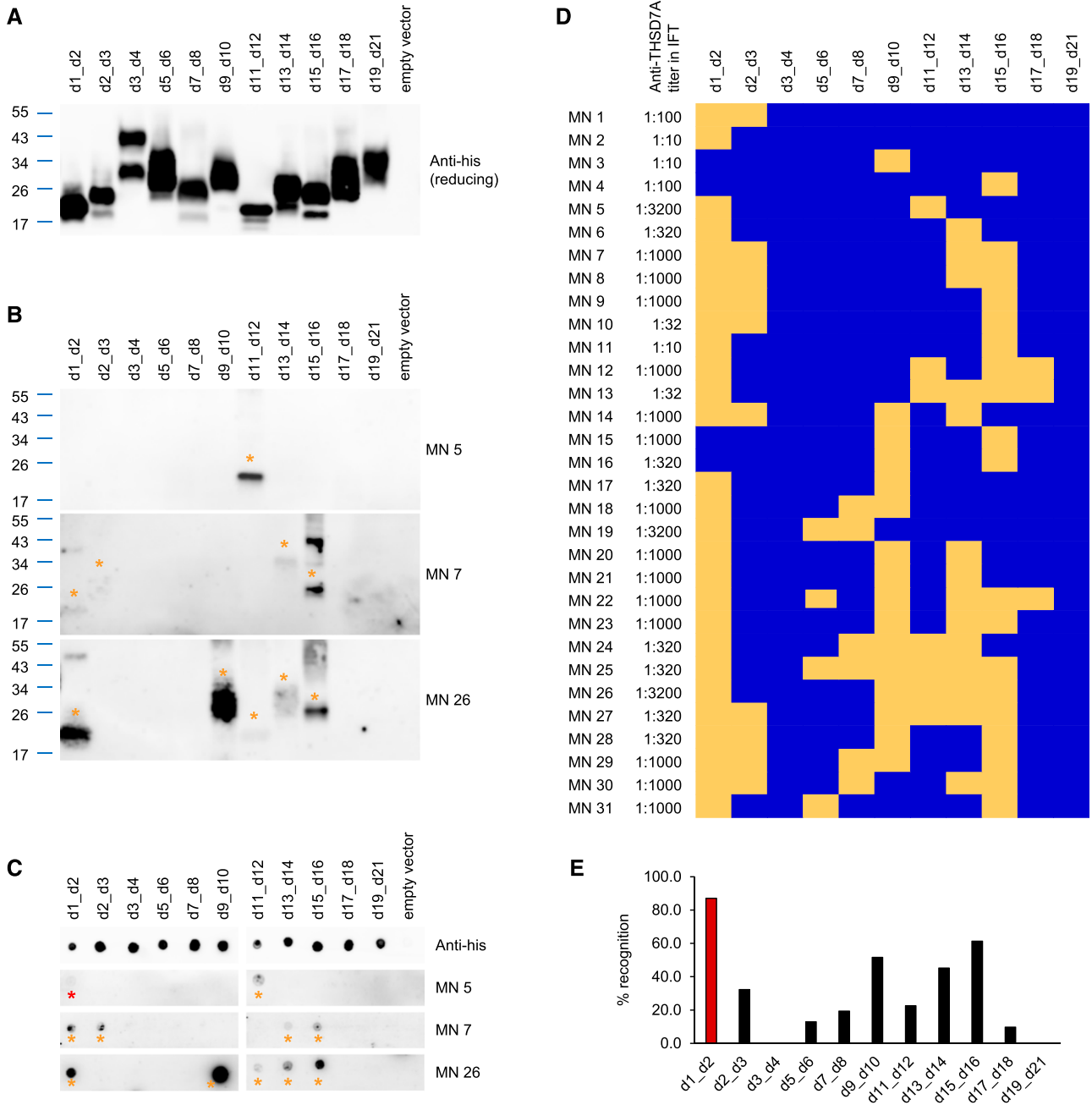


Figure 3. Patient autoantibodies recognize multiple epitopes in thrombospondin type 1 domain-containing 7A (THSD7A) with a predominance for the most N-terminal region. (A) Western blot of HEK293 cell-expressed soluble thrombospondin type 1 (TSP-1) domain constructs with an anti-his antibody under reducing conditions. (B) Representative Western blots of the TSP-1 domain constructs with three different sera under nonreducing conditions (serum dilution 1:100, anti-IgG4 as secondary antibody). Asterisks mark the recognized TSP-1 domain constructs. (C) Native blot (dot blot) analyses of the TSP-1 domain constructs with an anti-his antibody (row 1) and three representative sera (rows 2–4). Yellow asterisks mark the recognized TSP-1 domain constructs that were also recognized using Western blotting, whereas the red asterisk marks an additional TSP-1 domain recognition (MN 5). (D) Heat map depicting reactivity profiles of sera from all 31 patients with the small TSP-1 domain constructs as deduced from nonreduced Western blotting and native blotting. Yellow indicates serum recognition of the construct, whereas blue indicates no reactivity. IFT, indirect immunofluorescence test. (E) Recognition of the individual TSP-1 domains by patient sera in percentages.

and mouse THSD7A cDNA. We have previously shown that these antibodies induce MN with severe nephrotic syndrome when transferred into mice.²¹ A detailed sequence analysis of

mouse THSD7A showed that it shares over 90% of amino acid sequence homology with human THSD7A and that it is also composed of 21 TSP-1 domains with the identical pattern of

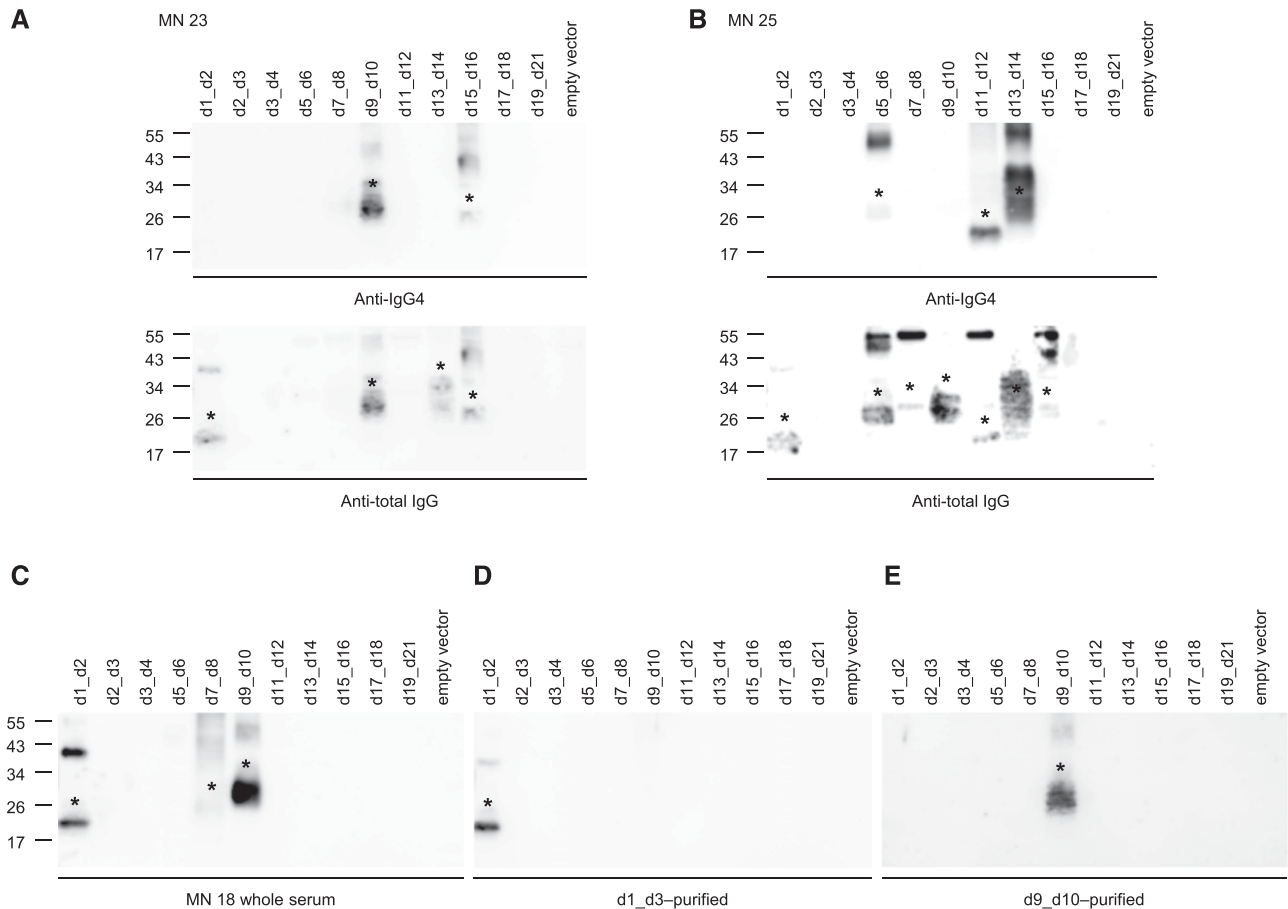


Figure 4. Patient autoantibodies are IgG4-predominant and domain-specific. (A and B) Western blot under nonreducing conditions of TSP-1 domain constructs with sera from two patients with thrombospondin type 1 domain-containing 7A (THSD7A)-associated membranous nephropathy (MN) using anti-IgG4 (upper panels) and anti-total IgG (lower panels) as secondary antibodies. Asterisks mark the recognized TSP-1 domain constructs. (C) Western blot under nonreducing conditions of TSP-1 domain constructs with serum from one patient with THSD7A-associated MN. (D and E) Antibodies that were purified using recombinant (D) d1_d3 and (E) d9_d10 exclusively bound d1_d2 and d9_d10, respectively. Asterisks mark the recognized TSP-1 domain constructs.

THBS1- and C6-like domains (Supplemental Figure 13). Consequently, we used the same cloning and expression techniques for the mouse TSP-1 domains as described for the human TSP-1 domains. All mouse TSP-1 domain constructs were well expressed in HEK293 cells and secreted to the culture medium (Figure 6A). We tested the three rabbit antisera for their recognition of human and mouse TSP-1 domains under nonreducing conditions. Strikingly, all three rabbit antisera recognized the most N-terminal region d1_d2 of both human and mouse THSD7A (Figure 6, B and C, Supplemental Figure 14), which was also the most frequently recognized epitope region in our patient cohort (Figure 3E). There is no lower homology between the rabbit, mouse, and human proteins in the d1_d2 region compared with the other TSP-1 domains (Supplemental Table 2). Therefore, a lack of homology in this region cannot be the reason for the preferred generation of autoantibodies against the most N-terminal region of THSD7A. Interestingly, the highly pathogenic rabbit

sera additionally recognized epitope domains in the more C-terminal region of mouse THSD7A, also resembling the situation found in our patient cohort.

In a similar approach, we immunized four mice by ballistic cDNA immunization with a mixture of human and mouse THSD7A cDNA. As controls, four mice were mock immunized. THSD7A-immunized mice generated antibodies that recognized human but not mouse THSD7A (Figure 6D), showing that self-tolerance could not be overcome with this particular immunization technique. Accordingly, mice did not show glomerular binding of mouse IgG in immunohistochemical analysis (Figure 6E) and did not develop proteinuria (not shown). Notably, sera from all THSD7A-immunized mice also recognized d1_d2 (Figure 6, F and G). As for rabbit and human THSD7A, the amino acid sequence homology in the N-terminal region of mouse and human THSD7A is comparable (approximately 90% identity) with that of the other TSP-1 domains (Supplemental Table 2), indicating that

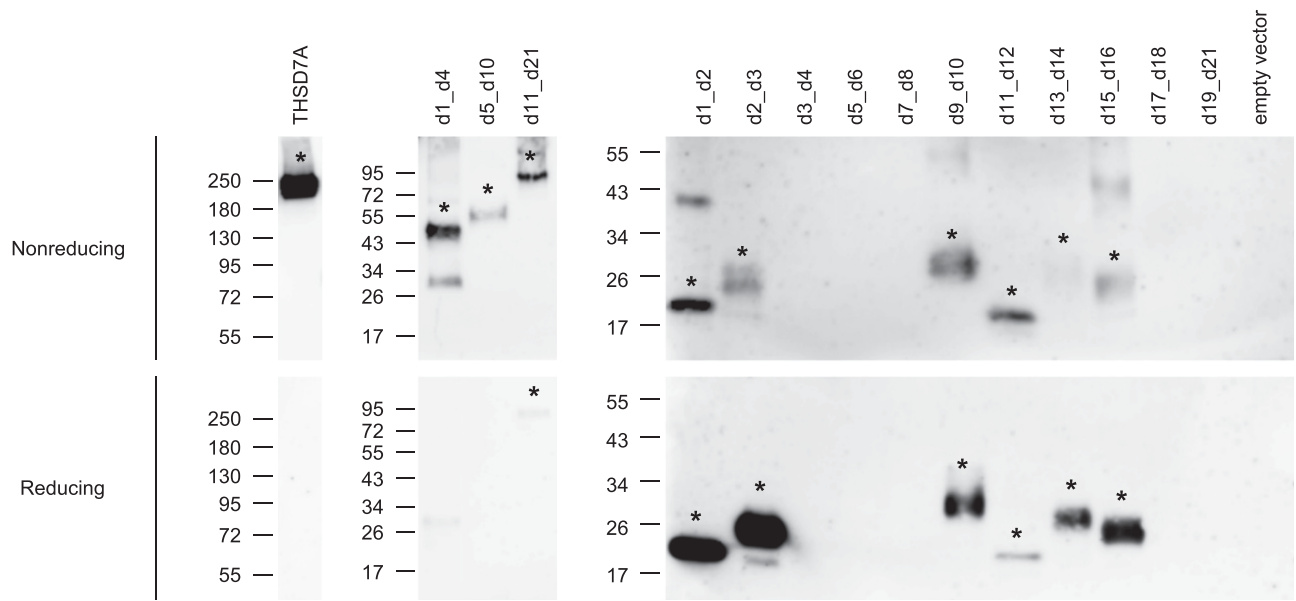


Figure 5. Patient autoantibodies recognize conformation-dependent epitopes in thrombospondin type 1 domain-containing 7A (THSD7A). Images depict Western blots of full-length THSD7A, the three THSD7A fragments, and the small thrombospondin type 1 (TSP-1) domain constructs with one representative serum (MN 27) under nonreducing (upper panels) and reducing conditions (lower panels).

differences in the amino acid sequence are not the predominant stimulus for the animals' immune system to target this region. Taken together, these data show that induced rabbit and mouse anti-THSD7A antibodies, like patient autoantibodies, predominantly target the most N-terminal domains of THSD7A.

DISCUSSION

This study identifies the epitope regions in THSD7A that are targeted by autoantibodies from patients with MN. Using comprehensive sequence alignments, we characterized the

extracellular part of THSD7A as a series of 21 TSP-1 domains. On the basis of their amino acid sequence, these TSP-1 domains can be further classified as either THBS1-like or C6-like. THBS1 itself acts as an adhesive glycoprotein that can interact with components of the extracellular matrix,^{27–30} cell receptors,^{31–37} and proteases,^{38,39} possibly leading to activation of downstream signaling pathways, alterations of protein localization, proteolytic processing, and protein internalization.⁴⁰ The homology of the THBS1-like domains in THSD7A with THBS1 may give a hint on the presently unknown biologic functions of THSD7A on podocytes and allow speculation on potential pathomechanisms in THSD7A-associated MN.

Table 1. Epitope recognition and clinical characteristics of the cohort

Clinical Characteristics	Sera with Recognition of One or Two TSP-1 Domain Constructs	Sera with Recognition of More Than Two TSP-1 Domain Constructs	P Value
No. of patients (%)	10 (32)	21 (68)	N/A
No. of epitopes, median (IQR)	2.0 (1.0–2.0)	4.0 (4.0–5.0)	<0.001
Age, yr, median (IQR)	67.0 (52.0–76.5)	65.0 (54.0–69.0)	0.75
Men (%)	5 (50)	14 (67)	0.45
Proteinuria, g/d, median (IQR)	5.8 (3.4–7.4)	7.7 (5.3–10.7)	0.07
Serum creatinine, mg/dl, median (IQR)	1.2 (0.9–1.6)	1.2 (0.8–1.8)	0.69
Anti-THSD7A antibody level, median (IQR)	210 (32–320)	1000 (320–1000)	0.02
Patients with malignancy (%)	3 (30)	6 (29)	>0.99
Patients with partial or complete remission of proteinuria during follow-up (%)	6 of 7 (86)	8 of 16 (50)	0.18

Follow-up data on proteinuria were available for 23 of the patients included in our cohort. TSP-1, thrombospondin type 1; N/A, not applicable; IQR, interquartile range; THSD7A, thrombospondin type 1 domain-containing 7A.

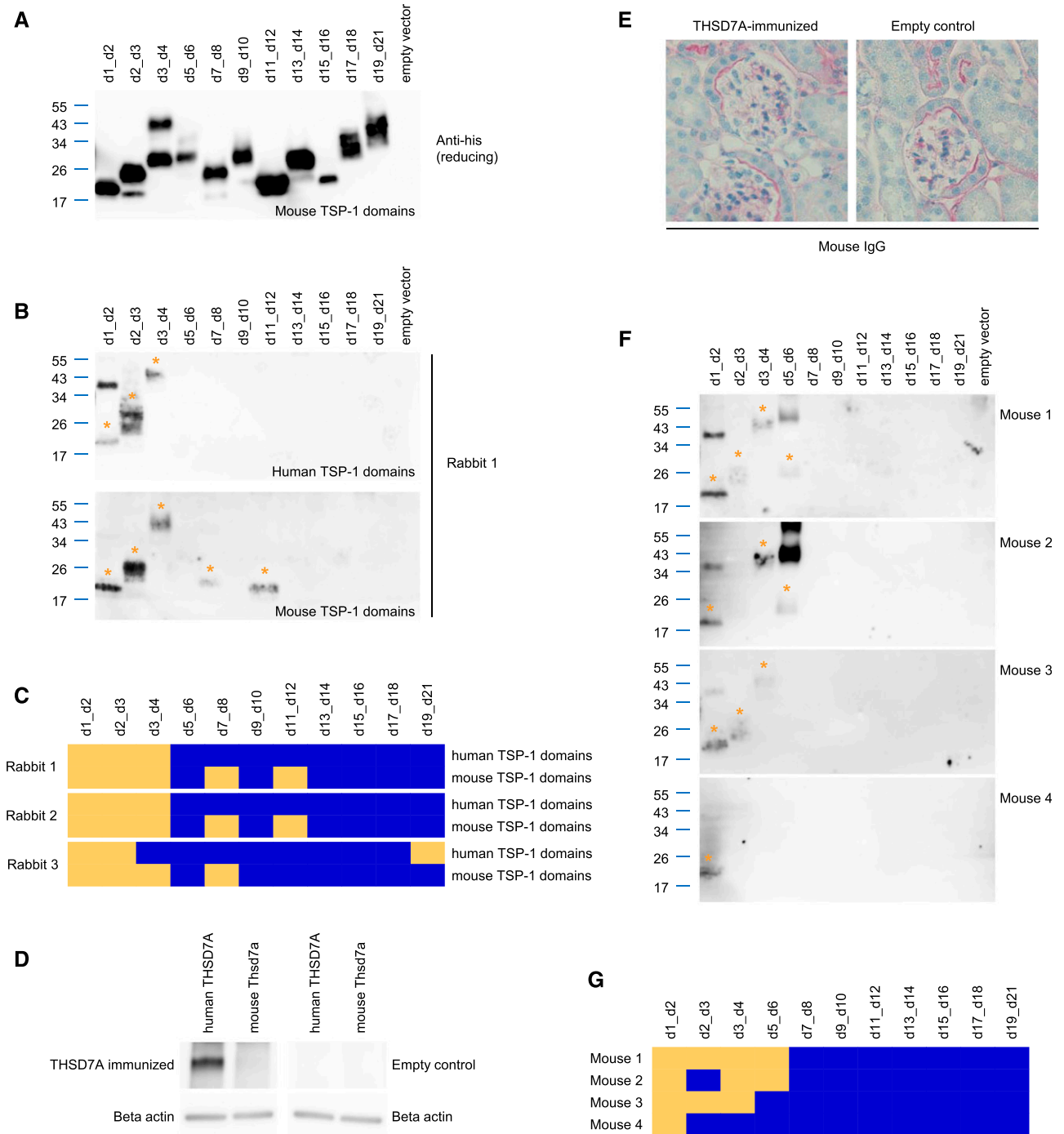


Figure 6. Rabbits and mice generate antibodies against the most N-terminal region of thrombospondin type 1 domain-containing 7A (THSD7A) after coimmunization with human and mouse THSD7A cDNA. (A) Western blot of HEK293 cell-expressed soluble mouse thrombospondin type 1 (TSP-1) domain constructs with an anti-his antibody under reducing conditions. (B) Western blot under non-reducing conditions of human (upper panel) and mouse (lower panel) TSP-1 domain constructs with one representative rabbit antiserum (serum dilution 1:100). Asterisks mark the recognized TSP-1 domain constructs. (C) Heat map depicting the reactivity profiles of three rabbit antisera with human and mouse TSP-1 domain constructs in Western blot analysis. Yellow indicates serum recognition of the construct, whereas blue indicates no reactivity. (D) Representative Western blot under nonreducing conditions of recombinant human and mouse THSD7A with serum from one of four mice that were immunized with a combination of human and mouse THSD7A cDNA. Four mice were mock immunized (empty control). (E) Representative immunohistochemical staining for mouse IgG in one THSD7A-immunized mouse and one control mouse. (F) Western blot under nonreducing conditions and (G) heat map analysis of reactivity of four mouse antisera with the human TSP-1 domain constructs. Asterisks in F mark the recognized TSP-1 domain constructs. Yellow in G indicates serum recognition of the construct, whereas blue indicates no reactivity.

In an unbiased approach to identify the epitope regions in THSD7A, we designed three consecutive fragments of the antigen and tested for recognition by patient autoantibodies. Most patient sera reacted with several THSD7A fragments with a predominance for the more N-terminal and the more C-terminal part of the antigen. Additional epitope mapping revealed that the d1_d2 construct (amino acids 48–192) was recognized by 87% of the sera, indicating that the dominant epitope in THSD7A-associated MN is located within the most N-terminal part of the antigen. In contrast, the reactivity in the more C-terminal part distributed over several epitope domains. Interestingly, the preference of autoantibodies for the most N-terminal region of the antigen is a similarity of THSD7A- and PLA2R1-associated MN. However, whereas patient autoantibodies bind to the most N-terminal region of PLA2R1 in all investigated patients,^{17,18} this is not the case for THSD7A. Furthermore, most sera from patients with THSD7A-associated MN recognize more than one antigen domain, and epitope profiles vary between the different patients. This is in contrast to PLA2R1, for which only three epitope regions have been identified so far.¹⁸ It is known from other antibody-mediated autoimmune diseases, such as Grave disease, pemphigus vulgaris, and anti-brush border antibody disease, that autoantibodies target a great variety of epitopes that distribute over the whole extracellular regions of the respective autoantigens but with an N-terminal predominance.^{41–44}

Compared with patients whose sera recognized only one or two TSP-1 domains, patients whose sera recognized more than two TSP-1 domains had higher anti-THSD7A antibody levels, tended to higher levels of proteinuria, and achieved a remission of proteinuria in the observation period less often. During follow-up, seven patients lost recognition of one or more epitopes, which paralleled a decrease in anti-THSD7A antibody levels and in most patients, a remission of proteinuria. From these data it is not clear whether it is the individual epitope profile, the number of recognized epitopes, the antibody titer alone, or a combination of these factors that drive disease. Further studies are needed to investigate these issues.

The phenomenon of epitope spreading has been described in human antibody-mediated autoimmune diseases^{45–49} and different autoimmune animal models.^{50–53} In the experimental MN model of Heymann nephritis, proteinuria increased with epitope spreading.⁵⁴ This is in accordance with PLA2R1-associated MN, where epitope spreading was reported to relate with disease outcome.^{18,19} In our study, we did not find clear evidence for epitope spreading over time due to the small number of patients with THSD7A-associated MN and serologic follow-up. In the future, larger cohorts of patients will be needed to further dissect the relationship of epitope profiles at diagnosis and the possible phenomenon of epitope spreading with disease activity and long-term clinical outcome.

Our study has several limitations. First, we did not use a quantitative method, such as ELISA, to determine domain-specific autoantibody titers. Therefore, we cannot compare domain-

specific antibody levels between patients and correlate domain-specific titers with disease activity and outcome. Second, Western blot experiments were standardized regarding protein loading (on the basis of anti-his reactivity under reducing conditions) and serum dilution (1:100) due to a limited amount of patient serum. It seems likely that a change in these parameters, such as higher or lower dilution of the used serum, may have led to slightly different epitope profiles for some patients. Third, antibody binding sites were mapped to peptides of 100–120 amino acids. Additional work is needed to define the genuine epitopes on the level of ten to 15 amino acids.

To investigate antibody generation against THSD7A, we analyzed rabbits and mice that were immunized with a combination of human and mouse THSD7A cDNA. Remarkably, all animals raised an antibody response against the first two N-terminal domains d1_d2 of both mouse and/or human THSD7A, and most animals recognized several other domains, resembling the situation in our patient cohort. Thereby, the N-terminus of THSD7A does not predispose to antibody formation due to a particularly low homology in this area between the three species orthologs. This indicates that other features of the N-terminal region, such as epitope accessibility, might be responsible for the predominant antibody response. However, autoantibodies were induced against foreign proteins in these experiments, and importantly, the pathogenicity of antibodies targeting specific domains within the antigen remains to be investigated in future studies.

Identification of the epitopes that are targeted by autoantibodies from patients with THSD7A-associated MN is of high interest for future investigations for the following reasons. (1) Autoimmunity may emerge as a result of molecular mimicry between microbial or tumor antigens and host proteins.^{55,56} Defining the precise antibody binding site(s) would allow alignments with microbial proteins to uncover yet unknown links between infections or tumors and primary MN. (2) The TSP-1 domains in THSD7A might differentially interact with other molecules and/or induce intracellular signaling.⁴⁰ Interference of autoantibodies with these functions could represent a pathomechanism in the mediation of podocyte damage in MN. (3) Epitope blocking/competition therapy or systemic autoantibody extraction using the antibody binding fragment could constitute innovative therapies for patients with antibody-mediated autoimmune diseases.⁵⁷ Also, expression of epitope-containing domains on T cells in combination with intracellular signaling domains can direct T cells to eliminate autoantibody-producing B cells through specific binding to the B cell receptor,⁵⁸ representing another potential therapeutic intervention for patients with autoimmune primary MN that requires knowledge of the antibody binding domains.

In conclusion, our study shows that an autoimmune process with polyreactive IgG is part of the pathogenesis of THSD7A-associated MN. Additionally, we provide clinical and experimental evidence that the principal immune response targets the most N-terminal part of the protein, potentially enabling epitope-specific therapies in the future.

ACKNOWLEDGMENTS

The authors thank Eugen Kinzler and Daniela Bergleiter (III. Medizinische Klinik, University Medical Center Hamburg-Eppendorf, Hamburg, Germany) for technical assistance and Gudrun Dubberke, Fabienne Seyfried, and Sarah Hewald (Institute of Immunology, University Medical Center Hamburg-Eppendorf, Hamburg, Germany) for technical assistance with cDNA immunization.

This study was supported by grants from the Deutsche Forschungsgemeinschaft as part of the Sonderforschungsbereich 1192 (project B1 to E.H. and R.A.K.S.; project B2 to G.Z., R.A.K.S., and N.M.T.; and project B5 to F.K.-N.). E.H. is supported by the Else Kröner-Fresenius Stiftung.

The following colleagues participated in the recruitment of the patients for this study (in alphabetical order): Bahte S, Beckmann S, Bokemeyer D, Born B, Boser M, Budde K, Dellanna F, Ferber J, Fielitz JG, Floege J, Gerth J, Groll J, Grosser S, Hegner B, Hetzel GR, Hollenbeck M, Hoyer J, Isbell LK, Jabs W, Jacobson J, Kidder D, Koch C, Köhler S, Kortus-Götze B, Köstler F, Kresse S, Langer T, Leidig B, Messtorff K, Möller J, Peitzmeier C, Rosenburg C, Rump C, Sass C, Schmidtmann K, Schnegelsberg O, Tacuri-Strasser D, Thiele I, Tiedeken P, Treiber W, Vitu J, Vosskühler A, Walz G, Weiner S, and Worch P.

DISCLOSURES

None.

REFERENCES

- Ruggenti P, Fervenza FC, Remuzzi G: Treatment of membranous nephropathy: Time for a paradigm shift. *Nat Rev Nephrol* 13: 563–579, 2017
- Beck LH Jr., Bonegio RG, Lambeau G, Beck DM, Powell DW, Cummins TD, et al.: M-type phospholipase A2 receptor as target antigen in idiopathic membranous nephropathy. *N Engl J Med* 361: 11–21, 2009
- Tomas NM, Beck LH Jr., Meyer-Schwesinger C, Seitz-Polski B, Ma H, Zahner G, et al.: Thrombospondin type-1 domain-containing 7A in idiopathic membranous nephropathy. *N Engl J Med* 371: 2277–2287, 2014
- Hofstra JM, Beck LH Jr., Beck DM, Wetzels JF, Salant DJ: Anti-phospholipase A₂ receptor antibodies correlate with clinical status in idiopathic membranous nephropathy. *Clin J Am Soc Nephrol* 6: 1286–1291, 2011
- Hoxha E, Harendza S, Pinnschmidt H, Panzer U, Stahl RA: PLA2R antibody levels and clinical outcome in patients with membranous nephropathy and non-nephrotic range proteinuria under treatment with inhibitors of the renin-angiotensin system. *PLoS One* 9: e110681, 2014
- Hoxha E, Harendza S, Pinnschmidt H, Panzer U, Stahl RA: M-type phospholipase A2 receptor autoantibodies and renal function in patients with primary membranous nephropathy. *Clin J Am Soc Nephrol* 9: 1883–1890, 2014
- Beck LH Jr., Fervenza FC, Beck DM, Bonegio RG, Malik FA, Erickson SB, et al.: Rituximab-induced depletion of anti-PLA2R autoantibodies predicts response in membranous nephropathy. *J Am Soc Nephrol* 22: 1543–1550, 2011
- Hofstra JM, Debiec H, Short CD, Pellé T, Kleta R, Mathieson PW, et al.: Antiphospholipase A2 receptor antibody titer and subclass in idiopathic membranous nephropathy. *J Am Soc Nephrol* 23: 1735–1743, 2012
- Stahl R, Hoxha E, Fechner K: PLA2R autoantibodies and recurrent membranous nephropathy after transplantation. *N Engl J Med* 363: 496–498, 2010
- Gupta G, Fattah H, Ayalon R, Kidd J, Gehr T, Quintana LF, et al.: Pre-transplant phospholipase A2 receptor autoantibody concentration is associated with clinically significant recurrence of membranous nephropathy post-kidney transplantation. *Clin Transplant* 30: 461–469, 2016
- Hoxha E, Beck LH Jr., Wiech T, Tomas NM, Probst C, Mindorf S, et al.: An indirect immunofluorescence method facilitates detection of thrombospondin type 1 domain-containing 7A-specific antibodies in membranous nephropathy. *J Am Soc Nephrol* 28: 520–531, 2017
- Hoxha E, Wiech T, Stahl PR, Zahner G, Tomas NM, Meyer-Schwesinger C, et al.: A mechanism for cancer-associated membranous nephropathy. *N Engl J Med* 374: 1995–1996, 2016
- Wang J, Cui Z, Lu J, Probst C, Zhang YM, Wang X, et al.: Circulating antibodies against thrombospondin type-I domain-containing 7A in Chinese patients with idiopathic membranous nephropathy. *Clin J Am Soc Nephrol* 12: 1642–1651, 2017
- Pedchenko V, Bondar O, Fogo AB, Vanacore R, Voziyan P, Kitching AR, et al.: Molecular architecture of the Goodpasture autoantigen in anti-GBM nephritis. *N Engl J Med* 363: 343–354, 2010
- Roth AJ, Ooi JD, Hess JJ, van Timmeren MM, Berg EA, Poulton CE, et al.: Epitope specificity determines pathogenicity and detectability in ANCA-associated vasculitis. *J Clin Invest* 123: 1773–1783, 2013
- Kao L, Lam V, Waldman M, Glassock RJ, Zhu Q: Identification of the immunodominant epitope region in phospholipase A2 receptor-mediated autoantibody binding in idiopathic membranous nephropathy. *J Am Soc Nephrol* 26: 291–301, 2015
- Fresquet M, Jowitt TA, Gummadova J, Collins R, O’Cualain R, McKenzie EA, et al.: Identification of a major epitope recognized by PLA2R autoantibodies in primary membranous nephropathy. *J Am Soc Nephrol* 26: 302–313, 2015
- Seitz-Polski B, Dolla G, Payré C, Girard CA, Polidori J, Zorzi K, et al.: Epitope spreading of autoantibody response to PLA2R associates with poor prognosis in membranous nephropathy. *J Am Soc Nephrol* 27: 1517–1533, 2016
- Seitz-Polski B, Debiec H, Rousseau A, Dahan K, Zaghrini C, Payre C, et al.: Phospholipase A2 receptor 1 epitope spreading at baseline predicts reduced likelihood of remission of membranous nephropathy. *J Am Soc Nephrol* 29: 401–408, 2018
- Jäger V, Büssow K, Wagner A, Weber S, Hust M, Frenzel A, et al.: High level transient production of recombinant antibodies and antibody fusion proteins in HEK293 cells. *BMC Biotechnol* 13: 52, 2013
- Tomas NM, Meyer-Schwesinger C, von Spiegel H, Kotb AM, Zahner G, Hoxha E, et al.: A heterologous model of thrombospondin type 1 domain-containing 7A-associated membranous nephropathy. *J Am Soc Nephrol* 28: 3262–3277, 2017
- Klenotic PA, Page RC, Misra S, Silverstein RL: Expression, purification and structural characterization of functionally replete thrombospondin-1 type 1 repeats in a bacterial expression system. *Protein Expr Purif* 80: 253–259, 2011
- Aleshin AE, Schraufstatter IU, Stec B, Bankston LA, Liddington RC, DiScipio RG: Structure of complement C6 suggests a mechanism for initiation and unidirectional, sequential assembly of membrane attack complex (MAC). *J Biol Chem* 287: 10210–10222, 2012
- Pääkkönen K, Tossavainen H, Permi P, Rakkolainen H, Rauvala H, Raulo E, et al.: Solution structures of the first and fourth TSR domains of F-spondin. *Proteins* 64: 665–672, 2006
- Venkatesh B, Lee AP, Ravi V, Maurya AK, Lian MM, Swann JB, et al.: Elephant shark genome provides unique insights into gnathostome evolution. *Nature* 505: 174–179, 2014

26. Kuo MW, Wang CH, Wu HC, Chang SJ, Chuang YJ: Soluble THSD7A is an N-glycoprotein that promotes endothelial cell migration and tube formation in angiogenesis. *PLoS One* 6: e29000, 2011
27. Galvin NJ, Vance PM, Dixit VM, Fink B, Frazier WA: Interaction of human thrombospondin with types I-V collagen: Direct binding and electron microscopy. *J Cell Biol* 104: 1413–1422, 1987
28. Sercu S, Lambeir AM, Steenackers E, El Ghalbzouri A, Geentjens K, Sasaki T, et al.: ECM1 interacts with fibulin-3 and the beta 3 chain of laminin 332 through its serum albumin subdomain-like 2 domain. *Matrix Biol* 28: 160–169, 2009
29. Dardik R, Lahav J: Multiple domains are involved in the interaction of endothelial cell thrombospondin with fibronectin. *Eur J Biochem* 185: 581–588, 1989
30. Herndon ME, Stipp CS, Lander AD: Interactions of neural glycosaminoglycans and proteoglycans with protein ligands: Assessment of selectivity, heterogeneity and the participation of core proteins in binding. *Glycobiology* 9: 143–155, 1999
31. Asch AS, Silbiger S, Heimer E, Nachman RL: Thrombospondin sequence motif (CSVTCG) is responsible for CD36 binding. *Biochem Biophys Res Commun* 182: 1208–1217, 1992
32. Gao AG, Lindberg FP, Dimitry JM, Brown EJ, Frazier WA: Thrombospondin modulates alpha v beta 3 function through integrin-associated protein. *J Cell Biol* 135: 533–544, 1996
33. Gao AG, Lindberg FP, Finn MB, Blystone SD, Brown EJ, Frazier WA: Integrin-associated protein is a receptor for the C-terminal domain of thrombospondin. *J Biol Chem* 271: 21–24, 1996
34. Isenberg JS, Annis DS, Pendrak ML, Ptaszynska M, Frazier WA, Mosher DF, et al.: Differential interactions of thrombospondin-1, -2, and -4 with CD47 and effects on cGMP signaling and ischemic injury responses. *J Biol Chem* 284: 1116–1125, 2009
35. Calzada MJ, Sipes JM, Krutzsch HC, Yurchenco PD, Annis DS, Mosher DF, et al.: Recognition of the N-terminal modules of thrombospondin-1 and thrombospondin-2 by alpha6beta1 integrin. *J Biol Chem* 278: 40679–40687, 2003
36. Calzada MJ, Annis DS, Zeng B, Marcinkiewicz C, Banas B, Lawler J, et al.: Identification of novel beta1 integrin binding sites in the type 1 and type 2 repeats of thrombospondin-1. *J Biol Chem* 279: 41734–41743, 2004
37. Lawler J, Hynes RO: An integrin receptor on normal and thrombasthenic platelets that binds thrombospondin. *Blood* 74: 2022–2027, 1989
38. Bein K, Simons M: Thrombospondin type 1 repeats interact with matrix metalloproteinase 2. Regulation of metalloproteinase activity. *J Biol Chem* 275: 32167–32173, 2000
39. Yang Z, Strickland DK, Bornstein P: Extracellular matrix metalloproteinase 2 levels are regulated by the low density lipoprotein-related scavenger receptor and thrombospondin 2. *J Biol Chem* 276: 8403–8408, 2001
40. Resovi A, Pinessi D, Chiorino G, Taraboletti G: Current understanding of the thrombospondin-1 interactome. *Matrix Biol* 37: 83–91, 2014
41. Nagayama Y, Wadsworth HL, Russo D, Chazenbalk GD, Rapoport B: Binding domains of stimulatory and inhibitory thyrotropin (TSH) receptor autoantibodies determined with chimeric TSH-lutropin/chorionic gonadotropin receptors. *J Clin Invest* 88: 336–340, 1991
42. Futei Y, Amagai M, Sekiguchi M, Nishifuji K, Fujii Y, Nishikawa T: Use of domain-swapped molecules for conformational epitope mapping of desmoglein 3 in pemphigus vulgaris. *J Invest Dermatol* 115: 829–834, 2000
43. Sekiguchi M, Futei Y, Fujii Y, Iwasaki T, Nishikawa T, Amagai M: Dominant autoimmune epitopes recognized by pemphigus antibodies map to the N-terminal adhesive region of desmogleins. *J Immunol* 167: 5439–5448, 2001
44. Larsen CP, Trivin-Avillach C, Coles P, Collins AB, Merchant M, Ma H, et al.: LDL receptor-related protein 2 (megalin) as a target antigen in human kidney anti-brush border antibody disease. *J Am Soc Nephrol* 29: 644–653, 2018
45. Di Zenzo G, Thoma-Uszynski S, Calabresi V, Fontao L, Hofmann SC, Lacour JP, et al.: Demonstration of epitope-spreading phenomena in bullous pemphigoid: Results of a prospective multicenter study. *J Invest Dermatol* 131: 2271–2280, 2011
46. Hashimoto T, Tsuruta D, Dainichi T, Hamada T, Furumura M, Ishii N: Demonstration of epitope spreading in bullous pemphigoid: Results of a prospective multicenter study. *J Invest Dermatol* 131: 2175–2177, 2011
47. Chen JL, Hu SY, Jia XY, Zhao J, Yang R, Cui Z, et al.: Association of epitope spreading of antiglomerular basement membrane antibodies and kidney injury. *Clin J Am Soc Nephrol* 8: 51–58, 2013
48. McRae BL, Vanderlugt CL, Dal Canto MC, Miller SD: Functional evidence for epitope spreading in the relapsing pathology of experimental autoimmune encephalomyelitis. *J Exp Med* 182: 75–85, 1995
49. Goebels N, Hofstetter H, Schmidt S, Brunner C, Wekerle H, Hohlfeld R: Repertoire dynamics of autoreactive T cells in multiple sclerosis patients and healthy subjects: Epitope spreading versus clonal persistence. *Brain* 123: 508–518, 2000
50. Thrasvoulides A, Lymberi P: Evidence for intramolecular B-cell epitope spreading during experimental immunization with an immunogenic thyroglobulin peptide. *Clin Exp Immunol* 132: 401–407, 2003
51. Pöllinger B, Krishnamoorthy G, Berer K, Lassmann H, Bösl MR, Dunn R, et al.: Spontaneous relapsing-remitting EAE in the SJL/J mouse: MOG-reactive transgenic T cells recruit endogenous MOG-specific B cells. *J Exp Med* 206: 1303–1316, 2009
52. Vlase H, Nakashima M, Graves PN, Tomer Y, Morris JC, Davies TF: Defining the major antibody epitopes on the human thyrotropin receptor in immunized mice: Evidence for intramolecular epitope spreading. *Endocrinology* 136: 4415–4423, 1995
53. Schwarz-Lauer L, Pichurin PN, Chen CR, Nagayama Y, Paras C, Morris JC, et al.: The cysteine-rich amino terminus of the thyrotropin receptor is the immunodominant linear antibody epitope in mice immunized using naked deoxyribonucleic acid or adenovirus vectors. *Endocrinology* 144: 1718–1725, 2003
54. Shah P, Tramontano A, Makker SP: Intramolecular epitope spreading in Heymann nephritis. *J Am Soc Nephrol* 18: 3060–3066, 2007
55. Wucherpfennig KW: Mechanisms for the induction of autoimmunity by infectious agents. *J Clin Invest* 108: 1097–1104, 2001
56. Kain R, Exner M, Brandes R, Ziebermayr R, Cunningham D, Alderson CA, et al.: Molecular mimicry in pauci-immune focal necrotizing glomerulonephritis. *Nat Med* 14: 1088–1096, 2008
57. Ronco P, Debiec H: Pathophysiological advances in membranous nephropathy: Time for a shift in patient's care. *Lancet* 385: 1983–1992, 2015
58. Ellebrecht CT, Bhoj VG, Nace A, Choi EJ, Mao X, Cho MJ, et al.: Re-engineering chimeric antigen receptor T cells for targeted therapy of autoimmune disease. *Science* 353: 179–184, 2016

This article contains supplemental material online at <http://jasn.asnjournals.org/lookup/suppl/doi:10.1681/ASN.2017070805/-/DCSupplemental>.

SUPPLEMENTAL RESULTS

A

Alignments for THBS1-like domains

```

3r6b      -----INGGWGFWSPWDIC-----SVTGG--GVQKRSLICNNPTQFQGGK-----DCVGDVT-----ENQICNKQ--DCP
d1        QGEAEAPTLYWKT-GPWGRCMG-----DECGPG--GIQTFVWCAHVEGWTTLH-----TNCKQAER-----PNNQQNCFK--VCD
d2        -----LYDWRLL-GPWNQCQPVISKSLKPE-----LECIKGEEGIQVREIACIQKDKDIPAE-----DIICEYFEP-----KPLLEQACLI--PCQ
d5        -----YGRWT-TEWTECRVDPLLSQDQKRRG--NQTALCGG--GIQTRREVYCVQANENLLSQLSTHKNKEASKPMDLKLK--TGPI-----PNTTQLCHI--PCP
d7        -----DWKA-VRLGNCEPDNG-----KECGP--GTQVQEVVCI NSDGEVDR-----QLCRDAIF-----PI PVA--CDA--PCP
d9        -----VYHWQT-GPGQCIEDTSVSSFNNTTTWNGE-ASCSV--GMQTKVICVRVNVGVGVP-----KKCPESLR-----PETVRPCLL--PCK
d11       -----SYRWKT-HKWRRCQLVPWSVQDSPAQ--EGCGP--GRQAARITCRKQDGGQAGI-----HECLQYAG-----PVPALTQAQI--FCQ
d13       -----KYNAQPVGNWSDCILPEKGVVLLGMKVQGDIKECGQ--GYRYQAMACYDQNGRLVET-----SRCNSHG Y-----IEEACII--PCP
d15       -----QYLWVT-EPWSICKVTFVNM-----RENGGE--GVQTKVRCMQNTADGPSE-----HVEDYLC DPEEM-----PLGSRVCKL--PCP
d17       -----HYDYNV-TDWSICQLSEK-----AVCGN--GIKTMLDCVRS DGSVDL-----KYCEALGL-----EKNWQMN TSCMV--ECP
d19       -----RWQY-GQWSPCQVQE-----AOCGE--GTRTRNISCVVSDGSADD F-----SKVVDEEFCADIELIIDGNKNM VLEESCSQ--PCP
d21       --EYKWMASAWKGS SRTVWCQRSDGINVT-----GGLV M--SQPDADRS CNP-----PCSQP-----GSSQP-----HSYCS ETKTCH
  
```

Alignments for C6-like domains

```

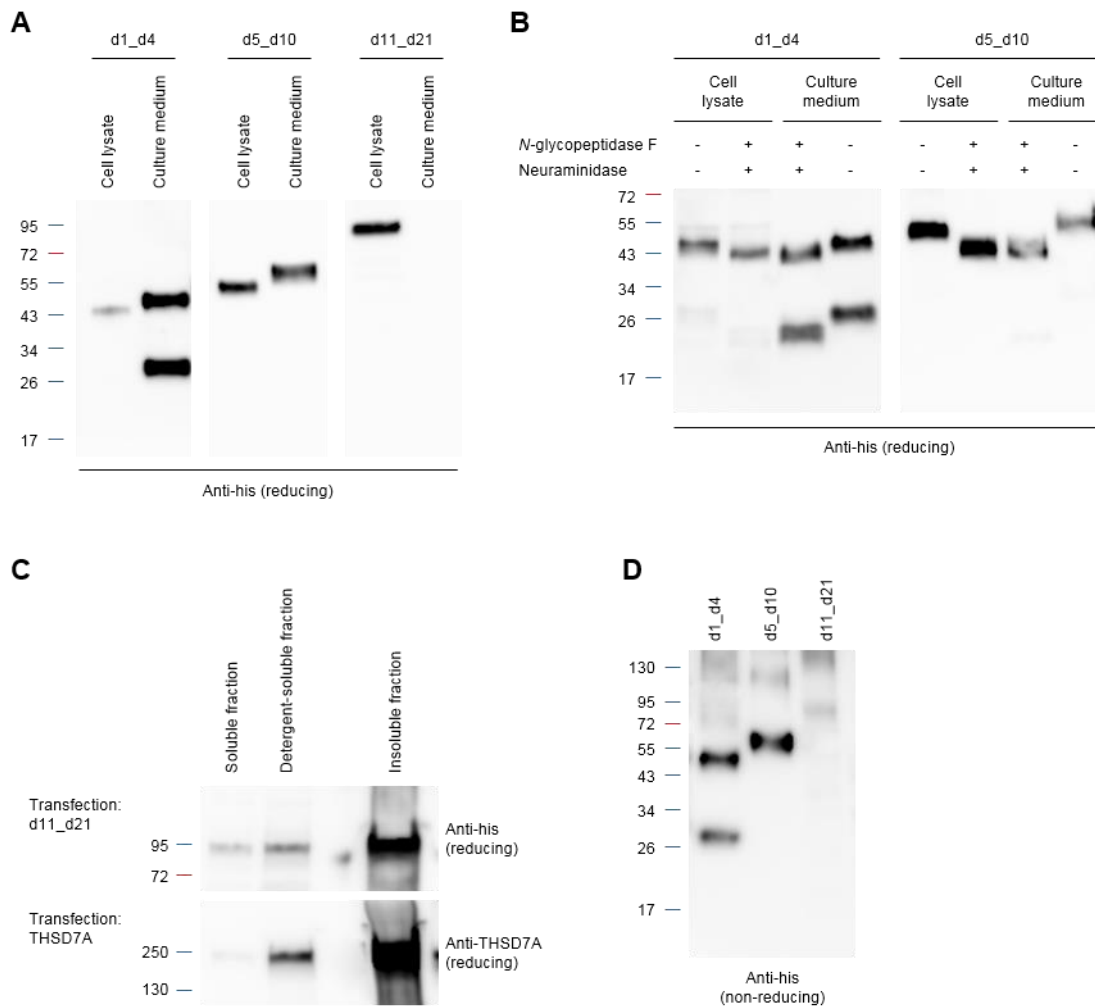
3t5o1     --CFCDHYAWTQWTSCK-TGN-----SGTQSRHRQIVVDKYQE--NFCBQICSKQ-----ETRECNWQ-----RCP----
3t502     --INCLLDGDFGWSDDC--PCI-----EKQSKVRSVLRPSQFG--GQPC TAP-----LVAFQPCIPSK-----LCKIE--
1sz1     GSETCIYSNWSFWACSSTC-----EKGKRMQMLKAQ--LDLSV--PCPDT-----QDFQC-----MGFGSDEDDG
d3        --QDCIVSEFSAWSECS-KTC-----GSLQHRTTHV VAPP-QFGGS--GCPNL-----TEFQVC-----QSSPCE----
d4        --KECQVSEWSEWSPCS-KTCHDMV--SPAGTRVTRTIRQFP-IGSEK--ECP EF-----EKEPELSQGDGVVPCA
d6        --TECEVSPWSAWGPTIYENCNDDQ--GKKGFKLRRRITNEPTGGSGVTGNCPHL-----LEAIPC-----EEPAC Y----
d8        --KDCVLTSTWTSWSSCS-HTC-SGK--TTEGKQIRARSILAYAGEEGGI--RCPNSA-----LQEVRS C-----NEHPT
d10       --KDCIVTFPYSDFWSSCP--SSCKEGD--SSIRKQSRHRVVIQLP-ANGGR--DCTDP-----LYEKA C-----EAPQA CQ----
d12       --DDCQLTWSKFSNCGD--GDC-----GAVTRKRLTLVGS--KKKE--KCKNSHLYP--LIETQY C-----PCD-----
d14       --SDCKLSEWNSWRSRCS-KSC-----GSGVKVRSKWLREKPYNGGR--PCPKLDHVNQAVVEVVP-----HSDCN----
d16       --EDCVISEWGWTCV-LPC-----NQSSFQRQSADPIRQ-ADGR--SCPNA-----VEKEPC-----NLNKNQY----
d18       --VNCQLSDWSSWQCS-QTC-----GLTGKMIKRRVTVQFP-QGDGR--PCPSLM-----DQSKP C-----PVKPCY----
d20       --GDCYLKDWSSWLSLQ-LTCVNGEDLFGGGIQVRSRPVIIQE-LENQH--LCPQM-----LETKSC-----YDGCQY----
  
```

B

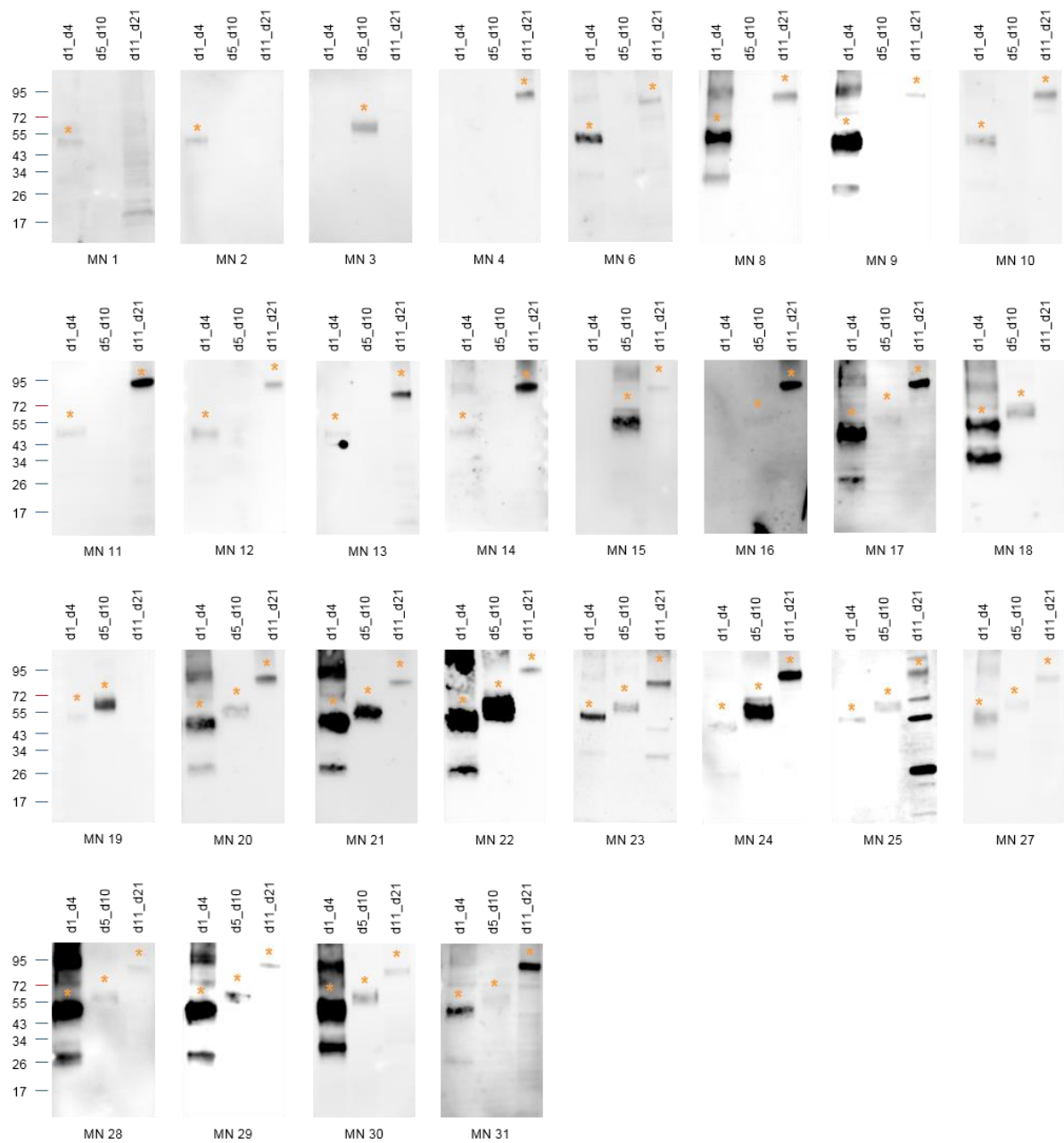
```

leader    MGLQARRWASGSRGAAGPRRGLVQLLPLPLPLLLLLLLLRPGAGRA
d1        AAQGEAEAPTLYWKTGPWGRCMGDECGPGGIQTRAVWCAHVEGWTTLHTNCKQAERPNNQQNCFKVC D
d2        WHKELYDWRLLGPWNQCQPVISKSLKPELECIKGEEGIQVREIACIQKDKDIPAEIDIICEYFEPKPLLEQA CLIPQC
d3        QDCIVSEFSAWSECSKTCCGSLQHRTRHV VAPPQFGGSGCPNLTEFQVCQSSPCE
cc        ABELRYSLHVGFWSTCSMPHSRQVRQARRGKNEREKDRSKGVKDEARELIIKKRNRNRQNRQENKYWDIQIGYQTR EVMCINKTKGAADLSFCQKELMPTFQSCVIT
d4        KECQVSEWSEWSPCSKTCHDMVSPAGTRVTRTIRQFP-IGSEKCEPEEKEPELSQGDGVVPCA
d5        TYGWRITTEWTECRVDPLLSQDQKRRGNQALCGGGIQTREVVYCVQANENLLSQLSTHKNKEASKPMDLKLCTGP IPIPTTQLCHIPC P
d6        TECEVSPWSAWGPTIYENCNDDQGGKGFKLRRRITNEPTGGSGVTGNCPHLEAIPC EEPAC Y
d7        DWKAVRLGNCEPDNGKECGPQTQVQEVVCI NSDGEVDRQLCRDAIFPIPVACADPC P
d8        KDCVLTSTWTSWSSCSHTCSGKTTTEGKQIRARSILAYAGEEGGI RCPNSALQEVRS CNEHPT
d9        VYHWQTGPNWQCIEDTSVSSFNNTTTWNGEASCSVMQTRKVICVRVNVGVGVPKCPESLRPETVRPCLLPCK
d10       KDCIVTFPYSDFWTSWSSCKEGDSSIRKQSRHRVVIQLPANGGRDCTDPLYEKA CEAFAQCQ
d11       SYRWKTHKWRRCQLVPWSVQDSPAQEGCGPGRQARAITCRKQDGGQAGIHECLQYAGFPV PALTQAQCI PCQ
d12       DDQQLTSWSKFSNCGDCAVTRRKRRLTLVGSKSKKCKNSHLYPLIETQYCPCD
d13       KYNAQPVGNWSDCILPEKGVVLLGMKVQGDIKECGQGYRYQAMACYDQNGRLVETSRCNSHG YIEEACII PCP
d14       SDCKLSEWNSWRSRCSKSGSVKRSKWLREKPYNGGRPCPKLDHVNQAVVEVVPVCHSDCN
d15       QYLWVTPEPWSICKVTFVNMRENGCEGVQTRKVRCMQNTADGPSEHVEDYLC DPEEMPLGSRVCKLPC P
d16       EDCVISEWGWTCVLPNCNQSSFQRQSADPIRQPADEGRSCPNAVEKEPCNLNKNQY
d17       HYDYNVTDWSICQLSEKAVCGNGIKRMLDCVRS DGSVDLKYCEALGLEKNWQMN TSCMV ECP
d18       VNCQLSDWSSWQCSQTCGLTGKMIKRRVTVQFPQGDGRPCPSLM DQSKP C P V K P C Y
d19       RWQYQGWSPCQVQEACQEGGTRTRNISCVVSDGSADD FSKVVDEEFCADIELIIDGNKNM VLEESCSQPC P
d20       GDCYLKDWSSWLSLQ LTCVNGEDLFGGGIQVRSRPVIIQELENQHLCPEQMLETKSCYDGCQY
d21       EYKWMASAWKGS SRTVWCQRSDGINVTGGCLVMSQPDADRS CNPCCSQPHSYCSETKTCH
stalk/tm CEEGYTEVMSSNTLEQCTLIPVVVLP T MEDKRGDVKTSRAVHPTQPSNPAGRGRTWFLQPFPGDRLK T W
cytosol   VYGAAGAFVLLIFIVSMIYLACKKPKKPRRQNNRKLPLT LAYDGDADM
  
```

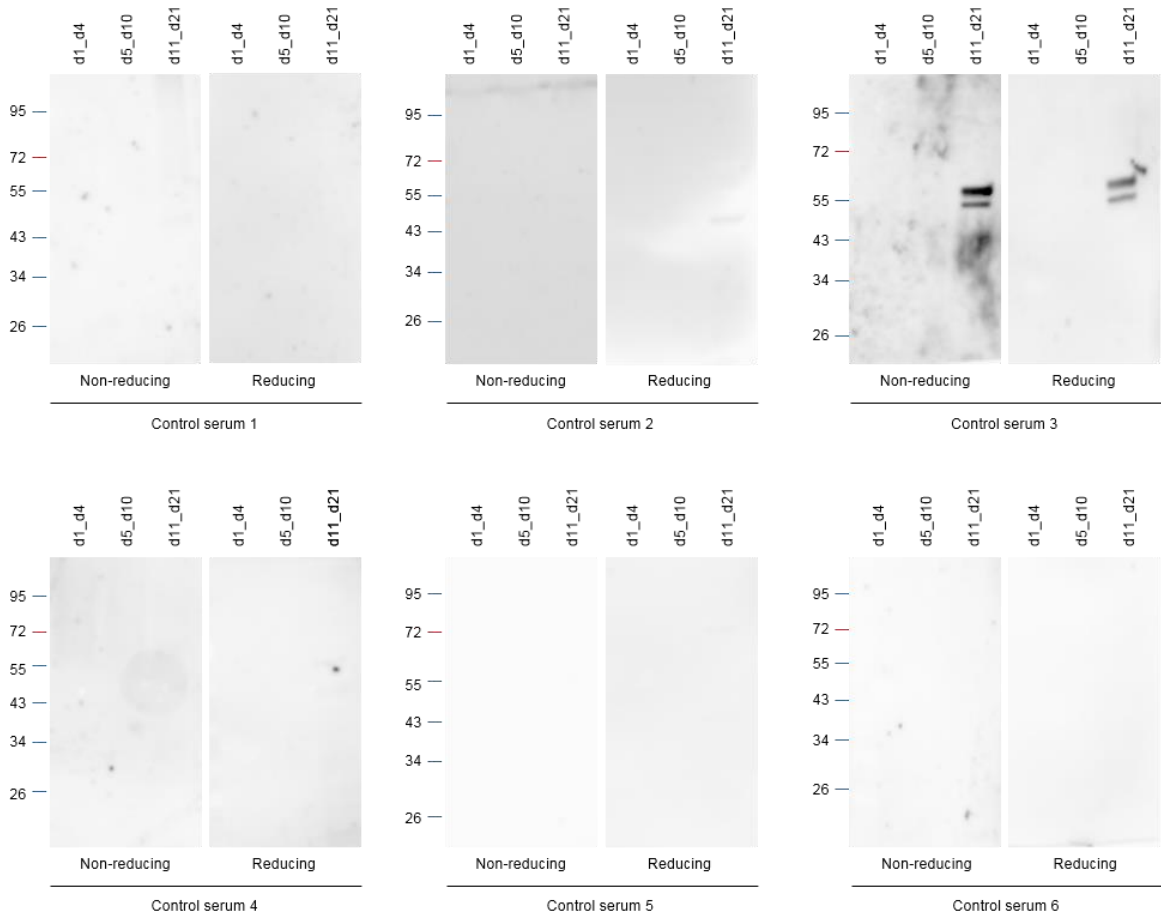
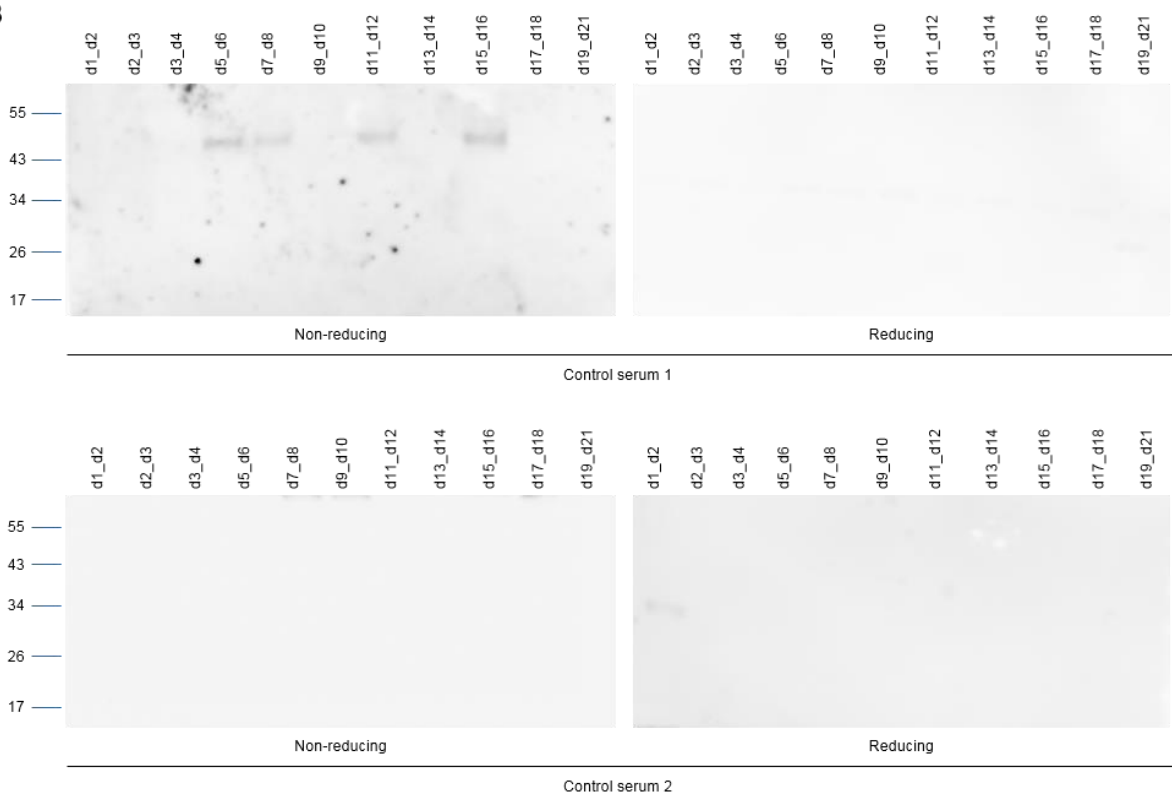
Supplemental Figure 1. Identification of TSP-1 domains and structure of human THSD7A. **(A)** Reference sequences for TSP-1 domains as in THBS1 (protein data bank [pdb] code 3r6b¹, upper panel) and for TSP-1 domains as in C6 (pdb code 3t5o²) or F-spondin (pdb code 1szl³) and alignment with the 21 TSP-1 domains of human THSD7A. Yellow, cysteine; magenta, tryptophane; cyan, arginine. **(B)** Amino acid sequence of full-length human THSD7A with colored tagging of all parts. Purple, leader peptide; red, THBS1-like TSP-1 domain; green, C6-like TSP-1 domain; blue, coiled coil (cc) domain; brown, extracellular stalk region, transmembrane (tm) region and cytosolic tail.

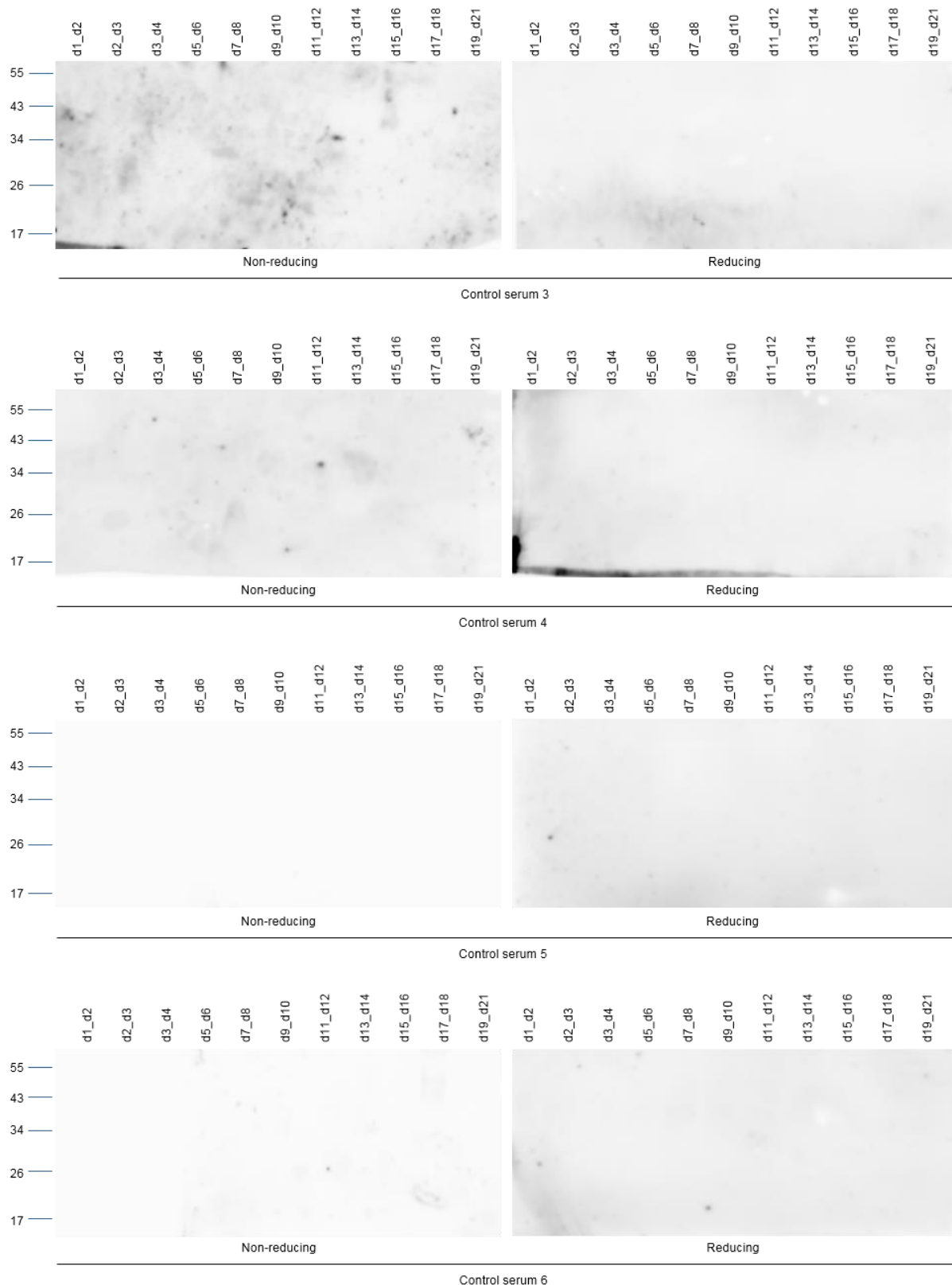


Supplemental Figure 2. Expression of three THSD7A fragments in HEK293 cells. **(A)** Western blot of cell lysates and culture media of transfected HEK293 cells with an anti-his antibody. Constructs d1_d4 and d5_d10, but not d11_d21, were secreted to the culture media. Secreted proteins showed a slightly higher molecular mass compared with the proteins in the cellular fraction. **(B)** Western blot of cell lysate and culture media fractions of d1_d4 and d5_d10 before and after enzymatic deglycosylation with *N*-glycopeptidase F and neuraminidase. Deglycosylated fragments migrated to the same molecular mass, demonstrating that the difference in size was due to incomplete glycosylation of the protein in the cellular fraction. **(C)** Western blot of different subcellular fractions of d11_d21-transfected HEK293 cells with an anti-his antibody. The d11_d21 construct was found in both the soluble and the detergent-soluble fraction (upper panel). As an experimental control, HEK293 cells transfected with full-length THSD7A were treated identically (lower panel). Both the d11_d21 construct and full-length THSD7A were also present in the insoluble fraction. **(D)** Western blot analysis of the three THSD7A fragments (culture media for d1_d4 and d5_d10 and cell lysate for d11_d21) with an anti-his antibody under non-reducing conditions.

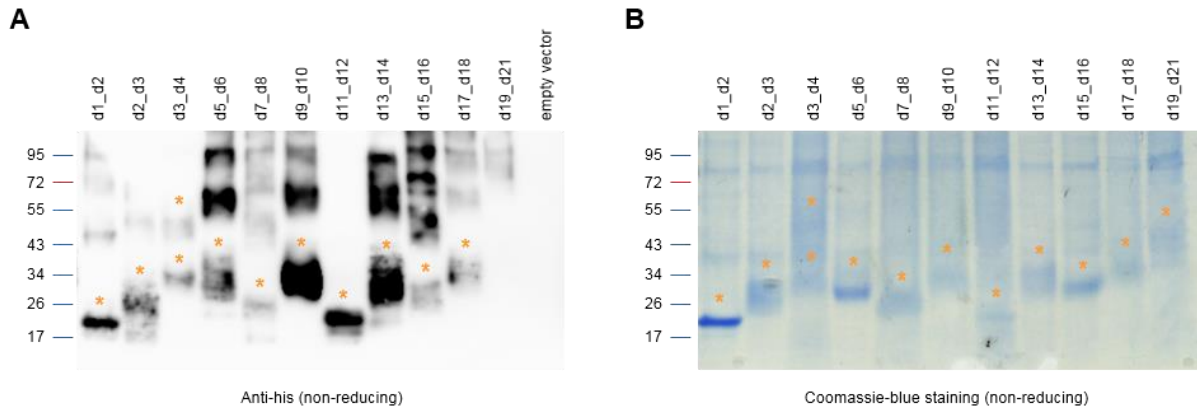


Supplemental Figure 3. Western blot analysis of the three THSD7A fragments d1_d4, d5_d10 and d11_d21 with sera from 28 patients with THSD7A-associated MN under non-reducing conditions (results of the remaining three patients are depicted in **Figure 2A** in the main body).

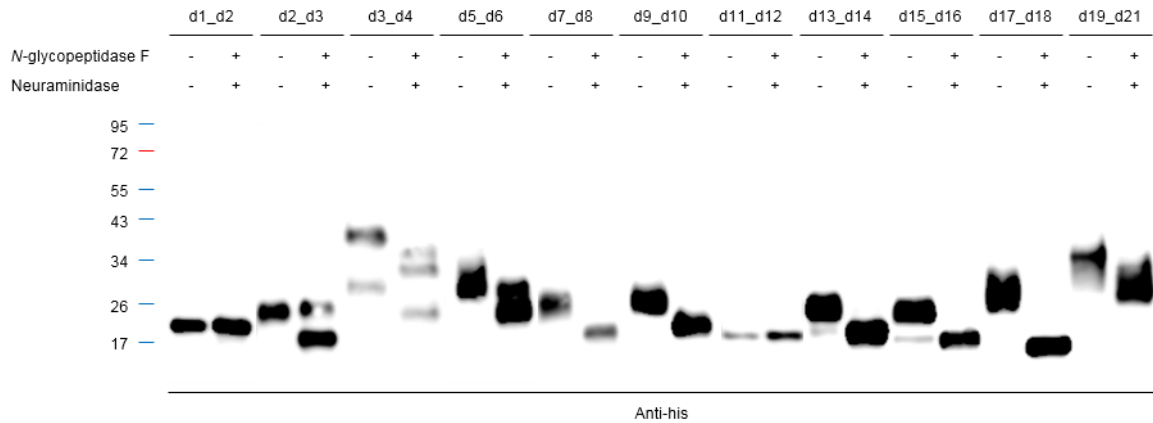
A**B**



Supplemental Figure 4. Baseline negative controls. (A, B) Images depict results of Western blot analyses of (A) the three larger THSD7A fragments and (B) the small TSP-1 domain constructs with serum from six healthy individuals (1:100) under non-reducing and reducing conditions.

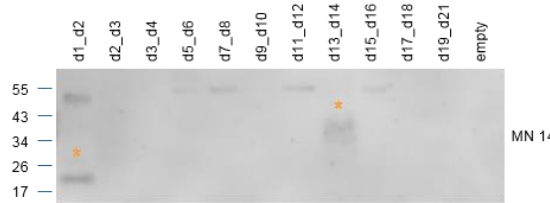
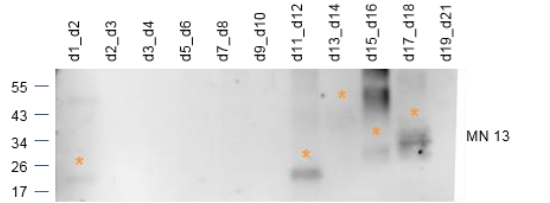
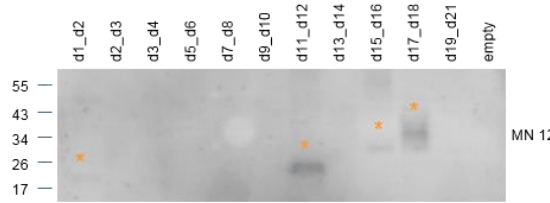
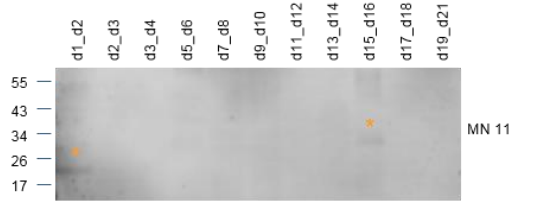
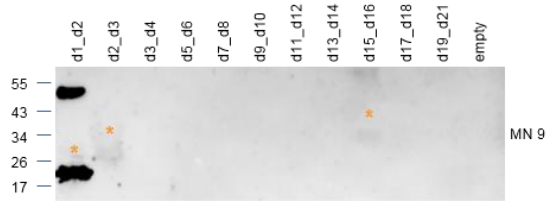
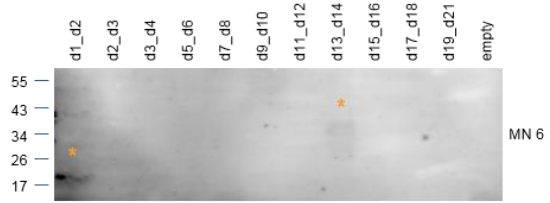
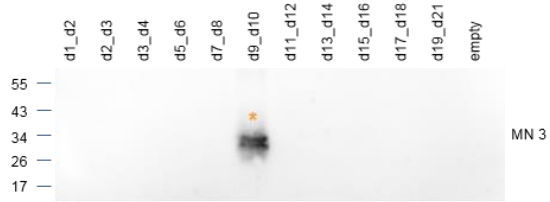
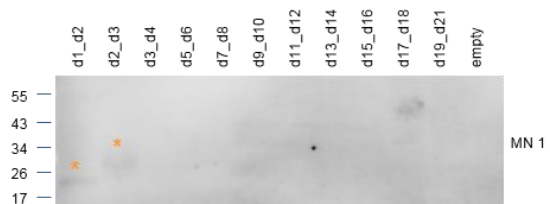


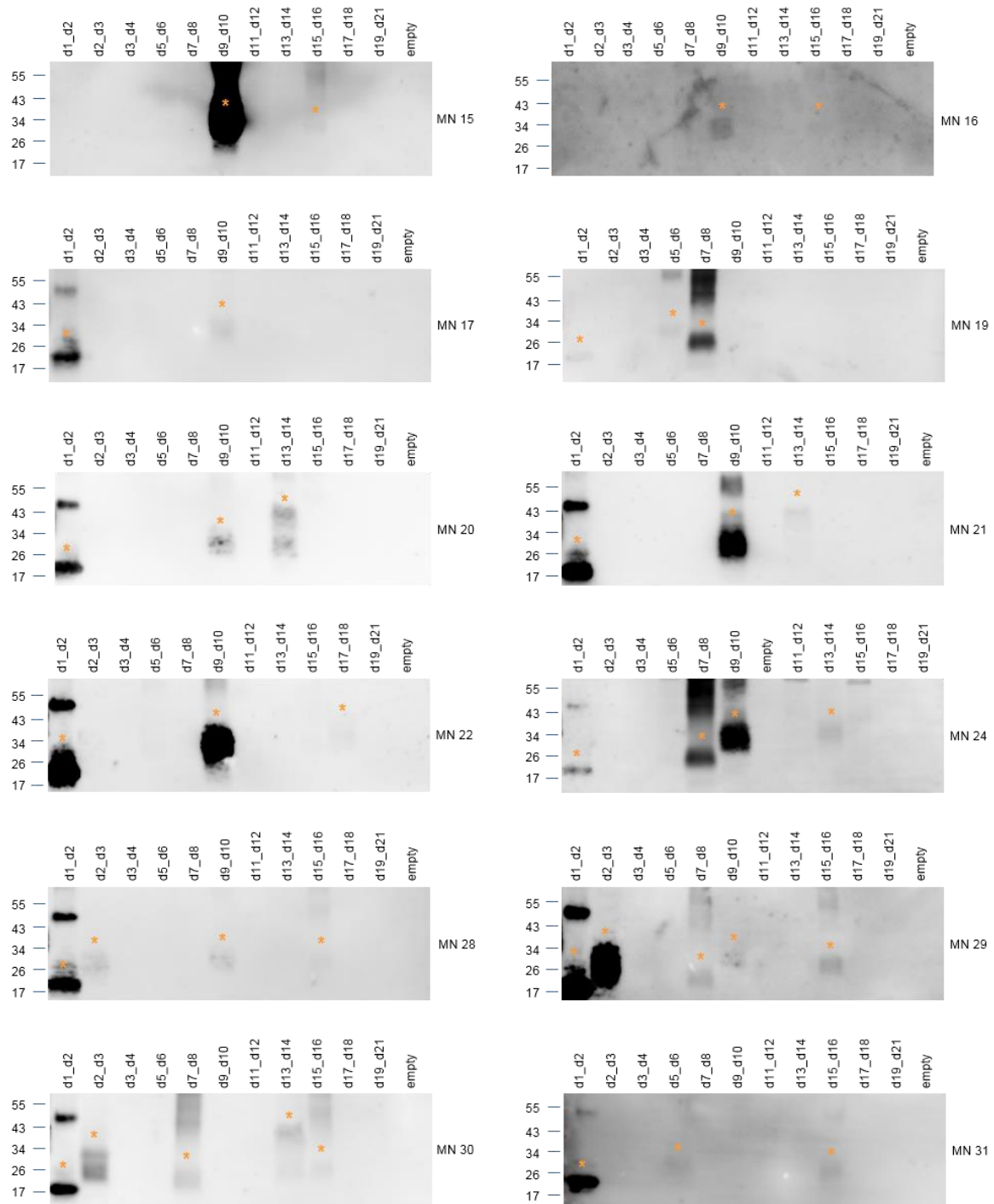
Supplemental Figure 5. (A) Western blot analysis under non-reducing conditions of cell culture supernatants of HEK293 cells expressing the soluble TSP-1 domain constructs. With the exception of d19_d21, all constructs were well recognized by the anti-his antibody despite good recognition of d11_d21 under reducing conditions (**Figure 3A** in the main body), suggesting that the 6x his-epitope in the d19_d21 construct lacks antibody accessibility under non-reducing conditions. Some of the constructs cross-link and build multimers, which were well recognized by the anti-his antibody. Asterisks mark the recognized TSP-1 domain constructs. (B) Coomassie-blue staining of cell culture supernatants of HEK293 cells expressing the soluble TSP-1 domain constructs. All eleven TSP-1 domain constructs can be detected using this method.

A**B**

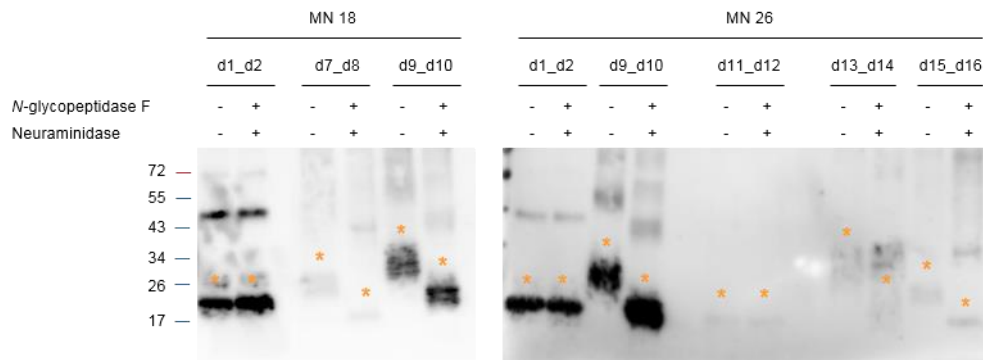
TSP-1 domain construct	Expected molecular mass	Molecular mass after deglycosylation
d1_d2	18	20
d2_d3	16	16
d3_d4	27	32
d5_d6	18	26
d7_d8	14	18
d9_d10	16	20
d11_d12	15	18
d13_d14	16	18
d15_d16	15	17
d17_d18	15	15
d19_d21	23	29

Supplemental figure 6. (A) Glycosylation of individual TSP-1 domain constructs. The TSP-1 domain constructs were enzymatically deglycosylated using *N*-glycopeptidase F and neuraminidase. Shifts in protein mass were evaluated by immunodetection with an anti-his antibody in Western blot analysis under reducing conditions. **(B)** Predicted molecular mass according to www.sciencegateway.org/tools/proteinmw.htm and molecular mass as estimated from migration in gel electrophoresis after enzymatic deglycosylation. The fragments corresponded well to their expected molecular masses or run slightly above.

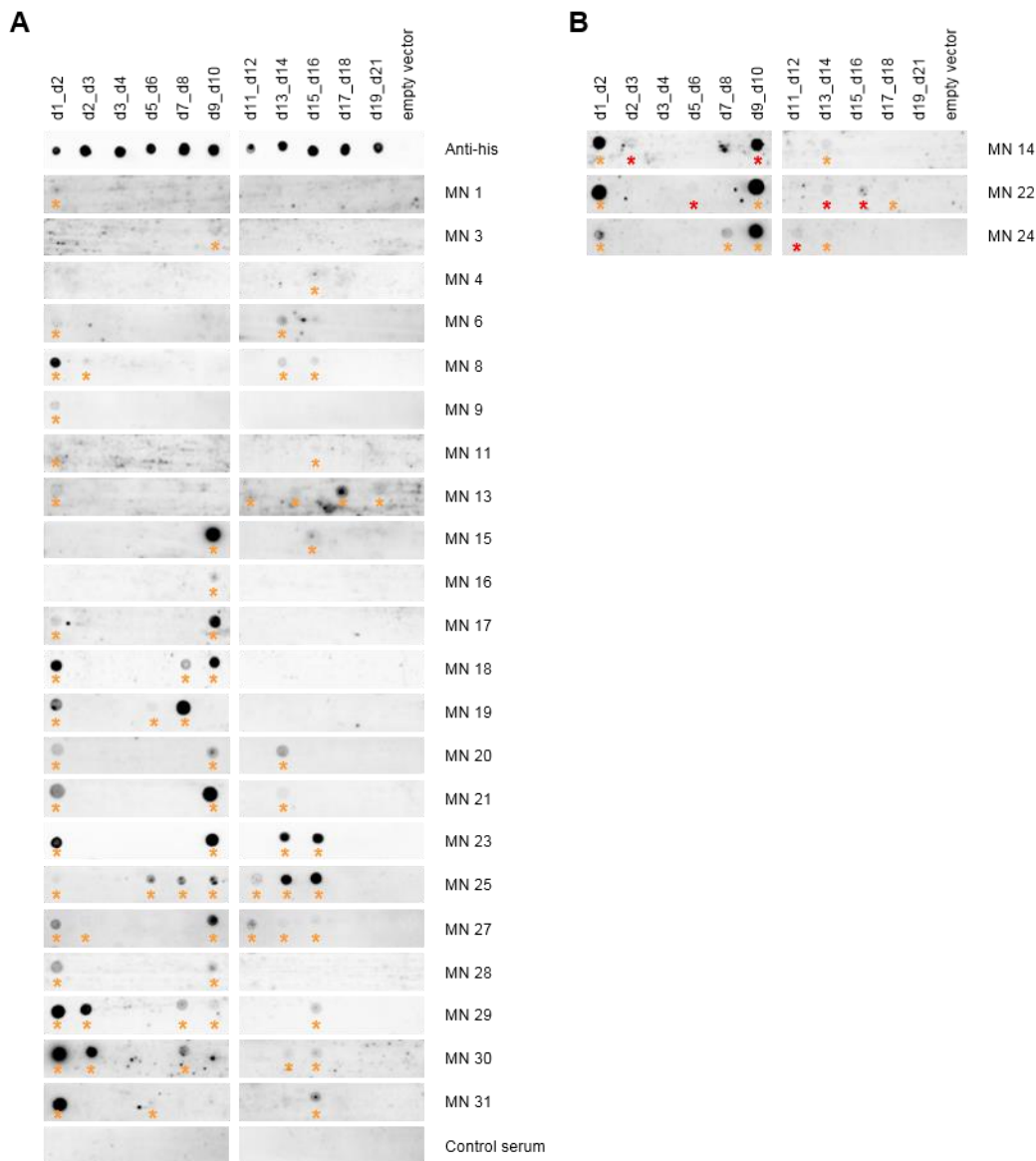




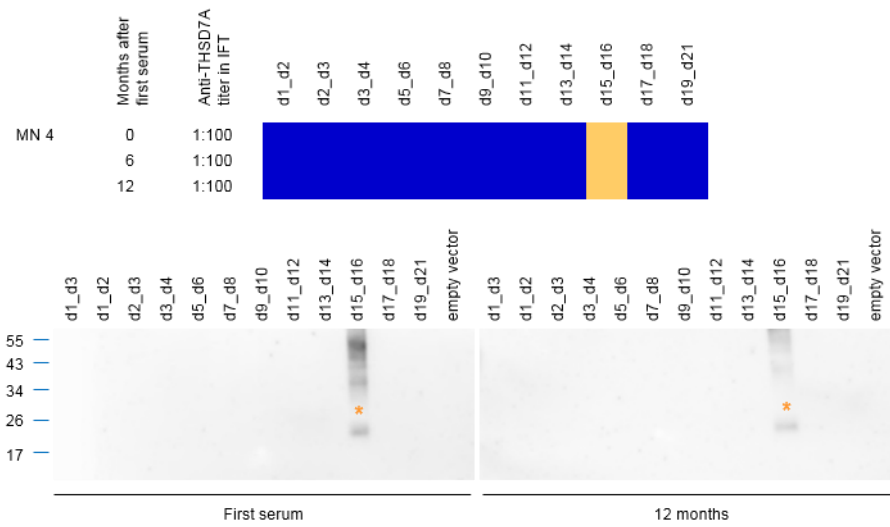
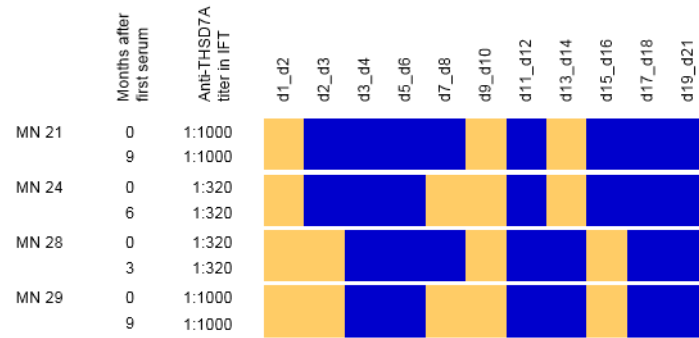
Supplemental Figure 7. Western blot analysis of the TSP-1 domain constructs with sera from the remaining 24 patients that are not depicted in the results section (**Figures 3B, 4 and 5**) with THSD7A-associated MN under non-reducing conditions (serum dilution 1:100). Asterisks mark the recognized TSP-1 domain constructs.



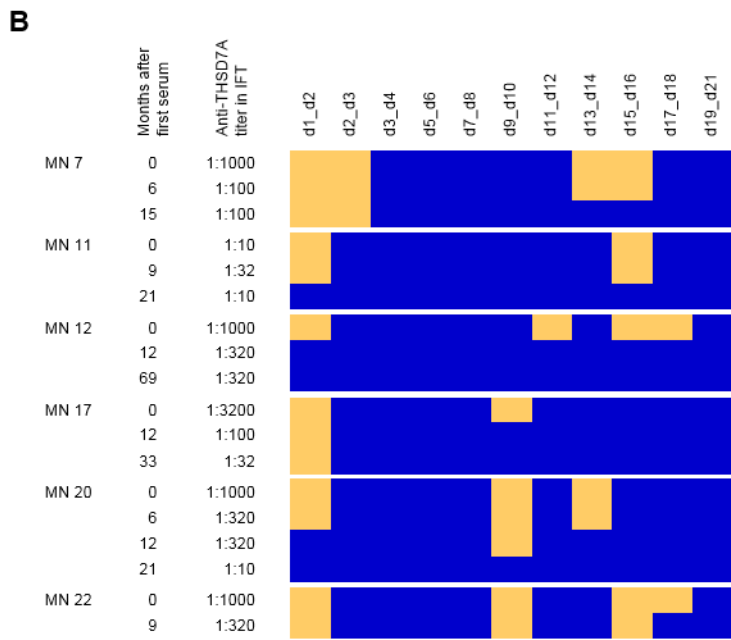
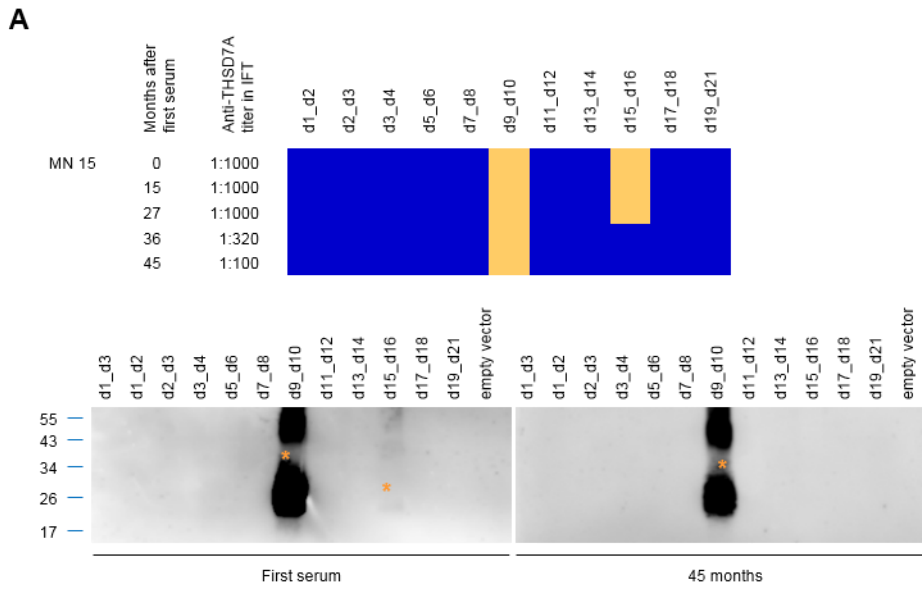
Supplemental Figure 8. Serum recognition of deglycosylated TSP-1 domain constructs. The TSP-1 domain constructs were enzymatically deglycosylated using *N*-glycopeptidase F and neuraminidase. Sera recognized both the glycosylated and deglycosylated forms in Western blot analysis under non-reducing conditions. Asterisks mark the recognized TSP-1 domain constructs.



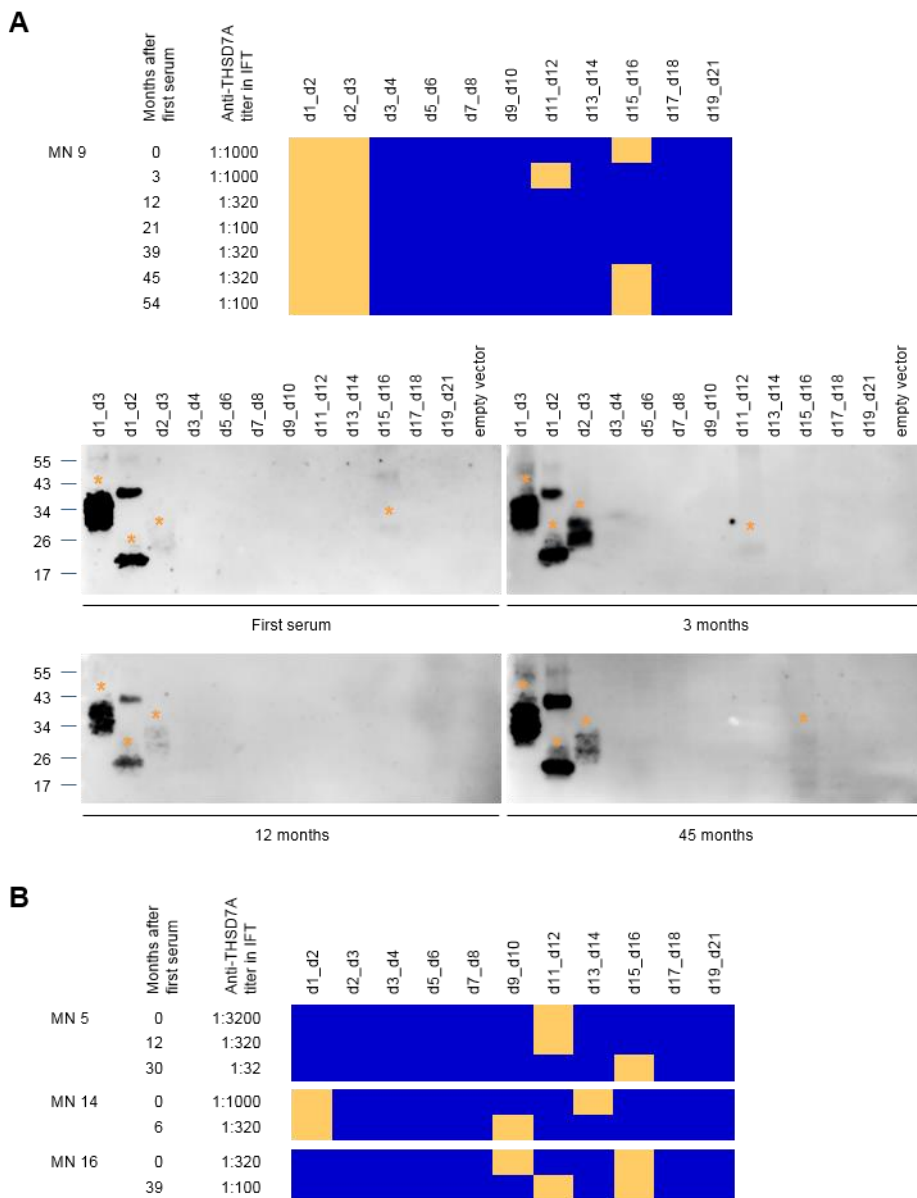
Supplemental Figure 9. Native blotting (dot blot analysis) of purified TSP-1 domain constructs with sera from patients with THSD7A-associated MN. (A, B) Dot blot analysis of TSP-1 domain constructs with sera that (A) recognized the same or less TSP-1 domain constructs or (B) showed additional reactivity with TSP-1 domain constructs when compared with Western blotting. MN 9, MN 16 and MN 28 failed to recognize a TSP-1 domain construct that was previously recognized in Western blotting and MN 2 and MN 12 failed to recognize any TSP-1 domain construct in native blotting (data not shown). Yellow asterisks mark the recognized TSP-1 domain constructs that were also appreciated in Western blotting while red asterisks mark additional TSP-1 domain recognition.

A**B**

Supplemental Figure 10. Anti-THSD7A antibody levels and epitope profiles during follow-up in patients with steady TSP-1 domain recognition. **(A)** In patient MN 4, epitope profiling showed serum recognition of the d15_d16 construct, which remained unchanged during the observation period. IFT titer also remained stable and proteinuria was constantly in the nephrotic range. The patient did not receive immunosuppressive therapy. Lower panels depict the Western blot analyses of the TSP-1 domain constructs with the first and last available serum from this patient. Asterisks mark the recognized TSP-1 domain constructs. **(B)** Anti-THSD7A antibody levels and epitope profiles of four more patients with stable TSP-1 domain recognition and persistent active disease. MN 21 and MN 28 received immunosuppressive therapy during follow-up.



Supplemental Figure 11. Anti-THSD7A antibody levels and epitope profiles during follow-up in patients with a loss of TSP-1 domain recognition. **(A)** In patient MN 15, epitope profiling showed serum recognition of the d9_10 and d15_d16 constructs. During follow-up, d15_d16 reactivity was lost, the anti-THSD7A antibody level decreased, and the patient had a partial remission of proteinuria. The patient did not receive immunosuppressive therapy. Lower panels depict the Western blot analyses of the TSP-1 domain constructs with the first and last available serum from this patient. Asterisks mark the recognized TSP-1 domain constructs. **(B)** Anti-THSD7A antibody levels and epitope profiles of six more patients with a loss of TSP-1 domain recognition. MN 7, MN 12, MN 16, and MN 22 received immunosuppressive therapy during follow-up.



Supplemental Figure 12. Anti-THSD7A antibody levels and epitope profiles during follow-up in patients with a change in TSP_1 domain recognition. **(A)** In patient MN 9, epitope analysis showed serum reactivity with the d1_d2, d2_d3, and d15_d16 constructs. While reactivity with d15_d16 was lost three months later, the serum additionally recognized d11_d12. The patient was treated with prednisone and cyclosporine A, had a partial remission of proteinuria associated with a decrease of anti-THSD7A antibody levels and a loss of reactivity with d11_d12. Proteinuria relapsed after 45 months, which was accompanied by renewed serum reactivity with d15_d16 in the presence of a persistent anti-THSD7A antibody titer of 1:320 in IFT. Lower panels depict the Western blot analyses of the TSP_1 domain constructs with several follow-up sera from this patient. **(B)** Anti-THSD7A antibody levels and epitope profiles of three more patients with a change in TSP_1 domain recognition. One patient (MN 5) achieved a partial remission during follow-up. No data on proteinuria during follow-up were available for the other two patients.

A

Alignments for THBS1-like domains

```
3r6b  ---INGGKGPWSPWDICSV-----TGG-GVQKHSRLNNPTQF-----GGKDCVG-----DVTENQIENK-QDCP
d1  QGDTEVPTLYLK-TGPMGRCMG-----DDCPGGIQTAVWCAHVEGWTT-----LHNCXQAV-----RPSNQNCF--KVC
d2  ---WHKELYDWR-LGTWDRCPVVISKSL---EKSRECVKGE-GIQVFEIMCIQKDKDIPA-----EDIIIEYFEP-----KPLLEQAACL--IP
d5  ---TYGWR-TTEWTECHVDPLLSQQD--KRRANQTALCGG-GVQTFEYICIQTNDNMLSHGNTQKDKKASKPVDSKLTGPF-----VPNTTQLCH--VPC
d7  ---DWK-SVRLGDCPEP-----NGKSCGP-GTQVQEVVCI NSDGEEV-----DRQLCRDA-----IFPIPVACD--APCP
d9  ---VYHQ-TGPGWQCIEDTSVSSFN-TTTWNGEASC SV-GMQTHKVICRVNVVGVV-----GPKCPESL-----RPETVRPCL--LPCR
d11 ---SYRWK-THKWRRCLVPSIQD---VPGAQEGCGP-GRQAFAITCRKQDGGQA-----SIQELQYA-----GVPALTAQACQ--IP
d13 ---KYNAQPVGNSDCILPEGKAEVLLGMKVQGDGSKGCG-GYRYQAMACYDNGRLV-----ETSRONS-----HGYIEEACI--IP
d15 ---QYIYW-TEPWSVCKVTFV-----DMRDNGE-GVQTFKVRMCQNTADGPESEHV-----EDYLCDEP-----DMPLGSRCK--LPC
d17 ---HYDYN-VTDWSTCQLS-----EKAVCN-GIKTSMMLDCVRSDDGKSV-----DLKYCELEL-----LEKNWPMNTSCT--VECP
d19 ---RWQ-YGQWSPCQVQ-----EAQCGE-GTTRTFNISCVVSDGSAEDFSKVV-----DEEFCANTELIIDGNKQIVLEETCT--QPC
d21 ---EYKWVASAWKGSRRVWCQRSDDGINV-----TGGGLV-VQPDTRSCNP-----PCSQ-----PHSYCSEMKTCT
```

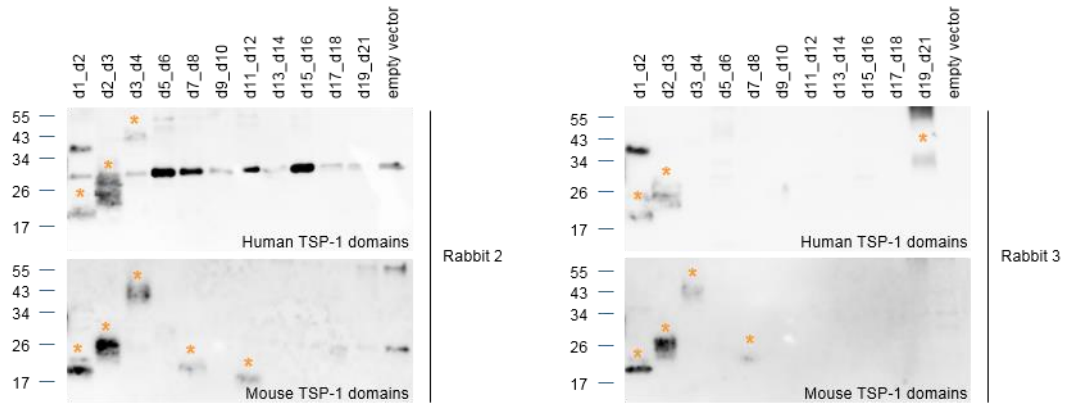
Alignments for C6-like domains

```
3t5o1  --CFDDHYAWTOWTSCSK-TCN-----SGTQSRHRQIVVDKYYQE---NFCQICSKQ----ETRECNWQ----RCP---
3t5o2  --INCLLDGFGPMSDCD--PCI-----EKQSKVRSVLRPSQFG---GQPOTAP-----LVAFQPCIPSK---LCKIE---
1sz1  GSETCIYSNWSMSSACSSSTCE-----RKGKMRQMLKALQDL---SVFPDPT-----QDFQPCMGF---GCSDEDDG
d3  --KDCIVSEFSPWSECSR-TCG-----SGLQHRTRHVVAAPPYQY---GSGCPNL-----TEFQVQCSN---PCE---
d4  --KEQVSENLWSPSCSK-TCNDVT---SPTGTRVTRTITQFPFGS---EKECPAL-----EKEPCVSGDGAVALCA---
d6  --IECEVSPWSSWSPCTYENCNDQQ--GKKGFKLRRIITNEPTGGSGATGNCPHL-----LEAIPCCEP---SCY---
d8  --KDCVLSANSSWSSCSH-TCGSKT---TEGKQTRARISILAYAGEEG--GIRCPNI-----SALQEVRSQNEH---PCT---
d10  --KDCVVTYSDWTPCPS-SCREGD--SGARKQSRQVVIQLPANG---GKECSDP-----LYEEKACEAPP---TCH---
d12  --DDCQFTSNWKFSSCNG-DCG-----AVRTRKRAIVGKSKK---KCKKNS---HLYPLIETQYC-----PCD---
d14  --SDCKLSEWNSRCSKSCG-SCG-----SGVKVRSKWLREKPYNG---GRPCPKLDHVNQAQVYEVVPCHS---DCN
d16  --EDCVISEWGPWTCAL-PCNP-----SGSNQRADPIRQPADE---GRAPDA-----VEKEPCSLNK---NCY---
d18  --VNCQLSDWSSWSQCSQTCGL---TGKMIKRTVTQPFQGD---GRPCPSL-----MEQSKPCVK---PCY---
d20  --GDCYLNDSWSSSLCQL-TCVNGEDLFGGGIQVRSRAVVIQLELEN---QHLCEPQ-----MLETKSCDDG---QCY---
```

B

```
leader  MGLRAGRLASPSRGLQLRLPLLLLLLSSGARGA
d1  AAQGDTEVPTLYLWKTPWNGRCMGDDCGPGGIQTAVWCAHVEGWTTLHNTCKQAVRPSNQNCFKVCD
d2  WHKELYDWRGLTWDRCQPVVISKLEKSRECVKGEIYQVREIMCIQKDKDIPAEDIICEYFEPKPLLEQAACLIP
d3  KDCIVSEFSPWSECSRTCGSLQHRTRHVVAAPPYQYGGSGCPNLTEFQVQCSN
cc  EDESLYSLQVGPWACSVPHTRQARARRRGNKEREKERGKAVKDPPEARLEIKKKRNRNRQNRQENRYWDIQIGYQTRDVTCLNRTGKSADLSFCQQRERLPMFTQSCVIT
d4  KEQVSENLWSPSCSKTCHDVTSPGTGTRVTRTITQFPFGSKECPALEEKEPCVSGDGAVALCA
d5  TYGWRTEWTECHVDPLLSQQDKRRANQTALCGGQVQTFEYICIQTNDNMLSHGNTQKDKKASKPVDSKLTGPFVPNTTQLCHVPCP
d6  IECEVSPWSSWSPCTYENCNDQQGKKGFKLRRIITNEPTGGSGATGNCPHLLEAIPCCEPSCY
d7  DWKSVRLGDCPEPNDGKSGPQVQEVVCI NSDGEEVDRQLCRDAIFPIPVACDAPCP
d8  KDCVLSANSSWSSCSHTEGKQTRARISILAYAGEEGGIRCPNISALQEVRSQNEHPCT
d9  VYHWQTPGPGWQCIEDTSVSSFNTTTTWNGEASC SVGMQTRKVICRVNVVGVVGPCKCPESLRPETVRPCLLPCR
d10  KDCVVTYSDWTPCPS-SCREGD- SGARKQSRQVVIQLPANGGKESDPLYEKACEAPPCH
d11  SYRWKTHKWRRCLVPSIQDVPGAQEGCGPGRQARAITCRKQDGGQASIQECLQYAGVPAALTQACQIP
d12  DDQFTSNWKFSSCNGDCGAVRTRKRAIVGKSKKKECKNSHLYPLIETQYCPCD
d13  KYNAQPVGNSDCILPEGKAEVLLGMKVQGDGSKGCGGYRYQAMACYDNGRLVETSRONS HGYIEEACIIP
d14  SDCKLSEWNSRCSKSCGSGVKVRSKWLREKPYNGGRPCPKLDHVNQAQVYEVVPCHSDCN
d15  QYIYWTEPWSVCKVTFVDMRDNGEGEVQTRKVRMCQNTADGPESEHVEDYLCDEPDMPLGSRCKLPCP
d16  EDCVISEWGPWTCALPCNPSSGSRQADPIRQPADEGRACPDAVEKEPCSLNKNKY
d17  HYDYNVTDWSTCQLSEKAVCGNGIKRMLDCVRSDDGKSVDLKYCELEGLKNWPMNTSCTVECP
d18  VNCQLSDWSSWSQCSQTCGLTGKMIKRTVTQPFQGDGRPCPSLMEQSKPCVKPCY
d19  RWQYQWSPCQVQEAQCGEGTRTRNISCVVSDGSAEDFSKVVDEEFCANTELIIDGNKQIVLEETCTQPCP
d20  GDCYLNDSWSSSLCQLTCVNGEDLFGGGIQVRSRAVVIQLELENHLCPEQMLETKSCDDGQCY
d21  EYKWVASAWKGSRRVWCQRSDDGINVTGGGLV-VQPDTRSCNPSPCSQPHSYCSEMKTCT
stalk/tm  CEEGYTEVMSSNSTLEQCTLIPVVVITVEDKRGDVKTSRAVHPTQPSINPAGRGRTWLQPFPGDGRKLTW
cytosol  VYGAAGAFAVLLVFIIVSMIYLACKPKKPKRRQNNRKLPLTLAYDGDADM
```

Supplemental Figure 13. Identification of TSP-1 domains and structure of mouse THSD7A. **(A)** Reference sequences for TSP-1 domains as in THBS1 (protein data bank [pdb] code 3r6b¹, upper panel) and for TSP-1 domains as in C6 (pdb code 3t5o²) or F-spondin (pdb code 1szl³) and alignment with the 21 TSP-1 domains of mouse THSD7A. Yellow, cysteine; magenta, tryptophane; cyan, arginine. **(B)** Amino acid sequence of full-length mouse THSD7A with colored tagging of all parts. Purple, leader peptide; red, THBS1-like TSP-1 domain; green, C6-like TSP-1 domain; blue, coiled coil (cc) domain; brown, extracellular stalk region, transmembrane (tm) region and cytosolic tail.



Supplemental Figure 14. (A) Western blot analysis of reactivity of two different rabbit antisera with the human and mouse TSP-1 domain constructs under non-reducing conditions. Asterisks mark the recognized TSP-1 domain constructs.

	Number of patients with epitope recognition	
	At study start	At the end of follow-up
d1_d2	6	3
d2_d3	0	0
d3_d4	0	0
d5_d6	0	0
d7_d8	4	2
d9_d10	1	0
d11_d12	2	0
d13_d14	5	1
d15_d16	2	0
d17_d18	0	0
d19_d21	6	3

Supplemental Table 1. Epitope pattern during follow-up in seven patients, in whom recognition of one or more epitopes was lost.

	Amino acid sequence homology (%)		
	Rabbit versus human	Rabbit versus mouse	Mouse versus human
Full-length THSD7A	92	90	91
d1_d2	92	88	91
d2_d3	91	85	90
d3_d4	87	84	85
d5_d6	91	88	86
d7_d8	95	93	94
d9_d10	90	89	90
d11_d12	98	96	95
d13_d14	99	97	98
d15_d16	94	91	89
d17_d18	94	92	94
d19_d21	92	90	92

Supplemental Table 2. Amino acid sequence homology in percent between rabbit, human and mouse TSP-1 domain orthologs.

SUPPLEMENTAL METHODS

Cell culture, cell transfection and recombinant protein expression

Two lines of human embryonic kidney cells (HEK) were kept in culture for recombinant expression of THSD7A fragments. HEK293-6E is a cell line that can be cultivated in the absence of serum and is especially suitable for the expression of secreted proteins.^{4,5} HEK293T is a standard cell line for recombinant protein expression.⁶ HEK293-6E cells were cultured in cell culture bottles with 10 ml of serum-free medium (Freestyle 293, Gibco by Life Technologies, Grand Island, USA). HEK293T cells were cultured in 10 cm dishes with 10 ml Dulbecco's Modified Eagle Medium (DMEM, Life Technologies, Grand Island, USA) with addition of 10% fetal bovine serum (Thermo Scientific, Cramlington, United Kingdom) and 1% Penicillin/Streptomycin (Life Technologies, Grand Island, USA).

All protein fragments were transfected to both cell types and expression efficiency was evaluated. The d11_d21 construct was the only one not to be secreted into the culture medium and expression was higher in HEK293T cells. Thus, we chose to express d11_d21 in HEK293T cells for further experiments. All other constructs were well secreted into the culture medium when expressed in HEK293-6E cells.

For transfection of HEK293-6E cells, a polythylenimine (PEI)-based method (Polyscience Inc., Warrington, USA) was used. For each approach, 126 μ L (40 μ g) of PEI was mixed with 124 μ L water and 250 μ L NaCl (300 mM) was added. 10 μ g Plasmid DNA in 250 μ L water was mixed with the same amount of NaCl in a separate tube. Subsequently, solutions were slowly mixed, vortexed and incubated for 30 min. The solution was then added to the cells. After 24 h the cells were fed with 250 μ L feeding medium (Freestyle 293 medium supplemented with 20% tryptone). Five days later, cells were collected using centrifugation at 300 g and the supernatant was centrifuged again at 14,000 g for 30 min.

For transfection of HEK293T cells, a calcium phosphate-based method was used.⁶ Ten μ g of plasmid DNA was mixed with 36 μ L of 2 M CaCl_2 and diluted with sterile water up to a volume of 300 μ L. This solution was gently mixed with an equal volume of 2x HEPES buffered saline (HBS, 275 mM NaCl, 55 mM HEPES, pH 7.0) and incubated 30 min at room temperature. The resulting solution was added drop wise to the cells. Medium was changed 24 h after transfection. After 48 h, cells were scraped, centrifuged at 1,500 rpm for 5 minutes, washed with PBS, and centrifuged again at 1,500 rpm for 5 minutes. Cells were then lysed in 50 mM Tris pH 7.4, 1 mM EDTA, 150 mM NaCl, 1% Triton after addition of a protease inhibitor cocktail (Roche Diagnostics, Indianapolis, USA), sonicated, and centrifuged at 14,000 g and 4 °C for 1 h. The supernatant was saved and protein concentration was determined using the Pierce BCA protein assay kit according to the manufacturer's instructions (Thermo Fisher, Waltham, USA). All expressions (medium and cell lysate) were validated by Western blot and

immunological detection using an anti-his antibody (1:1,000, Thermo Scientific, Cramlington, United Kingdom). For analyses with patient sera, the culture media of d1_d4- and d5_d10-transfected cells and the cell lysate of d11_d21-transfected cells were used.

Protein fractionation and deglycosylation

To determine the subcellular location of the d11_d21 construct, cells were first lysed in 50 mM Tris pH 7.4, 0.32 M sucrose and 10 mM EDTA with a protease inhibitor cocktail (as above), sonicated, rotated for 30 min at 4 °C, and centrifuged at 100,000 g for 1 h at 4 °C. The supernatant was taken and labeled as the soluble (cytoplasmatic) fraction. The pellet was then resuspended in 50 mM Tris pH 7.4, 150 mM NaCl, 0.1% SDS, 1% NP40 and 0.5% Na-DOC with a protease inhibitor cocktail (as above), sonicated, rotated for 30 min at 4 °C, and centrifuged at 100,000 g for 1 h at 4 °C. The supernatant was labeled as the detergent-soluble (membrane) fraction. The cell pellet was then resuspended in 50 mM Tris pH 7.4, 10 mM DTT and 8 M urea, sonicated, and labeled as the insoluble fraction. As a control experiment, HEK293 cells transfected with full-length THSD7A were treated identically.

Deglycosylation experiments were performed using a combination of *N*-glycopeptidase F and neuraminidase (both Roche Diagnostics, Mannheim, Germany). Protein samples were incubated overnight at 37 °C with deglycosylating enzymes or an equal volume of PBS (1 µl per 100 µg of total protein).

Western blot and immunological detection

Protein samples were prepared for Western blot analysis by addition of 5x Laemmli buffer (1.5 M Tris-HCl pH 6.8, 50% glycerol, 10% SDS, 1% bromophenol blue) and subsequent heating to 95 °C for 10 minutes. If reducing conditions were desired, 20% β-mercaptoethanol was added to the 5x loading buffer. Proteins were separated by electrophoresis in 4-15% gradient gels (Bio-Rad, Hercules, USA) in an electrophoresis chamber (Bio-Rad, Hercules, USA) in the presence of a migration buffer (25 mM Tris, 192 mM glycine, 0.1% SDS; Amresco, Solon, USA). Subsequently, proteins were transferred to methanol-soaked PVDF membranes (Millipore, Billerica, USA) under semi-dry conditions in the presence of 25 mM Tris pH 8.5, 192 mM glycine, ethanol 20% using the Transblot Turbo system (Bio-Rad, Hercules, USA) at 25 V constant for 35 min. Membranes were blocked in 5% dry milk with PBS plus Tween 0.05% (PBS-T) for 2 h at room temperature followed by the incubation with the primary antibody (anti-his antibody, 1:1,000, Thermo Scientific; anti-THSD7A antibody, 1:1,000, Atlas, #000923), human serum, rabbit serum or mouse serum (all 1:100) in 0.5% dry milk in PBS-T. The next day, membranes were washed three times with PBS-T the next day and incubated with the secondary antibody in 5% dry milk in PBS-T for 2 h. HRP-conjugated mouse anti-human IgG4 and HRP-conjugated mouse anti-human IgG (both 1:20,000, SouthernBiotech, Birmingham,

USA), were used to analyze serum reactivity with the various THSD7A constructs. HRP-conjugated goat anti-mouse IgG was used as secondary antibody for his detection and HRP-conjugated goat anti-rabbit for THSD7A detection (both 1:20,000, SouthernBiotech, Birmingham, USA). To visualize the protein bands, membranes were incubated in a chemiluminescent substrate (SuperSignal West Pico and SuperSignal West Femto, Thermo Scientific, Rockford, USA, used in a 4:1 ratio) followed by incremental luminescence detection for up to 12 minutes with a Fujifilm LAS imager 3000. For testing human serum, protein loading was standardized based on anti-his reactivity under reducing conditions and all sera were used in a 1:100 dilution at all times.

Native blotting (dot blot analysis) and immunological detection

His-tagged TSP-1 domain constructs (d1_d2 to d19_d21) were purified under native conditions using a Ni-NTA resin (His-Pur, Thermo Scientific, Rockford USA, #88221) applying the batch method according to the manufacturer's instructions. Equilibration, wash, and elution buffers were PBS-based (pH 7.4) and supplemented with 10 mM imidazol, 25 mM imidazole, and 250 mM imidazole, respectively. Protein purification was validated by Coomassie-blue staining of electrophoresed proteins. Purified proteins were dotted on nitrocellulose membranes (Protran, Whatman, Dassel, Germany) and allowed to dry for 10 minutes at room temperature. Membranes were then blocked in 4% dry milk in PBS plus Tween 0.08% (PBS-T) for 3 hours, followed by incubation with human serum (1:100) or anti-his antibody (1:1000) in PBS-T with 0.5% dry milk. A mixture of HRP-conjugated anti-human IgG and anti-human IgG4 or anti-mouse IgG (all 1:20,000, SouthernBiotech, Birmingham, USA) were used as secondary antibodies and visualization of the protein signal was performed as described above.

Immunohistochemical analyses

1 μ M paraffin sections of mouse kidneys were deparaffinized and rehydrated. Antigen retrieval was obtained for rabbit IgG by digestion with protease XXIV (5 μ g/mL, Sigma) for 15 min at 37°C. Nonspecific binding was blocked with 5% horse serum (Vector, Burlingame, USA) with 0.05% Triton X-100 (Sigma) in PBS for 30 min at room temperature prior to incubation at 4 °C overnight with biotinylated anti-rabbit IgG (1:400) in blocking buffer. Staining was visualized with the ZytochemPlus AP Polymer kit (Zytomed Systems, Berlin, Germany) according to the manufacturer's instruction with neufuchsin (Merck) as a color substrate. Nuclei were counterstained with hemalaun (Merck) and sections were mounted with gum Arabic (Sigma, St. Louis, USA). Negative controls were performed by omitting primary antibodies. Stainings were evaluated with an Axioskop using the Axiovision software (all Zeiss).

SUPPLEMENTAL REFERENCES

1. Klenotic, PA, Page, RC, Misra, S, Silverstein, RL: Expression, purification and structural characterization of functionally replete thrombospondin-1 type 1 repeats in a bacterial expression system. *Protein Expr Purif*, 80: 253-259, 2011
2. Aleshin, AE, Schraufstatter, IU, Stec, B, Bankston, LA, Liddington, RC, DiScipio, RG: Structure of complement C6 suggests a mechanism for initiation and unidirectional, sequential assembly of membrane attack complex (MAC). *J Biol Chem*, 287: 10210-10222, 2012
3. Paakkonen, K, Tossavainen, H, Permi, P, Rakkolainen, H, Rauvala, H, Raulo, E, Kilpelainen, I, Guntert, P: Solution structures of the first and fourth TSR domains of F-spondin. *Proteins*, 64: 665-672, 2006
4. Danquah, W, Meyer-Schwesinger, C, Rissiek, B, Pinto, C, Serracant-Prat, A, Amadi, M, Iacenda, D, Knop, JH, Hammel, A, Bergmann, P, Schwarz, N, Assuncao, J, Rotthier, W, Haag, F, Tolosa, E, Bannas, P, Boue-Grabot, E, Magnus, T, Laeremans, T, Stortelers, C, Koch-Nolte, F: Nanobodies that block gating of the P2X7 ion channel ameliorate inflammation. *Sci Transl Med*, 8: 366ra162, 2016
5. Zhang, J, MacKenzie, R, Durocher, Y: Production of chimeric heavy-chain antibodies. *Methods Mol Biol*, 525: 323-336, xv, 2009
6. Tomas, NM, Hoxha, E, Reinicke, AT, Fester, L, Helmchen, U, Gerth, J, Bachmann, F, Budde, K, Koch-Nolte, F, Zahner, G, Rune, G, Lambeau, G, Meyer-Schwesinger, C, Stahl, RA: Autoantibodies against thrombospondin type 1 domain-containing 7A induce membranous nephropathy. *J Clin Invest*, 126: 2519-2532, 2016

A novel mouse model of phospholipase A2 receptor 1-associated membranous nephropathy mimics podocyte injury in patients

Catherine Meyer-Schwesinger^{1,6}, Nicola M. Tomas^{2,6}, Silke Dehde², Larissa Seifert², Irm Hermans-Borgmeyer³, Thorsten Wiech⁴, Friedrich Koch-Nolte⁵, Tobias B. Huber² and Gunther Zahner²

¹Institute of Cellular and Integrative Physiology, University Medical Center Hamburg-Eppendorf, Hamburg, Germany; ²III. Department of Medicine, University Medical Center Hamburg-Eppendorf, Hamburg, Germany; ³Center of Molecular Neurobiology, University Medical Center Hamburg-Eppendorf, Hamburg, Germany; ⁴Institute of Pathology, University Medical Center Hamburg-Eppendorf, Hamburg, Germany; and ⁵Institute of Immunology, University Medical Center Hamburg-Eppendorf, Hamburg, Germany

The phospholipase A2 receptor 1 (PLA2R1) is the major autoantigen in patients suffering from membranous nephropathy. To date, the lack of endogenous glomerular expression of PLA2R1 in mice and rats has impeded the establishment of PLA2R1-dependent animal models of this disease. Here, we generated a transgenic mouse line expressing murine full-length PLA2R1 in podocytes. Furthermore, expression of murine PLA2R1 did not result in any morphological disturbance as high-resolution confocal microscopy demonstrated an intact nephrin distribution with normal foot processes. Transfer of rabbit anti-mPLA2R1 antibodies to these mice induced nephrotic range proteinuria, hypercholesterolemia, and histomorphological signs of membranous nephropathy. Immunohistochemical and immunofluorescence analyses revealed enhanced staining for murine PLA2R1 in the presence of unaffected staining for murine thrombospondin type-1 domain-containing 7A in the diseased mice, resembling what is classically found in patients with PLA2R1-associated membranous nephropathy. Thus, our mouse model of membranous nephropathy will allow investigation of PLA2R1-specific pathomechanisms and may help to develop and assess antigen-specific treatments *in vivo*.

Kidney International (2019) ■, ■-■; <https://doi.org/10.1016/j.kint.2019.10.022>

KEYWORDS: membranous nephropathy; mouse model; nephrotic syndrome; phospholipase A2 receptor 1 (PLA2R1); podocyte

Copyright © 2019, International Society of Nephrology. Published by Elsevier Inc. All rights reserved.

Correspondence: Gunther Zahner, III. Department of Medicine, University Medical Center Hamburg-Eppendorf, Martinistraße 52, 20246 Hamburg, Germany. E-mail: zahner@uke.de

⁶CM-S and NMT contributed equally.

Received 12 August 2019; revised 8 October 2019; accepted 24 October 2019; published online 9 November 2019

Translational Statement

Over the last decade, the measurement of anti-phospholipase A2 receptor 1 (PLA2R1) antibodies for the diagnosis and monitoring of patients with membranous nephropathy (MN) has been broadly implemented into clinical practice worldwide. Despite this major advance, MN pathomechanisms are still incompletely understood, and patient treatment relies on broad and unspecific immunosuppression. We envision that this model of PLA2R1-associated MN may help to dissect the molecular mechanisms that underlie podocyte injury in MN. The roles of the complement system and receptor-specific podocyte signaling programs represent subjects of future interest that can be addressed using this model. Additionally, innovative therapeutic strategies targeting MN-specific pathomechanisms can be investigated regarding their *in vivo* efficacy—a prerequisite for the translation to patient care in the future.

Membranous nephropathy (MN) is an autoimmune glomerular disease and a frequent cause of nephrotic syndrome. Morphologically, the disease is characterized by granular deposition of IgG and complement system components along the glomerular filtration barrier as well as by subepithelial electron-dense deposits and podocyte foot process effacement in electron microscopy.^{1,2} Circulating autoantibodies against the podocyte membrane proteins phospholipase A2 receptor 1 (PLA2R1) and thrombospondin type-1 domain-containing 7A (THSD7A) are found in around 75%–80% of cases.^{3,4} Although recent animal studies demonstrated a pathogenic role of anti-THSD7A antibodies in the development of MN,^{5,6} the lack of endogenous PLA2R1 expression in rodents⁷ precluded analogous antibody transfer studies. However, as the majority of MN cases are PLA2R1-associated, the development of a mouse model involving this antigen is fundamental in order to experimentally investigate the role of anti-PLA2R1 antibodies, understand the pathogenic route through which anti-PLA2R1 autoantibodies induce

disease, and develop and evaluate novel antigen-specific treatments.

RESULTS

Generation and basal characterization of mouse PLA2R1 (mPLA2R1)-positive mice

Mice expressing mPLA2R1 in podocytes (mPLA2R1-positive mice) and their littermate controls (mPLA2R1-negative mice) were generated using a transgenic knock-in approach (Supplementary Methods and Supplementary Figure S1). The transgenic mPLA2R1 protein was strongly expressed in the podocyte membrane and cytoplasm of mPLA2R1-positive mice, whereas mPLA2R1 expression was completely absent in podocytes of mPLA2R1-negative mice (Figure 1a). In mPLA2R1-positive mice, mPLA2R1 expression partially merged with the slit diaphragm protein nephrin, indicating a specific localization at podocyte foot processes. Expression of mPLA2R1 did not result in a morphologic disturbance of foot process morphology, as high-resolution confocal microscopy demonstrated an intact nephrin distribution with normal foot processes (Figure 1b). Electron microscopy confirmed a regular foot process morphology and demonstrated normal glomerular basement membranes and endothelium in all mice (Figure 1c). Additionally, light microscopy showed no alterations in overall glomerular and tubulointerstitial morphology (Figure 1d). The number of podocytes identified by p57 staining was also similar in the 2 groups (Figure 1e). Measurement of the albumin/creatinine ratio in the urine of these mice excluded an mPLA2R1-mediated altered permeability of the glomerular filtration barrier to protein, determined over the course of 15 weeks (Figure 1f). Finally, we found no activation of pathways indicating cellular stress (Supplementary Figure S2), excluding an overload of cellular degradation/repair systems related to the transgenic expression of mPLA2R1. Together, these results demonstrate the successful generation of an mPLA2R1-expressing mouse line.

Generation of rabbit anti-mPLA2R1 antibodies

Rabbit anti-mPLA2R1 antibodies were generated by means of cDNA immunization. Incubation of Chinese hamster ovary (CHO) cells cotransfected with mPLA2R1 and green fluorescent protein with rabbit antiserum, but not with serum taken before immunization, resulted in a specific fluorescent signal for membrane-bound rabbit IgG on those cells showing a nuclear green fluorescent protein signal, demonstrating the presence of mPLA2R1-specific serum antibodies (Supplementary Figure S3A). Total IgG purified from the rabbit serum after immunization (referred to as anti-mPLA2R1 IgG) showed strong and specific binding to mPLA2R1 present in mouse glomerular extracts purified from mPLA2R1-positive mice under nonreducing conditions, and a complete absence of binding when mPLA2R1 was reduced (Figure 2a). This finding is in accordance with the known characteristics of patient anti-PLA2R1 autoantibodies, which also recognize conformation-dependent epitopes within the target antigen.³ Of note, a faint signal could also be

detected in glomerular extracts from mPLA2R1-negative mice (and wild-type BALB/c mice, data not shown), possibly indicating a low intrinsic expression of mPLA2R1 in mouse glomeruli. The anti-mPLA2R1 IgG strongly recognized the N-terminal region of mPLA2R1 comprising the cysteine-rich domain, the fibronectin type II domain, and the first C-type lectin domain (CysR-CTLD1), and bound additional epitopes in the CTLD1-2, CTLD2-6, and CTLD2-8 regions, but not in the CTLD7-8 region (Supplementary Figure S3B).

Disease development after transfer of anti-mPLA2R1 IgG

We next injected anti-mPLA2R1 IgG (total IgG purified from mPLA2R1-immunized rabbits) or control IgG (total IgG purified from non-immunized rabbits) intraperitoneally into mPLA2R1-positive and/or mPLA2R1-negative mice. mPLA2R1-positive mice injected with anti-mPLA2R1 IgG, but not the other groups, rapidly developed proteinuria up to an albumin/creatinine ratio of 100 g/g that was sustained over the complete observation period of 7 days (Figure 2b). Urinary samples of these mice contained, in addition to albumin as the most prominent protein at 69 kDa, both low (below 69 kDa) and high (above 69 kDa) molecular weight proteins (Supplementary Figure S3C), indicating a major perturbation of the glomerular filtration barrier. When the amount of injected rabbit IgG was reduced, proteinuria also decreased, suggesting a dose-dependent effect (data not shown). We also analyzed proteinuria up to 21 days (during the autologous phase of the disease) in an independent experimental cohort and found that albumin-to-creatinine ratios slowly decreased below 100 g/g (data not shown).

In addition, serum cholesterol levels were significantly increased in mPLA2R1-positive mice receiving anti-mPLA2R1 positive rabbit IgG (Figure 2c), whereas serum urea nitrogen levels remained normal (Figure 2d). Taken together, these results demonstrate that anti-mPLA2R1 antibodies cause nephrotic-range proteinuria and hypercholesterolemia in mPLA2R1-positive mice.

Histologic and ultrastructural changes after transfer of anti-mPLA2R1 IgG

We next investigated the histologic changes in mice after transfer of anti-mPLA2R1 IgG. We found granular and sub-epithelial deposition of rabbit IgG in mPLA2R1-positive mice 5 and 7 days after injection of anti-mPLA2R1 IgG (Figure 2e; Supplementary Figure S4). In contrast, rabbit IgG staining along the glomerular filtration barrier was absent in mPLA2R1-positive mice treated with control IgG, as well as mPLA2R1-negative mice treated with anti-mPLA2R1 IgG (Figure 2e; Supplementary Figure S5), albeit the latter showed very faint positivity for rabbit IgG in the mesangial space, again possibly indicating some intrinsic mPLA2R1 expression in the glomeruli of these mice. However, attempts to localize intrinsic glomerular mPLA2R1 expression in wild-type and in mPLA2R1-negative mice by immunohistologic techniques were unavailing. Notably, mPLA2R1-positive mice treated with anti-mPLA2R1 IgG showed positivity for complement

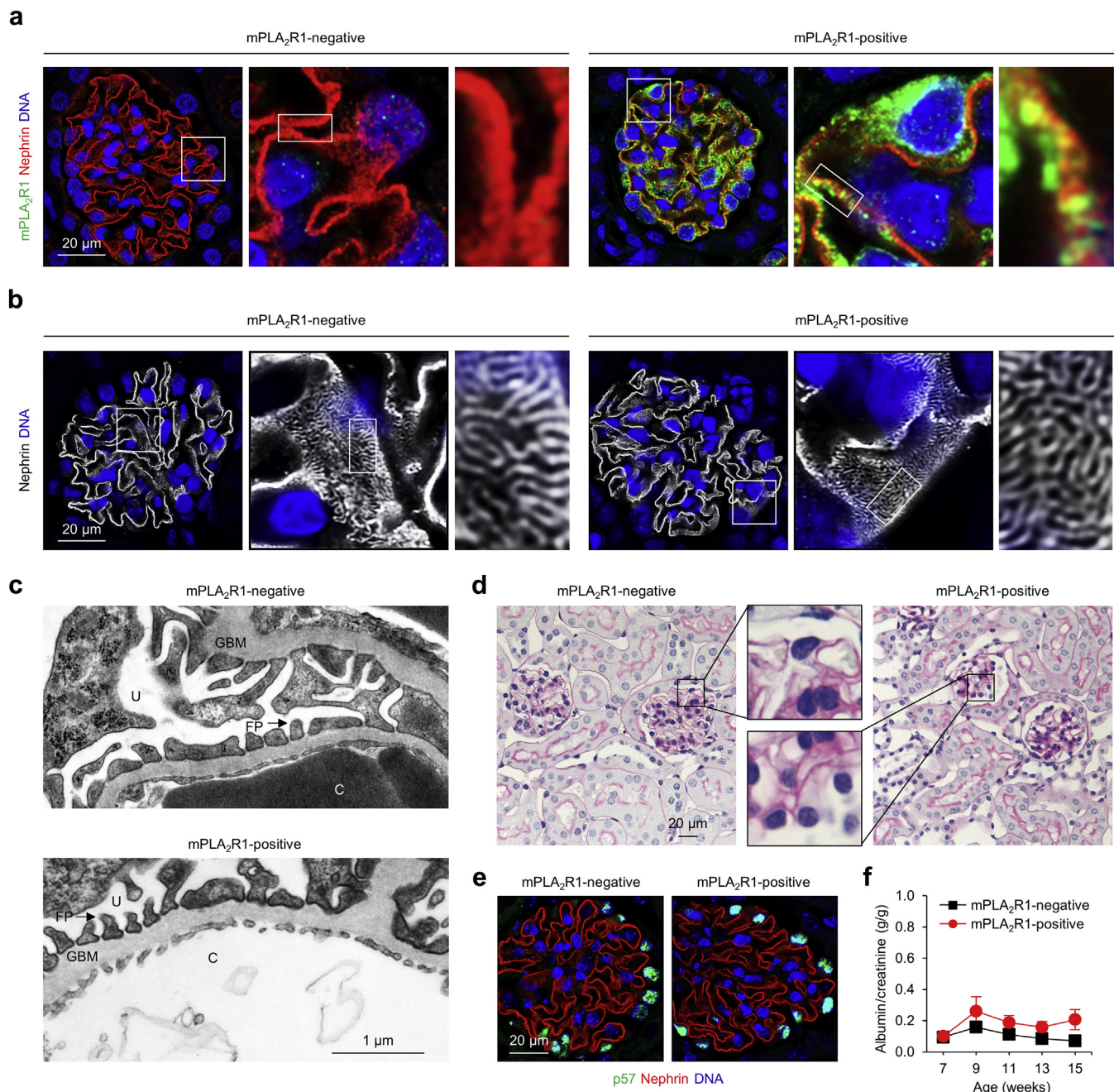


Figure 1 | Basal characterization of mouse phospholipase A2 receptor 1 (mPLA2R1)-positive mice. The basal phenotype of 15 week-old mPLA2R1-positive mice backcrossed to the BALB/c background in comparison to mPLA2R1-negative control littermates was evaluated. **(a)** Confocal microscopy shows the expression of mPLA2R1 (green) along the glomerular filtration barrier in close proximity to the slit diaphragm protein nephrin (red) and in the cytoplasm of podocytes exclusively in mPLA2R1-positive mice. Blue, nuclei. **(b)** High-resolution confocal microscopy staining for nephrin demonstrates regular foot process (FP) morphology in mPLA2R1-positive mice. Blue, nuclei. **(c)** Electron micrographs of the glomerular filtration barrier exhibit normal architecture of the endothelial cell layer, the glomerular basement membrane (GBM), and podocytes in mPLA2R1-positive mice. **(d)** Periodic acid-Schiff staining shows normal glomerular and tubulointerstitial morphology in mPLA2R1-positive mice. **(e)** The number of podocytes identified by p57 staining (green) was comparable between mPLA2R1-positive and -negative animals. Red, nephrin; blue, nuclei. **(f)** Albumin/creatinine ratios as measured by enzyme-linked immunosorbent assay from 7 up to 15 weeks of age. Values are expressed as mean \pm SEM; $n = 7$ for mPLA2R1-negative mice; $n = 11$ for mPLA2R1-positive mice. C, capillary; U, urine. To optimize viewing of this image, please see the online version of this article at www.kidney-international.org.

C3 in partial colocalization with the bound rabbit IgG at day 7, suggesting complement activation in the area of immune complex deposition (Figure 2f). This activation of the complement system was accompanied by oxidative stress as

indicated by an upregulation of superoxide dismutase 1 (SOD1) in podocytes (Supplementary Figure S6).

Antibody elution experiments from renal cryosections derived from mPLA2R1-positive mice 7 days after injection of

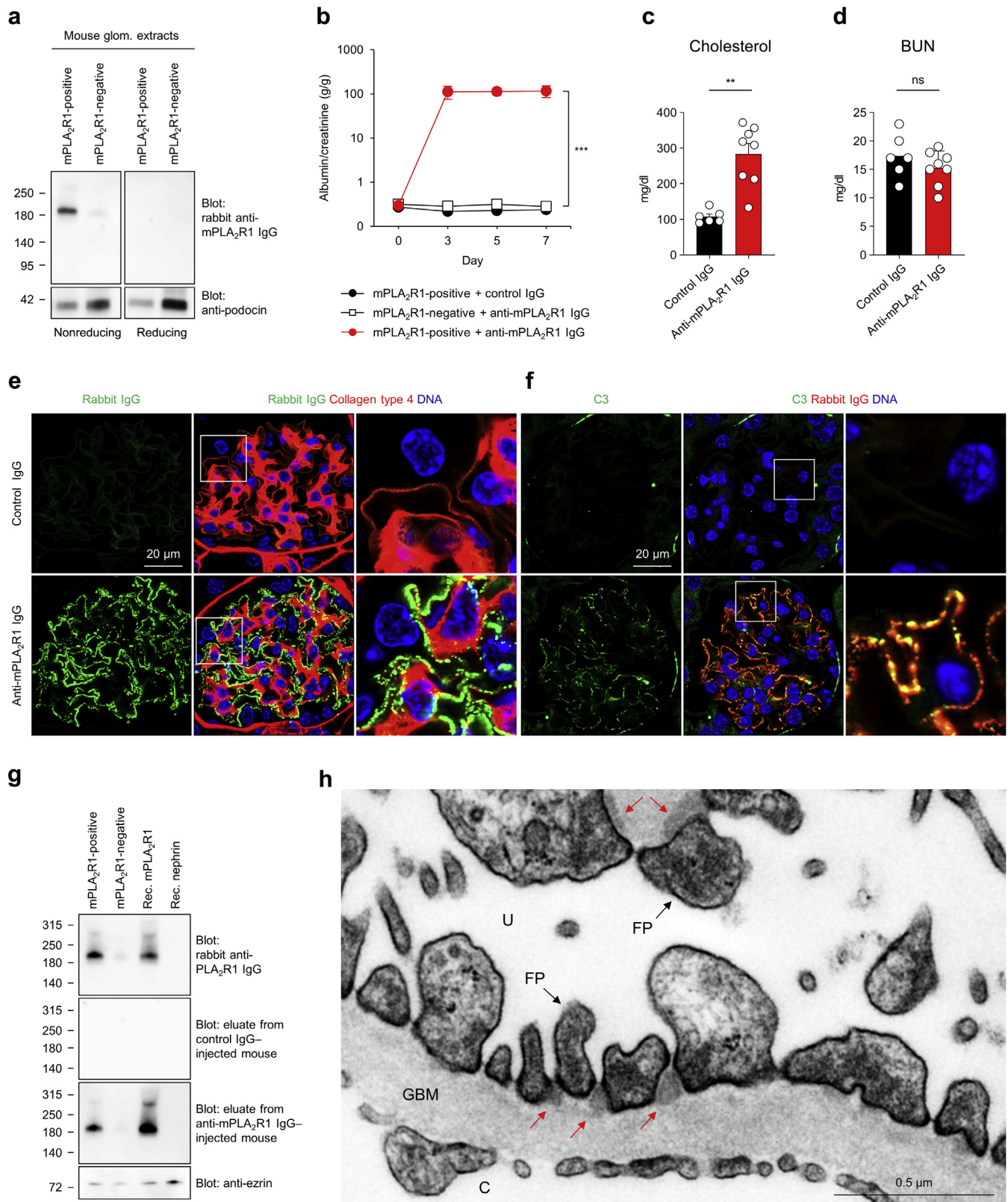


Figure 2 | Passive transfer of anti-mouse phospholipase A2 receptor 1 (mPLA2R1) IgG induces membranous nephropathy in mPLA2R1-positive mice. (a) Western blot analyses of mouse glomerular (glom.) extracts with anti-mPLA2R1 IgG under nonreducing and reducing conditions. Note the specific reactivity with mPLA2R1 at 180 kDa solely under nonreducing conditions. Anti-beta actin detection was used with the same membrane as a loading control. **(b)** Time-course of albuminuria as measured by albumin/creatinine ratio. Values are indicated as mean \pm SEM following the application of 3 milligrams of anti-mPLA2R1 IgG or control IgG to mPLA2R1-positive mice (continued)

either control or anti-mPLA2R1 IgG demonstrated specific binding of eluted antibodies to both recombinant mPLA2R1 and mPLA2R1 present in mouse glomerular extracts (Figure 2g). In periodic acid–Schiff stainings, mPLA2R1-positive mice treated with anti-mPLA2R1 IgG exhibited protein casts in dilated tubuli, reflecting the heavy proteinuria (Supplementary Figure S7A). Immunohistochemical and immunofluorescence analyses revealed enhanced staining for mPLA2R1 in the presence of unaffected staining for mouse THSD7A in the diseased mice (Supplementary Figure S7B–D), resembling the situation that is classically found in patients with PLA2R1-associated MN.^{4,8} In electron microscopic analyses, we found electron-dense deposits in a strictly subepithelial location within the glomerular basement membrane and areas of foot process broadening in mPLA2R1-positive mice injected with anti-mPLA2R1-positive IgG, but not in control mice (Figure 2h; Supplementary Figure S8). Of note, electron-dense deposits were found in close proximity to the podocyte slit diaphragms. In line, high-resolution confocal imaging revealed areas of foot process effacement and colocalization of mPLA2R1 and the deposited rabbit IgG with the slit-diaphragm protein nephrin (Supplementary Figure S9A), suggesting, as described previously for experimental THSD7A-associated MN,⁹ that the slit diaphragm is an early target of mPLA2R1-anti-mPLA2R1 antibody immune complex formation. Additionally, disruption of nephrin architecture indicated slit diaphragm alterations induced by the anti-PLA2R1 IgG (Supplementary Figure S9B).

Taken together, these results demonstrate that mPLA2R1-expressing mice develop the typical histomorphologic signs of human MN after transfer of anti-mPLA2R1 antibodies.

DISCUSSION

The purpose of this study was the establishment and characterization of a murine model of PLA2R1-associated MN. In this regard, we (i) developed a transgenic mouse line expressing mPLA2R1 in podocytes, (ii) generated mPLA2R1-specific antibodies in rabbits, and (iii) found that transfer of these antibodies causes MN in PLA2R1-expressing mice. Thus, the clinical and histologic features of MN could be

successfully reproduced in mice, representing an antigen-specific passive immunization model of PLA2R1-associated MN.

Previous attempts of our group to induce MN in mice expressing human PLA2R1 fused to a glycosylphosphatidylinositol anchor were unsuccessful (Zahner G, Helmchen U, Stahl RA. The generation of inducible specific human phospholipase A2 receptor transgenic mice [abstract]. *J Am Soc Nephrol.* 2012;23:568A; Zahner G, Tomas N, Hoxha E, et al. Development and morphologic characterization of a mouse model of membranous nephropathy involving the human phospholipase A2 receptor [abstract]. *J Am Soc Nephrol.* 2014;25:66A). This lack of success could be related to the complex structure of PLA2R1,¹⁰ resulting in insufficient antigen expression and membrane incorporation of the human protein in mice. In an attempt to circumvent these issues, we decided to transgenically express the murine PLA2R1 orthologue (mPLA2R1), which shares a moderate amino acid identity of 72% with human PLA2R1. We also injected a few mPLA2R1-positive mice with patient-derived anti-PLA2R1 IgG, but we could hardly detect any glomerular binding of human IgG, and the mice did not develop proteinuria. In Western blot analysis, we found a markedly reduced binding of patient serum with recombinant mPLA2R1, indicating that the human anti-PLA2R1 autoantibodies cannot bind the murine antigen to an extent sufficient to induce disease. This lack of disease development when using patient autoantibodies is a limitation of our model.

Application of this PLA2R1-specific MN model will help to address several important questions in the field of MN.^{11,12} Studies in the Heymann nephritis model indicated that local activation of the complement system with subsequent podocyte damage by the membrane attack complex C5b-9 is the key step in induction of proteinuria in MN.^{13,14} More recent studies suggest additional complement-independent mechanisms of antibody pathogenicity in MN, such as disturbance of cell adhesion to collagen type IV by anti-PLA2R1 antibodies,¹⁵ cytoskeletal rearrangement and alterations in focal adhesion signaling induced by anti-THSD7A antibodies,⁵ and inhibition of target antigen enzymatic activity by anti-neutral endopeptidase antibodies.^{16,17} Notably, we found some glomerular deposition of complement C3 in

Figure 2 | (continued) ($n = 11$ and $n = 9$, respectively) as well as the transfer of anti-mPLA2R1 IgG to mPLA2R1-negative mice ($n = 4$). ******* $P < 0.001$, 2-way analysis of variance. (c) Serum cholesterol and (d) blood urea nitrogen (BUN) levels in the serum of mPLA2R1-positive mice 7 days after the transfer of control IgG or anti-mPLA2R1 IgG. Values are expressed as mean \pm SEM, ****** $P < 0.01$, 2-tailed nonparametric Mann-Whitney U test. (e) Confocal microscopic analyses of rabbit IgG (green) in respect to the glomerular basement membrane (GBM) constituent collagen type 4 (red) in mPLA2R1-positive mice injected with anti-mPLA2R1 IgG or control IgG. Blue, nuclei. Only mPLA2R1-positive mice treated with anti-mPLA2R1 IgG showed an intensive granular subepithelial binding of rabbit IgG. (f) Confocal microscopic analyses of complement C3 (green) and rabbit IgG (red) in mPLA2R1-positive mice injected with anti-mPLA2R1 IgG or control IgG. Blue, nuclei. mPLA2R1-positive mice treated with anti-mPLA2R1 IgG showed pronounced complexes of C3 and rabbit IgG, suggesting complement activation at areas of rabbit IgG binding. (g) Bound IgG was eluted from frozen kidney sections from mPLA2R1-positive mice injected with anti-mPLA2R1 IgG or control IgG. The eluted rabbit IgG was used as the primary antibody in nonreducing Western blot analyses against mouse glom. extracts derived from mPLA2R1-positive and -negative mice as well as against recombinant (rec.) mPLA2R1 and nephrin (negative control). Ezrin detection was used as a loading control. (h) Electron microscopic analysis of the glom. filtration barrier in an mPLA2R1-positive mouse injected with anti-mPLA2R1 IgG. Note that electron-dense deposits are mainly located at the slit diaphragm (red arrows) of mPLA2R1-positive mice. C, capillary; FP, foot process; ns, not significant; U, urine. To optimize viewing of this image, please see the online version of this article at www.kidney-international.org.

our mouse model of PLA2R1-associated MN, in contrast to results in the recently published mouse model of THSD7A-associated MN,⁶ in which C3 was barely detectable. Future studies are needed to investigate the pathogenic relevance of glomerular complement activation and antibody-induced alterations in antigen function and podocyte signaling in experimental PLA2R1- and THSD7A-associated MN.

The identification of the antibody binding regions in PLA2R1^{18–20} and THSD7A²¹ will give rise to the development of novel and individualized therapies. For example, antibody clearance using epitope-specific immunoadsorption, trapping of pathogenic antibodies by antibody-binding fragments, and epitope blockage using specifically engineered antagonists represent therapeutic approaches that can be evaluated for their *in vivo* efficacy in this experimental passive model of PLA2R1-associated MN. The preclinical testing of innovative treatments targeting the autoantibody-producing cells,^{22,23} however, would require an animal model involving the production of autoantibodies by members of the B-cell lineage. Our mPLA2R1-expressing mice may enable the generation of such an active immunization model by means of immunization with either the mPLA2R1 protein or mPLA2R1 cDNA. Interestingly, recognition of epitopes in PLA2R1 beyond the cysteine-rich domain has been found to be associated with higher proteinuria, poor clinical outcome during follow-up, and reduced response to treatment with rituximab in patients with MN.^{20,24,25} However, it is unclear whether this diversified antigen recognition results from differential autoantibody repertoires already defined at disease initiation or from intramolecular epitope spreading over time. In Heymann nephritis, epitope spreading from the N-terminal toward the C-terminal region occurred when rats were immunized with a 236-mer N-terminal residue of megalin.²⁶ Whether this immunologic phenomenon is also part of the immune response against PLA2R1 could be investigated in such an active disease model. Furthermore, how antibody binding to single or multiple epitopes relates to disease severity can be addressed using the herein described passive model of PLA2R1-associated MN by means of domain-specific antibodies.

In conclusion, we generated a murine PLA2R1-dependent MN mouse model that can be robustly induced by rabbit anti-PLA2R1 antibodies and replicates human PLA2R1-associated MN. This model opens new avenues to comprehensive understanding of the molecular mechanisms that underlie podocyte injury in PLA2R1-associated MN and to investigation of innovative therapeutic strategies targeting MN-specific pathomechanisms regarding their *in vivo* efficacy—a prerequisite for translation to patient care in the future.

METHODS

Details on the transgenic generation of mPLA2R1-positive mice and rabbit anti-mPLA2R1 antibodies, antibody purification, conduction of animal experiments, histologic analyses, electron microscopy studies, cell culture, isolation of mouse glomeruli, antibody elution, and statistical analyses are presented in the [Supplementary Methods](#).

DISCLOSURE

NMT holds a patent: “Methods and Kits for Monitoring Membranous Nephropathy.” All the other authors declared no competing interests.

ACKNOWLEDGMENTS

This study was supported by grants from the Deutsche Forschungsgemeinschaft (DFG) as part of the Collaborative Research Center (CRC) 1192 (project B2 to GZ and NMT, project B3 to CMS, project B5 to FKN, and project B6 to TW). CMS holds a Heisenberg Professorship Grant (ME 2108). NMT holds an Emmy Noether Grant (TO 1013) of the DFG. TBH was supported by the DFG (CRC1192, CRC1140, CRC992, HU 1016/8-2), by the Bundesministerium für Bildung und Forschung (BMBF) (STOP-FSGS 01GM1901C), by the European Research Council (ERC grant 61689, DNCure) and by the H2020-IMI2 consortium BEAT-DKD (Innovative Medicines Initiative 2 Joint Undertaking under grant agreement No. 115974).

The authors thank Ronja Steinmetz, Marlies Sachs, Gudrun Dubberke, Fabienne Seyfried, Sarah Hewald, and Ulrike Langbehn for outstanding technical assistance.

SUPPLEMENTARY MATERIAL

Supplementary Methods and Supplementary References.

Figure S1. Generation of mPLA₂R1 full-length podocyte-specific transgenic mice.

Figure S2. Transgenic expression of mPLA₂R1 does not result in cellular/proteostatic stress.

Figure S3. Generation of anti-PLA2R1 antibodies in rabbits and antibody transfer.

Figure S4. mPLA₂R1-positive mice treated with rabbit anti-mPLA₂R1 antibodies but not with control rabbit IgG deposit rabbit IgG at the glomerular filtration barrier on day 5.

Figure S5. mPLA₂R1-negative mice treated with rabbit anti-mPLA₂R1 antibodies do not deposit rabbit IgG nor complement at the glomerular filtration barrier in comparison to mPLA₂R1-positive mice.

Figure S6. Superoxide dismutase 1 (SOD1) is upregulated in mPLA₂R1-positive mice treated with rabbit anti-mPLA₂R1 antibodies.

Figure S7. Light microscopic changes and mPLA₂R1 staining in mPLA₂R1-positive mice 7 days after the transfer of control IgG and anti-mPLA₂R1 IgG.

Figure S8. Electron microscopy studies.

Figure S9. High-resolution confocal and electron microscopic evaluations of immune complexes 7 days after the injection of rabbit anti-mPLA₂R1 IgG to mPLA₂R1-positive mice.

Supplementary material is linked to the online version of the paper at www.kidney-international.org.

REFERENCES

1. Fogo AB, Lusco MA, Najafian B, et al. AJKD atlas of renal pathology: membranous nephropathy. *Am J Kidney Dis.* 2015;66:e15–e17.
2. Segawa Y, Hisano S, Matsushita M, et al. IgG subclasses and complement pathway in segmental and global membranous nephropathy. *Pediatr Nephrol.* 2010;25:1091–1099.
3. Beck LH Jr, Bonegio RG, Lambeau G, et al. M-type phospholipase A2 receptor as target antigen in idiopathic membranous nephropathy. *N Engl J Med.* 2009;361:11–21.
4. Tomas NM, Beck LH Jr, Meyer-Schwesinger C, et al. Thrombospondin type-1 domain-containing 7A in idiopathic membranous nephropathy. *N Engl J Med.* 2014;371:2277–2287.
5. Tomas NM, Hoxha E, Reinicke AT, et al. Autoantibodies against thrombospondin type 1 domain-containing 7A induce membranous nephropathy. *J Clin Invest.* 2016;126:2519–2532.
6. Tomas NM, Meyer-Schwesinger C, von Spiegel H, et al. A heterologous model of thrombospondin type 1 domain-containing 7A-associated membranous nephropathy. *J Am Soc Nephrol.* 2017;28:3262–3277.

7. Rinschen MM, Godel M, Grahammer F, et al. A multi-layered quantitative *in vivo* expression atlas of the podocyte unravels kidney disease candidate genes. *Cell Rep.* 2018;23:2495–2508.
8. Hoxha E, Kneissler U, Stege G, et al. Enhanced expression of the M-type phospholipase A2 receptor in glomeruli correlates with serum receptor antibodies in primary membranous nephropathy. *Kidney Int.* 2012;82:797–804.
9. Herwig J, Skuza S, Sachs W, et al. Thrombospondin type 1 domain-containing 7A localizes to the slit diaphragm and stabilizes membrane dynamics of fully differentiated podocytes. *J Am Soc Nephrol.* 2019;30:824–839.
10. Dong Y, Cao L, Tang H, et al. Structure of human M-type phospholipase A2 receptor revealed by cryo-electron microscopy. *J Mol Biol.* 2017;429:3825–3835.
11. Ronco P, Debiec H. Pathophysiological advances in membranous nephropathy: time for a shift in patient's care. *Lancet.* 2015;385:1983–1992.
12. Salant DJ. Unmet challenges in membranous nephropathy. *Curr Opin Nephrol Hypertens.* 2019;28:70–76.
13. Salant DJ, Belok S, Madaio MP, et al. A new role for complement in experimental membranous nephropathy in rats. *J Clin Invest.* 1980;66:1339–1350.
14. Baker PJ, Ochi RF, Schulze M, et al. Depletion of C6 prevents development of proteinuria in experimental membranous nephropathy in rats. *Am J Pathol.* 1989;135:185–194.
15. Skoberne A, Behnert A, Teng B, et al. Serum with phospholipase A2 receptor autoantibodies interferes with podocyte adhesion to collagen. *Eur J Clin Invest.* 2014;44:753–765.
16. Debiec H, Guignonis V, Mougnot B, et al. Antenatal membranous glomerulonephritis due to anti-neutral endopeptidase antibodies. *N Engl J Med.* 2002;346:2053–2060.
17. Vivarelli M, Emma F, Pelle T, et al. Genetic homogeneity but IgG subclass-dependent clinical variability of alloimmune membranous nephropathy with anti-neutral endopeptidase antibodies. *Kidney Int.* 2015;87:602–609.
18. Kao L, Lam V, Waldman M, et al. Identification of the immunodominant epitope region in phospholipase A2 receptor-mediated autoantibody binding in idiopathic membranous nephropathy. *J Am Soc Nephrol.* 2015;26:291–301.
19. Fresquet M, Jowitt TA, Gummadova J, et al. Identification of a major epitope recognized by PLA2R autoantibodies in primary membranous nephropathy. *J Am Soc Nephrol.* 2015;26:302–313.
20. Seitz-Polski B, Dolla G, Payre C, et al. Epitope spreading of autoantibody response to PLA2R associates with poor prognosis in membranous nephropathy. *J Am Soc Nephrol.* 2016;27:1517–1533.
21. Seifert L, Hoxha E, Eichhoff AM, et al. The most N-terminal region of THSD7A is the predominant target for autoimmunity in THSD7A-associated membranous nephropathy. *J Am Soc Nephrol.* 2018;29:1536–1548.
22. Ellebrecht CT, Bhoj VG, Nace A, et al. Reengineering chimeric antigen receptor T cells for targeted therapy of autoimmune disease. *Science.* 2016;353:179–184.
23. Kansal R, Richardson N, Neeli I, et al. Sustained B cell depletion by CD19-targeted CAR T cells is a highly effective treatment for murine lupus. *Sci Transl Med.* 2019;11.
24. Seitz-Polski B, Debiec H, Rousseau A, et al. Phospholipase A2 receptor 1 epitope spreading at baseline predicts reduced likelihood of remission of membranous nephropathy. *J Am Soc Nephrol.* 2018;29:401–408.
25. Seitz-Polski B, Dahan K, Debiec H, et al. High-dose rituximab and early remission in PLA2R1-related membranous nephropathy. *Clin J Am Soc Nephrol.* 2019;14:1173–1182.
26. Shah P, Tramontano A, Makker SP. Intramolecular epitope spreading in Heymann nephritis. *J Am Soc Nephrol.* 2007;18:3060–3066.

Supplementary Methods

Generation of the murine PLA₂R1 full-length knock-in target vector

To generate the Rosa26 based knock-in, target vector construct of the complete mouse PLA₂R1 protein, a full-length mPLA₂R1 verified sequence (NM_008867; No.: MC224554 OriGene, Rockville, MD, USA) was PCR-amplified. For PCR, 5 ng of full-length murine PLA₂R1 cDNA was specifically amplified with 10 mM mPLA₂R1-forward (FW) and -reverse (Rev) primers, including Ascl sites at their 5' ends respectively. PCR was performed for 35 cycles (denaturing: 15 sec at 98°C, annealing: 15 sec at 66°C, extension 6 min at 72°C) using 5 U Phusion-DNA polymerase (Thermo Fisher Scientific) and subsequently cut for two hours at 37°C with 10 U Ascl (NEB, Ipswich, MA, USA). For cloning, 5 µg of the Rosa26/CAG/Stop/eGFP knock-in target vector (Addgene, #15192) was also digested over night at 37°C with 25 U Ascl (NEB).¹ The DNA-fragment and the vector were purified by phenol/chloroform extraction and ethanol-precipitation for one hour at -80°C. Ligation was performed with 100 ng vector-DNA and different molar ratios of the PCR-fragment (3:1, 1:1, 1:3) using 1 U T4-DNA ligase (NEB) at 12°C over night and subsequently transformed in competent XL10 E. coli (Agilent Technologies, Santa Clara, CA, USA) for 30 seconds at 42°C. The cloning was verified by PCR screening and DNA-sequencing of the complete mPLA₂R1 cDNA at Seqlab (Göttingen, Germany) according to their recommendations. Finally, 70 µg of one positive mPLA₂R1 full-length clone was linearized in 300 µl 10 mM Tris/HCl pH 8.0 with 200 U AsiSI (NEB) over night at 37°C, purified by sequential phenol and chloroform extractions and ethanol precipitated. The dried DNA-pellet was reconstituted in H₂O and integrity was verified by agarose gel electrophoresis.

Generation of mPLA₂R1 full-length knock-in (mPLA₂R1-positive) mice

R1-embryonic stem (ES)-cells were a kind gift from Dr. Nagy, Samuel Lunenfeld Research Institute, Mount Sinai Hospital, Toronto, Canada.² They were obtained at passage 11 and expanded to passage 14 and 15. R1-ES-cells were grown on gelatinated cell culture plates supplemented with a confluent layer of inactivated mouse embryo fibroblast (MEF) feeder cells. R1-ES-cells were passaged every second day. In order to obtain mice that specifically express mouse PLA₂R1 on podocytes, ES-cells containing a Rosa26/CAG/Stop/mPLA₂R1 knock-in target vector¹ (Supplemental Figure 1A) were generated and 1 x 10⁷ R1-ES-cells were electroporated with 50 µg of the linearized murine mPLA₂R1 knock-in target vector in a 0.4 cm gap-electroporation-cuvette (Life Technologies) and subsequently selected in a medium containing 200 µg geneticin (G418, Life Technologies) for one week. Correct targeting was verified by Southern blotting of EcoRI digested genomic DNA derived from isolated clones using a 5' external ROSA probe. Positive R1-ES-cell clones were further expanded before

injection into blastocysts. For blastocyst injection, 15 trypsinized R1-ES-cells with clearly visible, small, round nuclei without vacuoles were collected and injected into one blastocyst. Eight of these blastocysts were implanted into the uterus of a female mouse mated with vasectomized males at day 2.5 post coitum. The resulting chimeric males were mated with wild-type BALB/c females. Littermates of the F1 generation were genotyped by PCR to obtain offsprings that pass on the mPLA₂R1 knock-in. These mice carried the transgenic information of mPLA₂R1 under the control of a floxed stop-cassette to prevent transactivation by the CAG-enhancer. These animals are referred to as mPLA₂R1-negative precursor mice and were further used for breeding with NPHS2-Cre mice³ to obtain a podocyte-specific mPLA₂R1 expression. Due to the podocyte-specific action of the NPHS2 (podocin) promoter-triggered Cre-recombinase, the stop cassette was removed and mPLA₂R1 expression on glomerular podocytes was initiated, these mice are herein further referred to as mPLA₂R1-positive mice. mPLA₂R1-negative mice were backcrossed into the BALB/c background for 9 generations. The last backcross was performed with heterozygous Podocin Cre BALB/c mice to obtain mPLA₂R1-positive and -negative mice. Almost all mPLA₂R1-positive animals express mPLA₂R1 in podocytes in more than 90% of Glomeruli. The different genotypes were verified by three PCRs (Supplemental Figure 1B) either showing the presence of Cre (PodoCre) and the mPLA₂R1 transgene and the allele-frequency of the transgene (R26 wt).

Generation of rabbit antibodies against mPLA₂R1

Two rabbit antisera recognizing mPLA₂R1 were produced by cDNA immunization essentially as described previously.^{4,6} The expression construct encoding full-length mPLA₂R1 (OriGene) was conjugated to 1 μ m gold particles (Bio-Rad Laboratories) and ballistically injected into two rabbits at the antibody core unit of the University Medical Center Hamburg-Eppendorf. The rabbits received four immunizations in 3-6 week intervals, each with 12 shots of plasmid-conjugated gold particles (1 μ g DNA/mg gold per shot). Serum was obtained 3 weeks after the last DNA immunization and antiserum-specificity for native mPLA₂R1 was verified using immunofluorescence staining of CHO cells transiently transfected with mPLA₂R1 for 24 hours with serial dilutions of the antisera and using Western blotting on mouse glomerular extracts. Bound antibodies were detected with phycoerythrin- or HRP-conjugated anti-rabbit IgG antibodies (Dianova), respectively.

Animal Experiments

Fourteen week-old male mPLA₂R1-positive or -negative mice were injected intraperitoneally with 3 mg of purified rabbit IgG. To determine albuminuria, urine was collected using metabolic cages. Urine albumin content was quantified using a commercially available ELISA system (Bethyl) according to the manufacturer's instructions. Albumin values were standardized

against urinary creatinine values (as determined according to Jaffé) of the same sample. BUN and cholesterol levels were measured by standard procedures at the Department of Clinical Chemistry at the University Medical Center Hamburg-Eppendorf.

Mice were euthanized after seven days for the final removal of blood, urine and kidneys. All animals had free access to tap water and standard animal chow and were bred in the animal facility of the University Medical Center Hamburg-Eppendorf according to national and institutional animal care and ethical guidelines. Animal experiments were approved by the veterinarian agency of Hamburg and the local animal care committee.

Immunofluorescence analyses

For immunolocalization of nephrin (guinea pig pAB, 1:200; Acris), murine PLA₂R1 (rabbit pAB K1115, 1:600 and rat mAB B16/2 1:50, both self-made), rabbit IgG (AF488-rbIgG H+L, 1:200; Jackson ImmunoResearch Laboratories), C3 (FITC-goat pAB, 1:50; Cappel), THSD7A (goat pAB, 1:200; Santa Cruz); pIRE1 α (rabbit pAB, 1:100; Cell Signaling, LMP7 (rabbit pAB, 1:300 Abcam), Lamp2 (rabbit pAB, 1:500; Sigma), or LC3B (rabbit pAB, 1:50; Cell Signaling), collagen-type 4 (goat pAB, 1:400; Southern Biotechnologies), laminin (rabbit pAB, 1:1000; Sigma), p57 (rabbit pAB, 1:500; Santa Cruz) 3 μ M paraffin sections of experimental mouse kidneys were deparaffinized and rehydrated to water. Antigen retrieval was obtained by boiling in citrate buffer at pH 6.1 (30-60 minutes at constant 98°C), or by digestion with protease XXIV (5 μ g/ml; Sigma-Aldrich) for 15 minutes at 37°C. Unspecific binding was blocked with 5% horse serum (Vector Laboratories) with 0.05% Triton X-100 (Sigma-Aldrich) in PBS for 30 minutes at room temperature before incubation at 4°C overnight with primary antibodies in blocking buffer. Staining was visualized with fluorochrome-conjugated secondary antibodies (all affinity purified from Jackson ImmunoResearch Laboratories; 1:400) for 30 minutes at room temperature in 5% horse serum with 0.05% Triton X-100. To control for cross-reactivity of the anti-rabbit secondary antibodies with the injected and bound rabbit anti-PLA₂R1 IgG, intrinsic IgG was destroyed by excessive boiling. Furthermore, TrueBlot anti-rabbit antibodies (1:200; eBioscience) were used, which only bind to native rabbit IgG. Additionally, every individual mouse was controlled by omitting the primary antibody. Nuclei were counterstained with Hoechst (1:1000; Molecular Probes). Stainings were evaluated with a confocal LSM800 with airyscan using the ZEN blue software (all Zeiss), or by an Axioskop using the Axiovision software for light microscopy (all Zeiss). Fiji software was used for quantification of mPLA₂R1 staining intensity in relation to glomerular capillary tuft area. For immunohistochemistry to PLA₂R1, THSD7A and rabbit IgG, stainings were visualized using the AP-Polymer kit (Zytochem) following the manufacturer's instructions. Neufuchsin (Sigma) was used for color development, nuclei were counterstained with hemalaun (Sigma).

Periodic Acid-Schiff (PAS)-Staining

1.5 μ M paraffin sections of experimental mouse kidneys were deparaffinized and rehydrated to water. In order to oxidize diols to aldehydes, sections were incubated in 1% periodic acid for 15 min. These aldehydes then reacted for 40 minutes at RT with the Schiff reagent (Sigma) to obtain a purple-magenta color. Then counterstaining of nuclei was performed with hemalaun and following dehydration sections were mounted with Eukitt (O. Kindler GmbH).

Electron microscopy

Electron microscopic analyses were performed on kidneys that were fixed in 4% buffered paraformaldehyde. The specimen was transferred into a 0.1 M sodium-cacodylate buffer for 10 minutes at 80° C. Afterwards osmiumtetroxyde and sucrose were applied for two hours. Next, the specimens were washed in cacodylate buffer plus sucrose for 5 minutes. Tissue was post-fixed in rising ethanol concentrations for 5 minutes each, followed by tert-Methyl *tert*-butyl ether (MTBE) twice for 5 minutes. Afterwards the specimens were embedded in a MTBE plus epoxid-mixture (in a 1:3 dilution) at 60° for at 48 hours and for 11 ½ hours at 100°C.

Semithin and ultrathin sections were cut (Reichert-Jung Ultracut-E701704 microtome) and contrasted for one hour with uranyl acetate in methanol followed by lead citrate. Micrographs were generated with a transmission electron microscope (EM 109, Zeiss, Jena, Germany) equipped with a digital electron microscope camera (Tröndle, Moorenweis, Germany).

Coomassie-blue protein staining

Urine samples were normalized to creatinine and separated on a 4-15% Mini-PROTEAN® TGX™ Precast Protein Gel (Biorad). The gel was Coomassie Blue stained over night at RT and then thoroughly destained with water according to the manufacturer's instructions (Thermo Scientific).

Purification of rabbit IgG

NAb™ Spin Columns (Thermo Scientific) were used according to manufacturer's protocol. Briefly, 5 ml rabbit serum was given to a PBS-equilibrated 5 ml NAb™ Spin Column, washed with 20 ml 1 x PBS and eluted two times with 5.4 ml IgG Elution Buffer (Thermo Scientific) neutralized with 0.6 ml 1M Tris/HCl pH 9.0. Both elution fractions were rebuffered via PD-10 columns (GE Healthcare) to PBS and concentrated using Vivaspin 50,000 MWCO PES (Sartorius).

Glomeruli isolation

Mice were anesthetized by isofluorane and both kidneys were removed as one package. Kidneys were perfused over the renal artery with Dynabeads (Thermo Scientific) diluted in

HBSS. Then kidneys were unpacked, minced into small pieces, digested in collagenase solution (1.2 mg/ml collagenase 1A, 100U/ml DNaseI in HBSS) at 37°C for 15 min with gentle agitation. Collagenase-digested tissue was gently pressed through a 100 µm cell strainer followed by a 10 ml wash with HBSS. This solution was passed through a new 100 µm cell strainer followed by a 10 ml wash with HBSS. The glomerular suspension was then centrifuged at 200x g for 5 min. The glomerular pellet was resuspended in 6 ml HBSS and transferred into four 2 ml cups. Glomeruli containing Dynabeads were collected by a magnetic particle concentrator and washed for three times with HBSS 0.5% BSA, combined with HBSS, glomeruli were counted and centrifuged at 4000x g for 5 min. The glomerular pellet was snap frozen and kept at -80°C. The entire procedure was performed at 4°C with the exception of the collagenase digestion at 37°C. For the generation of mouse glomerular extracts, frozen pellets were homogenized in 100 µl of P1 (100 mM Tris/HCl pH 8.0, 1 mM MgCl₂) under liquid nitrogen. Then, the powder was immediately lysed in 100 µl P2 (50 mM Tris/Cl pH 7.4, 150 mM NaCl, 0.1 SDS, 1% NP-40, 0.5% Sodium-Deoxycholate containing protease inhibitor cocktail "Plus" (Roth, Karlsruhe, Germany) for 1 h at 4°C. The insoluble debris was pelleted at 20,000 x g for 10 minutes at 4°C and the supernatant was incubated over night at 4°C with 50 µl ProteinG resin (Thermo Fisher Scientific) to remove any mouse IgG. Finally, the ProteinG resin was pelleted for 5 minutes at 20,000x g and 4°C before the supernatant was further used for immunoblot analysis

HEK cell transfection

Full-length mPLA₂R1 and all other mPLA₂R1 sub-fragments used were cloned into the pcDNA3.1 vector (Invitrogen) containing a C-terminal hexahistidine tag and HEK293T cells were PEI-transfected using this construct. Three days post-transfection, cells were lysed in a native lysis buffer (50 mM Tris/HCl pH 7.4, 150 mM NaCl, 1 mM EDTA, 1% Triton X100) to obtain recombinant complete mPLA₂R1.

Antibody Elution

100 to 120 (10 µm thick) cryo-sections from mouse renal tissue were thawed in 1 ml PBS and centrifuged at low speed for 1 min. After washing three times in 1 ml PBS, the pellets were resuspended in 150 µl of 25 mM citrate buffer pH 3.2 and incubated on ice for 20 min with occasional shaking. Then, the samples were centrifuged for 5 min at 14,000 rpm and the supernatants were mixed with an equal volume of 1 M Tris/HCl, pH 8.0. In a second elution step, the pellets were resuspended in 25 mM citrate buffer, pH 2.5, incubated on ice, and centrifuged again. Finally, the supernatants were added to the first elution and diluted in 2 ml of 5% dry-milk in PBS-0.05% Tween 20. These samples were used as primary antibody source in Western blot analysis.

Statistical analyses

Data are expressed as mean \pm standard error of the mean (SEM). For statistical analyses we performed the non-parametric Mann-Whitney *U* test to enable robust conclusions on effect significance in case of departures from normality associated with small sample sizes or the two-tailed Student's *t*-test in parametric data sets. For comparison of more than two conditions, non-parametric one-way ANOVA was performed, for paired observations the two-way ANOVA was used.

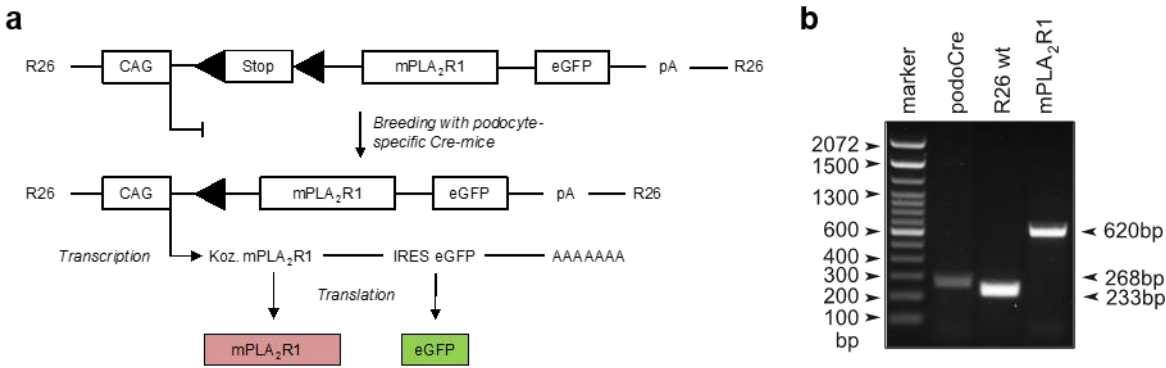
Immunoblot analyses

Similar amounts of total protein obtained from mouse glomerular extracts were loaded on a 4-15% Mini-PROTEAN® TGX™ Precast Protein Gel (Biorad) and separated under non-reducing conditions. Proteins were transferred to polyvinylidene difluoride membranes (Bio-Rad) under semi-dry conditions using Trans-blot Turbo (Bio-Rad) at 25 V constant for 25 min. After protein transfer, membranes were blocked for one hour at 4°C in 5% dry-milk, PBS-0.05% Tween 20 and incubated overnight with rabbit sera at a 1:10.000 dilution. HRP-conjugated goat anti-rabbit IgG 1:20.000 (Sigma-Aldrich) was used as the secondary antibody. Signals were detected using a chemiluminescent substrate (ECL Clarity, Biorad) with a Luminescent Detection Imager 600 (GE Healthcare).

Supplementary References

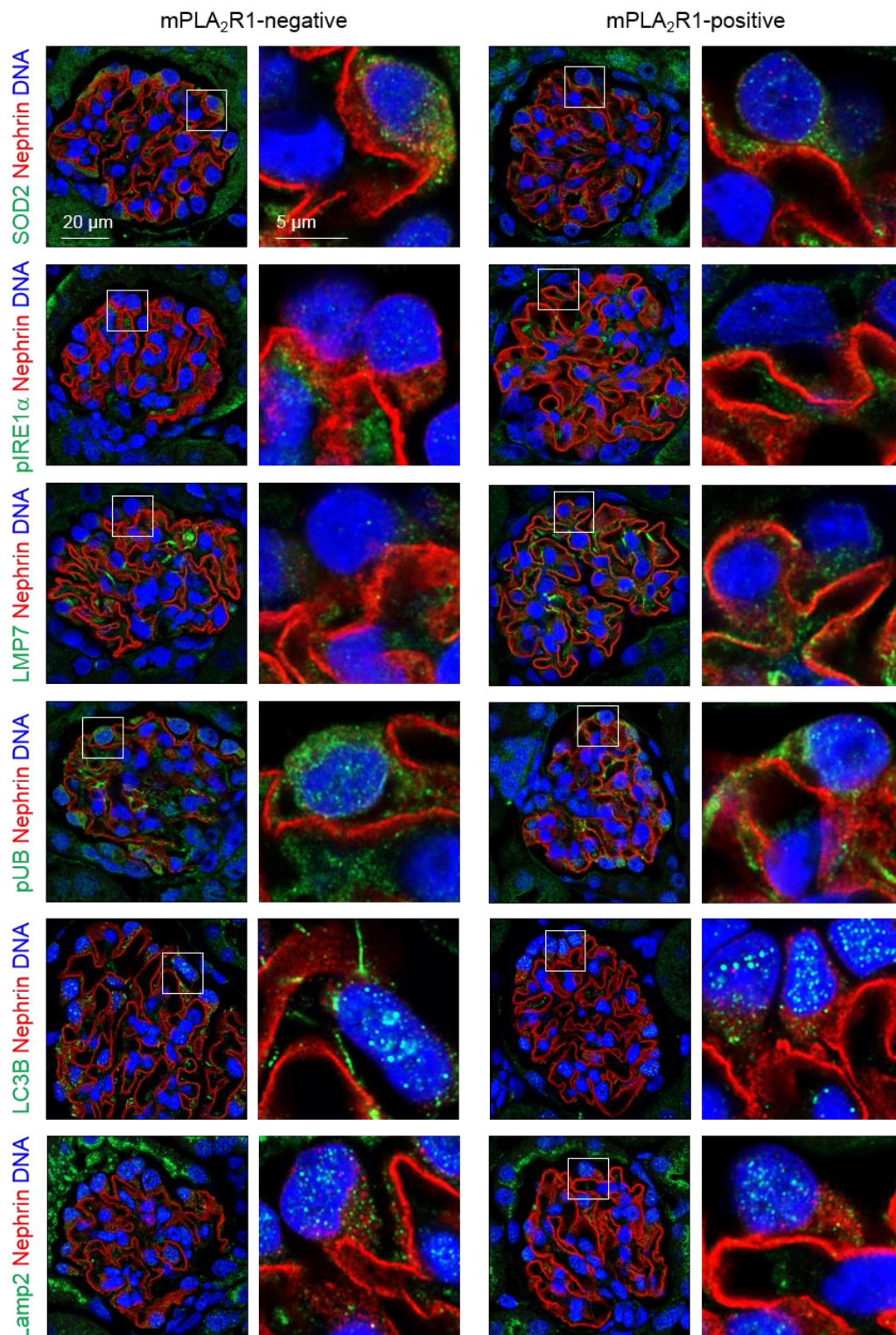
1. Thai, TH, Calado, DP, Casola, S, et al. Regulation of the germinal center response by microRNA-155. *Science*. 2007;316:604-608.
2. Nagy, A, Rossant, J, Nagy, R, et al. Derivation of completely cell culture-derived mice from early-passage embryonic stem cells. *Proc Natl Acad Sci U S A*. 1993;90:8424-8428.
3. Moeller, MJ, Sanden, SK, Soofi, A, et al. Podocyte-specific expression of cre recombinase in transgenic mice. *Genesis*. 2003;35:39-42.
4. Adriouch, S, Dubberke, G, Diessenbacher, P, et al. Probing the expression and function of the P2X7 purinoceptor with antibodies raised by genetic immunization. *Cell Immunol*. 2005;236:72-77.
5. Tomas, NM, Hoxha, E, Reinicke, AT, et al. Autoantibodies against thrombospondin type 1 domain-containing 7A induce membranous nephropathy. *J Clin Invest*. 2016;126:2519-2532.
6. Moller, S, Jung, C, Adriouch, S, et al. Monitoring the expression of purinoceptors and nucleotide-metabolizing ecto-enzymes with antibodies directed against proteins in native conformation. *Purinergic Signal*. 2007;3:359-366.

Supplementary Figures

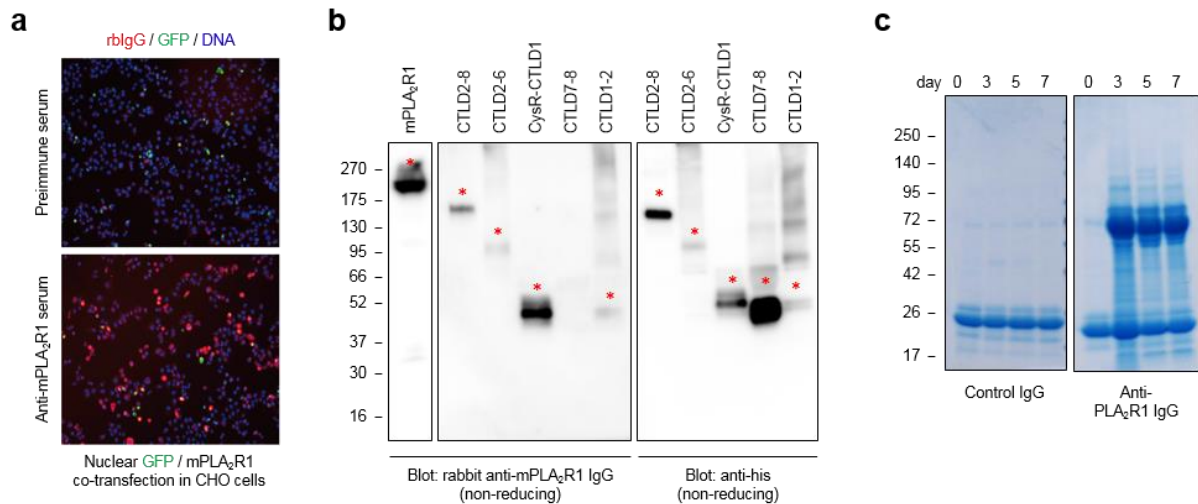


Supplementary Figure S1: Generation of mPLA₂R1 full-length podocyte specific transgenic mice.

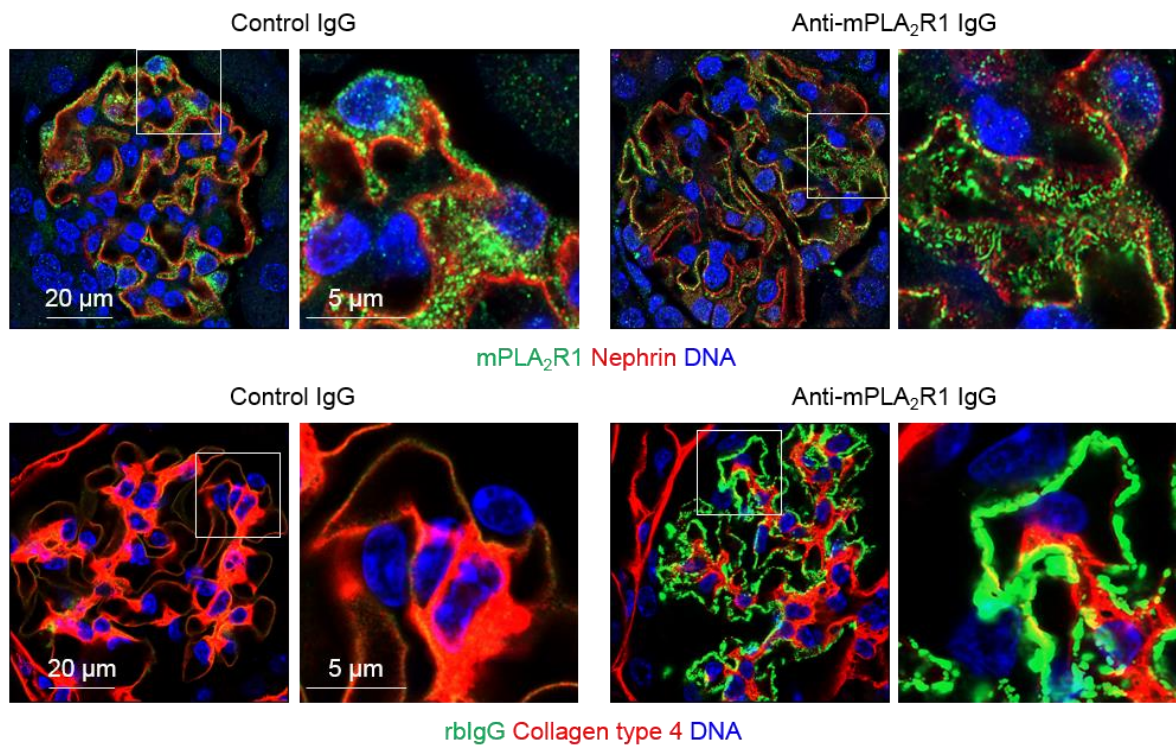
(a) Schematic depiction of the Rosa 26-based mPLA₂R1 full-length specific knock-in target construct including the transactivation by the CAG enhancer. After breeding with NPHS2 Cre deleter mice, mPLA₂R1-positive mice are obtained which express mPLA₂R1 specifically in podocytes. (b) PCR-based genotyping demonstrating the identification of the Cre-recombinase (268 bp), the mPLA₂R1 transgene (620 bp), as well as the determination of the mPLA₂R1 allele frequency by R26 wt (233 bp).



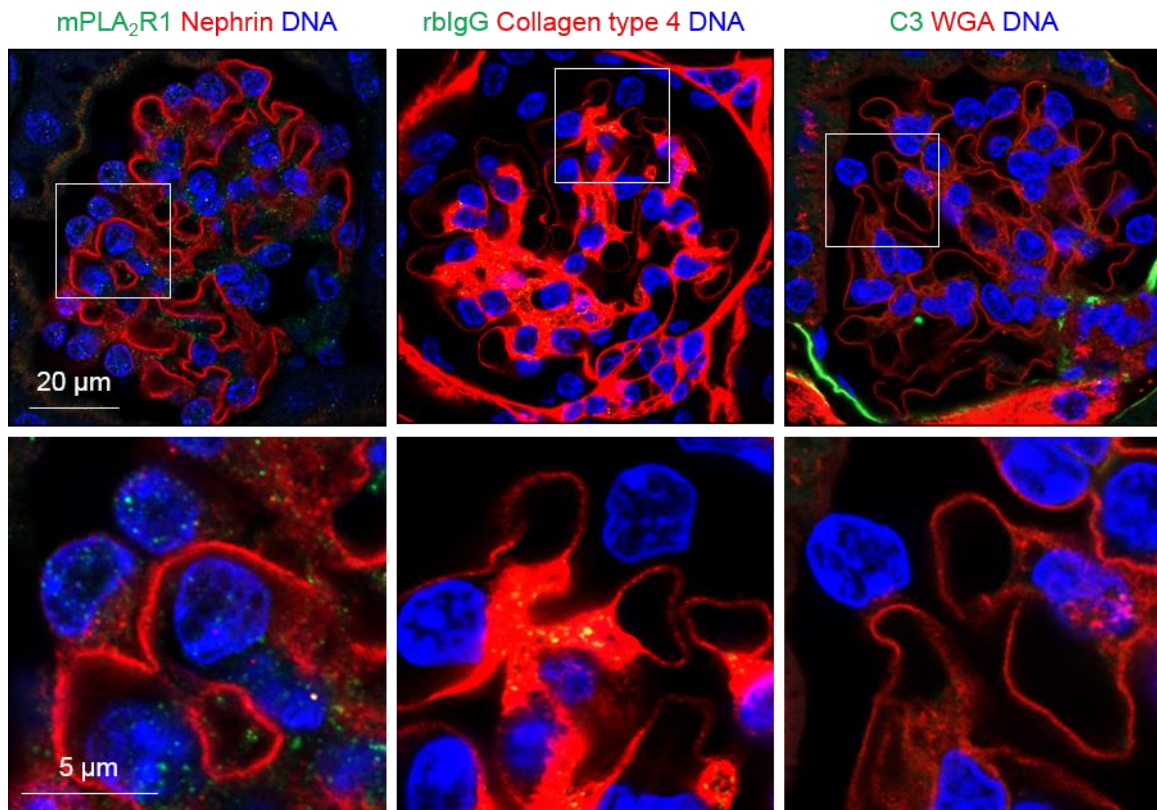
Supplementary Figure S2: Transgenic expression of mPLA₂R1 does not result in cellular/proteostatic stress. Representative confocal images to marker proteins such as superoxide dismutase (SOD2, oxidative stress), pIRE1a (endoplasmic reticulum stress), LMP7 (immunoproteasome subunit) and polyubiquitinated proteins (both markers for proteostatic stress in the proteasomal system), and autophagosomal LC3B and lysosomal Lamp2 (both indicators of an autophagosomal-lysosomal reaction) in conjunction with nephrin (red). Blue: Nuclei. The stress levels of mPLA₂R1-positive and -negative mice are similar.



Supplementary Figure S3: Generation of anti-PLA₂R1 antibodies in rabbits and antibody transfer. (a) CHO cells were co-transfected with nuclear GFP and mPLA₂R1 and stained with either rabbit preimmune or rabbit anti-mPLA₂R1 immune serum at a dilution of 1:400. Rabbit IgG bound to mPLA₂R1 was detected with an AF586 anti-rabbit antibody (red). Note red fluorescence in CHO-cells stained with rabbit anti-mPLA₂R1 antibody positive serum but not with rabbit preimmune serum. (b) Western blot analyses of lysates from HEK cells that were transiently transfected with flag-tagged full-length mPLA₂R1 and the his-tagged mPLA₂R1 mutants CTLD2-8, CTLD2-6, CysR-CTLD1, CTLD7-8 and CTLD1-2 with rabbit anti-mPLA₂R1 IgG diluted 1:10,000 under non-reducing conditions. Western blot of the same lysates with an anti-his antibody under non-reducing conditions demonstrates successful recombinant protein expression. Asterisks indicate specific bands. (c) Coomassie-blue staining of urinary samples from a mPLA₂R1-positive mouse injected with control IgG (left) and a mPLA₂R1-positive mouse injected with anti-mPLA₂R1 IgG (right).

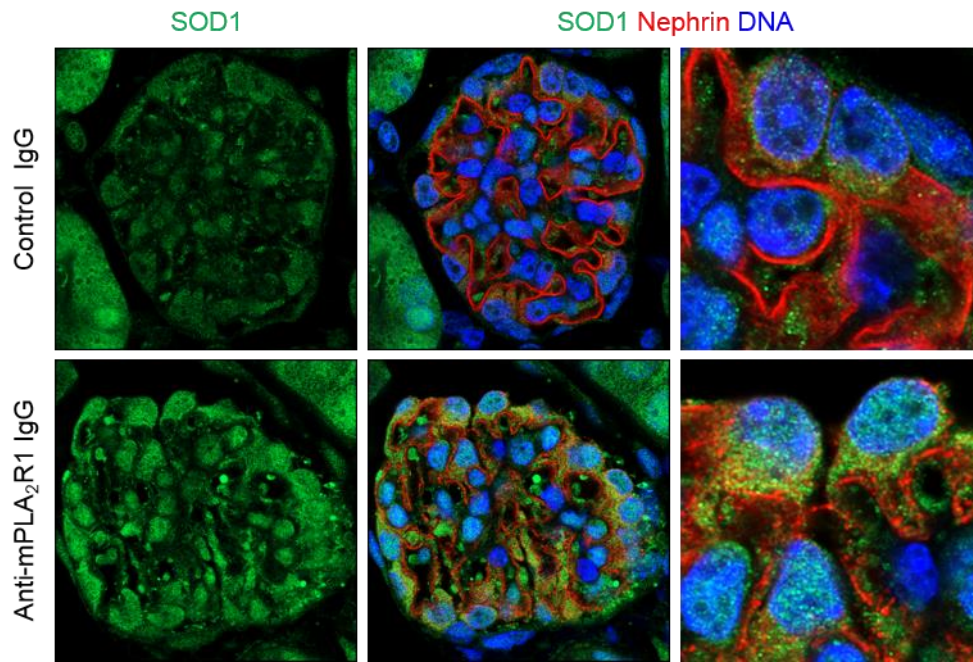


Supplementary Figure S4: mPLA₂R1-positive mice treated with rabbit anti-mPLA₂R1 antibodies but not with control rabbit IgG deposit rabbit IgG at the glomerular filtration barrier on day 5. Mice were stained for mPLA₂R1 expression (upper panels, green) in relation to nephrin (red) and for the occurrence of subepithelial rabbit IgG deposits (lower panels, green) in relation to the glomerular basement membrane protein collagen type 4 (red).

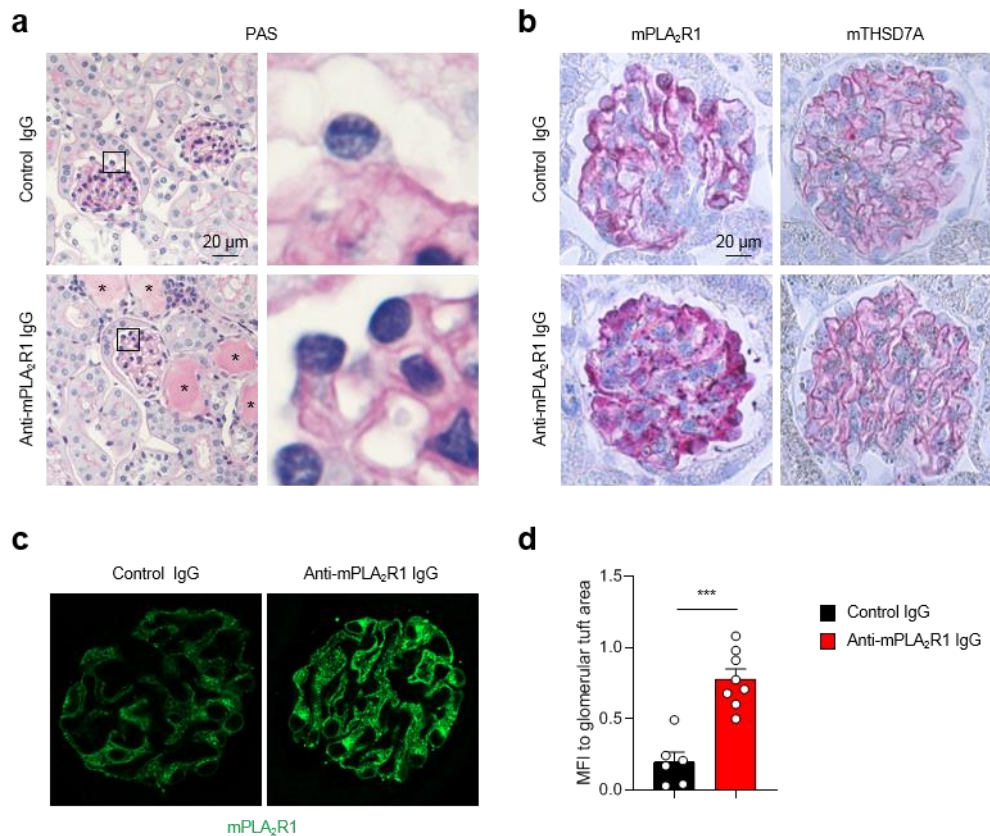


mPLA₂R1-negative mouse 7 days after treatment with anti-mPLA₂R1 rIgG

Supplementary Figure S5: mPLA₂R1-negative mice treated with rabbit anti-mPLA₂R1 antibodies do not deposit rabbit IgG or complement at the glomerular filtration barrier in comparison to mPLA₂R1-positive mice. On day 7, mice were stained for mPLA₂R1 expression (green) in relation to nephrin (red), for the occurrence of subepithelial rabbit IgG deposits (green) in relation to the glomerular basement membrane protein collagen type 4 (red), or for the occurrence of complement C3 (green) deposition. WGA = Wheat germ agglutinin, DNA (blue).

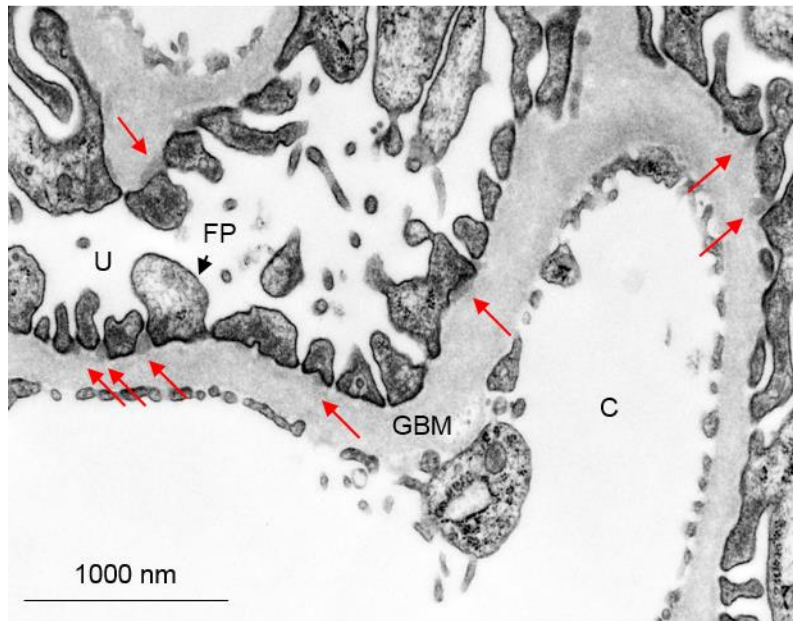


Supplementary Figure S6: Superoxide dismutase 1 (SOD1) is upregulated in mPLA₂R1-positive mice treated with rabbit anti-mPLA₂R1 antibodies. On day 7, mice were stained for SOD1 expression (green) in relation to nephrin (red). Note the strong positivity for SOD1 in mPLA₂R1-positive mice treated with anti-mPLA₂R1 IgG.

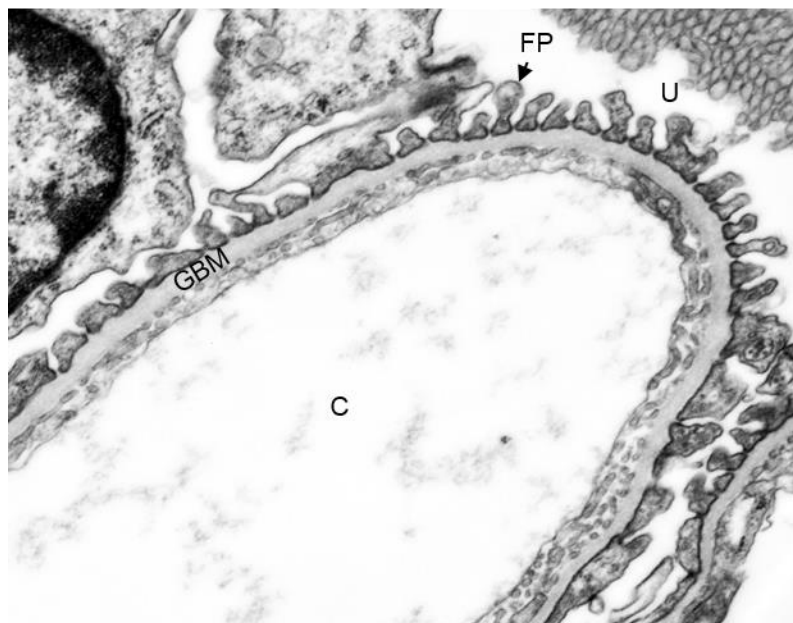


Supplementary Figure S7: Light microscopic changes and mPLA₂R1 staining in mPLA₂R1-positive mice seven days after transfer of control IgG and anti-mPLA₂R1 IgG. (a) Evaluation of renal cortex tissue integrity using PAS-staining. No major glomerular alterations (magnification) were observed in mPLA₂R1-positive mice treated with anti-mPLA₂R1 IgG, while signs of heavy proteinuria, such as protein casts (asterisks) in dilated tubuli, were visible under these conditions. (b) Immunohistochemical staining for mPLA₂R1 and mTHSD7A. Note the typical pathological picture of a PLA₂R1-associated MN with enhanced and granular PLA₂R1 staining and unaltered linear THSD7A expression. (c) Representative immunofluorescence staining for mPLA₂R1 in mPLA₂R1-positive mice after transfer of control IgG or anti-mPLA₂R1 IgG, demonstrating enhanced staining for mPLA₂R1 in the diseased mouse. (d) Quantification of mPLA₂R1 staining from mPLA₂R1-positive mice injected with control IgG (n=6 mice analyzed) or anti-mPLA₂R1 IgG (n=8 mice analyzed). MFI, mean fluorescence intensity. ****P*<0.001, two-tailed nonparametric Mann-Whitney *U* test.

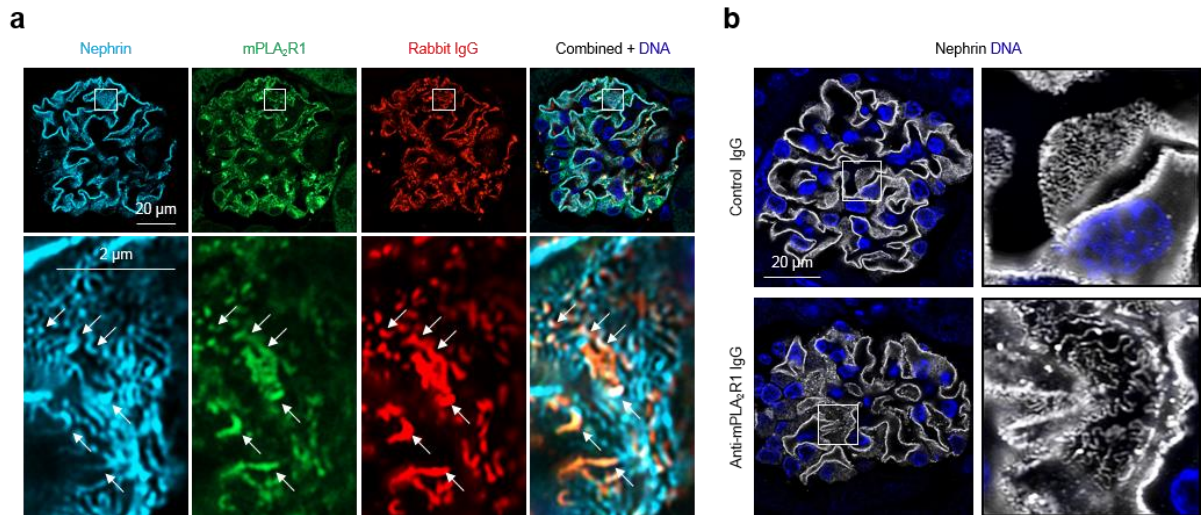
mPLA₂R1-positive mouse treated with anti-mPLA₂R1 IgG



mPLA₂R1-positive mouse treated with control IgG



Supplementary Figure S8: Electron microscopy studies. Representative electron microscopic images demonstrating electron dense deposits (red arrows) in mPLA₂R1-positive mice treated with anti-mPLA₂R1 antibodies but not in mPLA₂R1-positive mice treated with control IgG on day 7. C = capillary space, U = urinary space, FP = foot process, GBM = glomerular basement membrane.



Supplementary Figure S9: High resolution confocal and electron microscopic evaluations of immune complexes seven days after injection of rabbit anti-mPLA₂R1 IgG to mPLA₂R1-positive mice. (a) High-resolution confocal analysis of rabbit IgG (red) and mPLA₂R1 (green) in relation to the slit diaphragm protein nephrin (light blue). Note in the magnified transversal plane (lower panels) of the glomerular filtration barrier the co-localization of deposited rabbit IgG and mPLA₂R1 with nephrin (arrows). (b) High-resolution confocal microscopy for the slit diaphragm protein nephrin (white) revealed focal foot process effacement in mPLA₂R1-positive mice treated with anti-mPLA₂R1 IgG on day seven, but not in mice treated with control IgG. Blue, nuclei.